UNIVERSITY OF MISKOLC
FACULTY OF MECHANICAL ENGINEERING AND INFORMATICS

OPTIMIZING ENERGY EFFICIENCY BY INTEGRATING PHASE CHANGE MATERIALS INTO BUILDING ENVELOPES

PHD THESES

Prepared by

Ammar Saliby
Mechanical Power Engineering (BSc),
Solar Power Engineering (MSc),
Mechanical Power Engineering (MSc)

ISTVÁN SÁLYI DOCTORAL SCHOOL OF MECHANICAL ENGINEERING SCIENCES
TOPIC FIELD OF BASIC ENGINEERING SCIENCES
TOPIC GROUP OF TRANSPORT PROCESSES AND MACHINES

Head of Doctoral School

Dr. Gabriella Bognár
DSc, Full Professor

Head of Topic Group

Dr. László Baranyi
Full Professor

Scientific Supervisor

Dr. Béla Kovács

Miskolc
2026

CONTENTS

SUPERVISOR'S RECOMMENDATIONS

Date 22/07/2025

Ammar Saliby is a Ph.D. candidate specializing in mechanical engineering with a focus on energy-efficient building systems and thermal energy storage technologies. During his master studies, he developed expertise in building energy management and thermal modelling, which provided a strong foundation for his doctoral research. He commenced his Ph.D. studies at the University of Miskolc in the autumn of 2021, supported by the Stipendium Hungaricum scholarship program. Throughout his doctoral work, Ammar has demonstrated outstanding academic performance, completed all coursework, and actively contributed to scientific research within the field of sustainable building technologies. His research focuses on the integration and optimization of PCMs in building envelopes to enhance thermal performance and reduce energy consumption. He has made significant contributions to this field by developing validated CFD simulation models to analyze PCM behaviour, optimizing PCM layer configurations, and investigating encapsulation geometry for improved energy efficiency. Notably, his work explores the novel integration of PCMs into traditional masonry structures, such as Flemish bond walls, demonstrating a unique combination of architectural heritage and modern thermal storage solutions. Ammar has authored multiple scientific publications, including peer-reviewed journal articles and conference papers, all of which are indexed in Scopus, reflecting his commitment to high-quality research dissemination. He has actively presented his findings at national and international conferences, highlighting his dedication to advancing knowledge in the field of energy-efficient construction and thermal energy storage. The most significant contribution of his research lies in the development of practical, simulation-based methodologies for PCM application in building envelopes, providing new insights into the optimization of PCM placement, encapsulation geometry, and integration within traditional and modern wall assemblies. His work contributes to the advancement of sustainable building practices, offering solutions that improve energy performance while preserving architectural aesthetics. In recognition of these achievements, I, Dr. Béla Kovács, Associate Professor and supervisor of Ammar Saliby, consider his Ph.D. studies to be highly successful and commend his valuable contributions to the fields of mechanical engineering, energy efficiency, and sustainable building design.

Supervisor

Dr. Béla Kovács

LIST OF SYMBOLS AND ABBREVIATIONS

LATIN LETTERS

C_p	*Specific heat at constant pressure* [J/kgK]	p	*Pressure [Pa]*
E_{latent}	*Overall heat storage capacity* [kJ]	q	*Heat flux* [W]
f	*Liquid-fraction*	S	*Source term*
h	*Sensible heat* [J/kg]	t	*Time* [sec]
H	*Enthalpy of the material* [kJ/kg]	T_{ex}	*External surface temperature* [°C]
ΔH	*Latent heat content* [J/kg]	T_{in}	*Internal surface temperature* [°C]
h_{ex}	*External heat transfer coefficient* [W/m^{2}K]	T_L	*Liquids temperature of PCM* [°C]
h_{in}	*Internal heat transfer coefficient* [W/m^{2}K]	T_{ref}	*Reference temperature* [°C]
h_{ref}	*Reference enthalpy* [J/kg]	T_S	*Solidus temperatures of PCM* [°C]
k	*Thermal conductivity* [W/mK]	V	*Volume* [m^3]
L_H	*Latent heat of fusion* [kJ]	v	*Velocity of the fluid* [m/s]
m	*Mass* [kg]	x	*Element thickness* [m]
n	*Number of PCM cycles*		

GREEK LETTERS

α	*Thermal diffusivity* [m^2/s]	ρ	*Density of the material* [kg/m^3]
μ	*Dynamic viscosity* [Pa.s]		

ACRONYMS

ASHRAE	*American Society of Heating, Refrigerating and Air-Conditioning Engineers*
CFD	*Computational Fluid Dynamics*
DSC	*Differential Scanning Calorimetry*
IEA	*International Energy Agency*
LHS	*Latent Heat Storage*

PCM	*Phase Change Material*
PDE	*Partial Differential Equation*
PRESTO	*PREssure STaggering Option*
SIMPLE	*Semi-Implicit Method for Pressure-Linked Equations*
UDFs	*User Defined Functions*

1. INTRODUCTION

1.1. Energy Impacts of Heating and Cooling Loads in Buildings

Globally, buildings are becoming major energy consumers, with heating and cooling alone representing up to 40 % of commercial building energy and as much as 61 % of homes. The International Energy Agency (IEA) identifies the building sector as the largest single user of energy worldwide and warns that if nothing changes, demand for space heating could climb by 12 % and for cooling by 37 % by 2050 [1].

The building envelope (walls, roof, windows, and floors) works as the primary interface between indoor and outdoor environments. It not only protects occupants from the weather, but also governs how much thermal energy enters or escapes. A substantial portion of heating and cooling demand is associated with heat transfer through the envelope, while additional loads arise from ventilation, infiltration and internal gains. Reflecting this, the IEA reports that the greater part of recent investment in the sector has gone toward renovating and constructing higher-performance envelopes, as shown in Fig. 1.1, and that building operations plus construction accounted for 39 % of energy-related CO_2 emissions and 36 % of final energy use in buildings in 2018 [2].

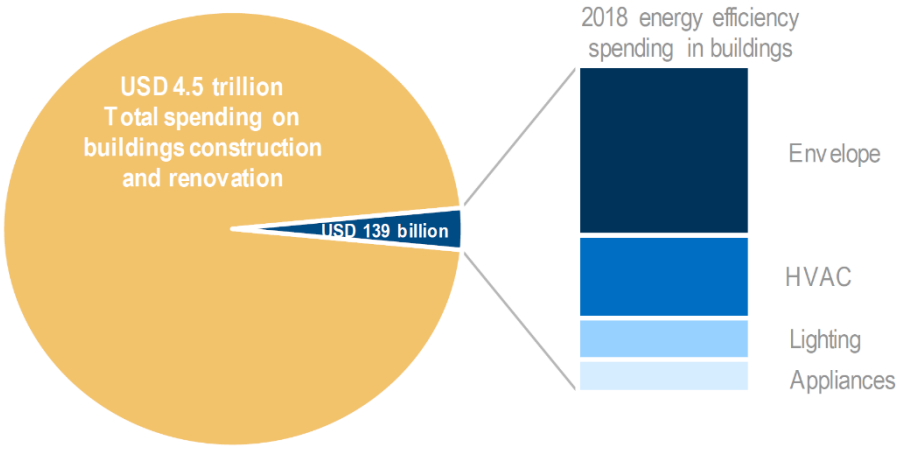

Fig. 1.1: *Investments in energy efficiency globally and total building spending* [2]

To reduce these loads, researchers and practitioners have explored a variety of envelope-focused strategies [3,4]. One of the most promising approaches is embedding phase change materials (PCMs) into building components. By absorbing and releasing latent heat as it melts and solidifies, PCMs can smooth out temperature swings, reducing heating and cooling demands while maintaining thermal comfort [5-11]. Recent studies [12-14] continue to investigate new PCM

formulations and ways to integrate them most effectively. As Fig. 1.2 shows, publications on PCM-enhanced envelopes have surged since 2012, reflecting the growing interest in this flexible energy storage solution.

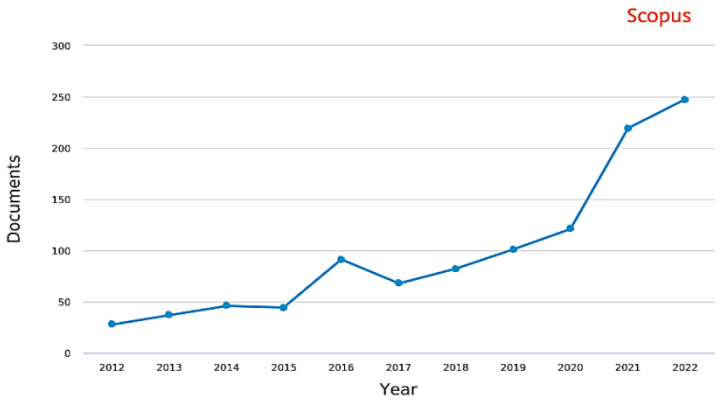

Fig. 1.2: *Published papers per journal throughout the last 10 years using the Scopus database*

1.2. Thermal Energy and Load Reduction Techniques in Buildings

Most of us, over 85 % of our lives are spent indoors, relying on buildings to keep us comfortable, healthy, and safe from the weather. Researchers have offered many definitions of comfort, but they generally agree that it hinges on the interplay between our bodies and the surrounding environment, especially when it comes to thermal comfort, well-being, and our ability to control conditions [15].

The building envelope significantly influences the comfort levels, natural lighting, ventilation, and how much energy is needed to heat and cool a building. If current trends continue, global cooling demand could surge by nearly 150 % by 2050, and by an astonishing 300-600 % in developing regions. Simple, cost-effective measures like reflective paints on walls and roofs, exterior shading devices, and low-emissivity window films can dramatically reduce cooling loads in hot climates [16]. Conversely, smart envelope design and advanced glazing can capture passive solar heat to reduce energy needs in colder areas.

Researchers are exploring a spectrum of passive and active strategies to boost an envelope's thermal performance and storage capacity. Together, these innovations hold the promise of cutting building energy use by up to 20 % by 2030 [17]. Among the most exciting developments is the integration of PCMs. By absorbing heat as it melts and releasing it when it solidifies, PCMs offer a dynamic way to balance peaks in building loads, bridging the gap between energy supply and demand, and are rapidly gaining traction in the construction sector.

1.3. The Idea Behind PCMs

PCMs can absorb and release heat during phase transition (from the solid to liquid state and *vice versa*) under a constant temperature, as seen in Fig. 1.3. These materials can absorb and release large amounts of heat for a limited unit volume by storing heat during the melting and

charging phases and releasing it during the solidification and discharge phases. PCMs may effectively manage energy in a variety of applications. This helps to regulate the required amount of energy. Additionally, by delaying and reducing peak thermal loads, PCMs can shift part of the heating and cooling demand to off-peak periods, which may reduce peak HVAC capacity requirements and improve operational performance depending on the building system and control strategy [18,19].

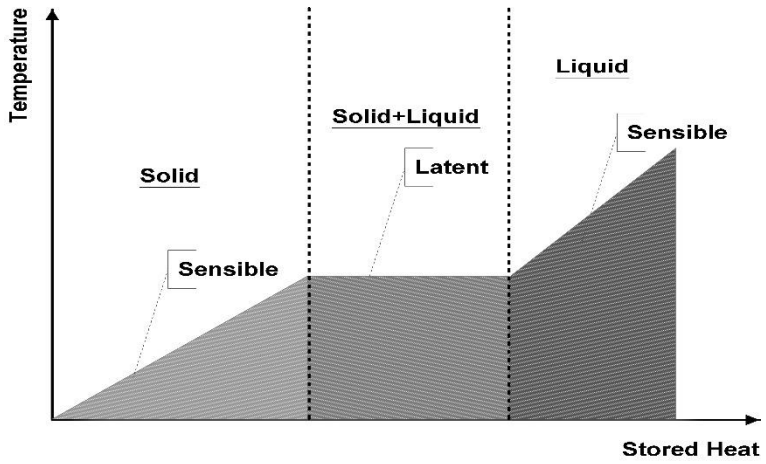

Fig. 1.3: *Heat transition regions*

1.4. Classification of PCMs

PCMs are typically grouped into three main categories: organic, inorganic, and eutectic, based on their chemical composition, as illustrated in Fig. 1.4. Each of these PCM categories offers distinct thermal characteristics and operating temperature ranges, as shown in Fig. 1.5, making certain types more suitable for specific applications than others.

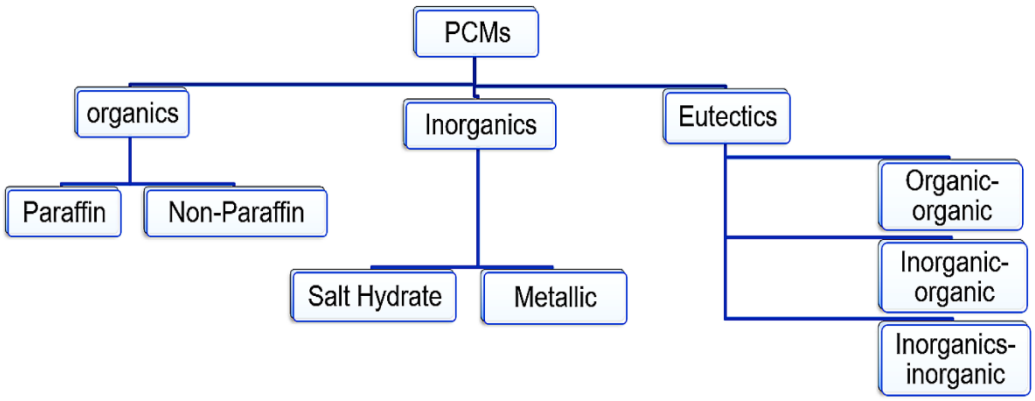

Fig. 1.4: *Classification of PCMs* [20]

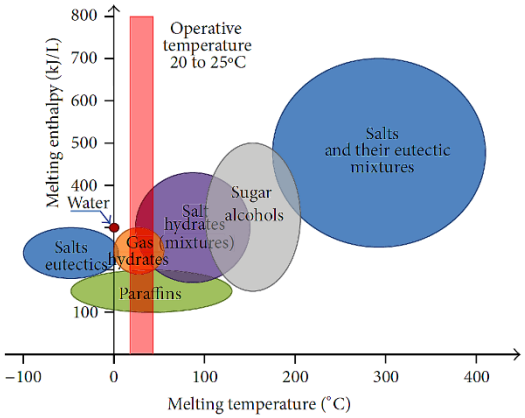

Fig. 1.5: *Melting temperatures and phase change enthalpy for PCMs* [21]

Table 1.1 summarizes the key advantages and disadvantages associated with these PCM types. Beyond their basic thermal properties, selecting the ideal PCM depends significantly on matching its melting point with the specific temperature range of the intended application.

Table 1.1: *Characteristics of PCMs* [22,23]

	PCM type		
	Organics (Paraffin wax, fatty acids, and vegetable oils)	Inorganic (Salt hydrates)	Eutectic
Advantages	Wide temperature range of availability	High thermal storage capacity	Sharp melting and boiling points
	The high heat of fusion	Good thermal conductivity	Higher volumetric storage density than the organic PCM
	physical and chemical stability	Low cost	
	Environmentally safe	Available easily	
	No subcooling	Nonflammable	
	No segregation	Low vapor pressure	
Disadvantages	Low thermal conductivity	Show subcooling	Costly
	Large volume change during phase transition	Considerable change in volume	Limited data available for thermophysical properties
	Unstable at high temperatures	Show phase segregation	

No sharp phase transition	Incompatible with metallic containers
Low enthalpy	
Flammable	

1.5. Applications of PCMs

PCMs have emerged as highly promising solutions for storing energy and managing heat transfer across various applications. Recent studies have particularly emphasized their potential within solar energy systems, demonstrating strong performance in numerous heat transfer scenarios [24]. Moreover, researchers have explored PCMs as effective thermal storage options in both heating and cooling installations [25], thermal storage tanks [26], and solar cooking devices [27]. Additionally, PCMs are increasingly integrated into electronic systems as effective heat sinks to regulate device temperatures [28]. Their incorporation into building envelopes further showcases their versatility and significant contributions toward energy efficiency.

1.6. PCM-Incorporated Building Envelope

Building components such as roofs, floors, external walls, and windows form the primary protective barrier, insulating indoor spaces from external conditions. This building envelope significantly influences thermal loads, determines heating and cooling needs, and directly impacts occupant comfort. To effectively harness their energy storage potential, PCMs can be integrated into building envelopes using various techniques and configurations. However, incorporating PCMs into building materials is not straightforward, it involves carefully navigating numerous interrelated parameters. These factors are closely related to the specific thermal properties of PCMs and the practical challenges associated with their integration into different building components.

1.6.1. PCMs Selection

Choosing the right PCM type for a given application is important by carefully considering the needed features. These properties can be categorized as follows:

- *Thermophysical properties:* play a crucial role in determining the effectiveness of PCMs in building applications. Important characteristics include melting points that closely match the typical temperature range of the intended application, high latent heat storage capacity, strong specific heat, effective thermal conductivity, minimal subcooling, significant density, low vapor pressure, and stable performance over many melting-solidification cycles. Table 1.2 summarizes these essential PCM characteristics as investigated by various studies.

Table 1.2 *Thermophysical properties of PCM reported in different literature*

PCM type	Melting temperature [°C]	Heat of fusion [kJ/kg]	Thermal conductivity [W/mK]		Density [kg/m^3]		Specific heat [kJ/kgK]		Ref.
			Liquid	Solid	Liquid	Solid	Liquid	Solid	
Organic PCMs									
Paraffin	23	200	0.2	0.2	-	860	-	2.1	[29]
Bio PCM	27-29	245	-	0.2	770	880	-	2	[30]
PCM wallboard	25.8	28.7	-	0.134	-	-	-	1.2	[31]
PCM-27	27	172.42	0.58	1.05	1710	1530	2.22	1.42	[32]
RT-18	17-19	225	-	0.2	770	880	-	2	[33]
Inorganic PCMs									
Salt hydrate	27.5	194	-	-	-	-	-	-	[34]
Salt hydrate	25-27	122.3	0.54	1.08	-	1100	2.31	1.34	[35]
Salt hydrate	28.9	190	-	1	-	1700	-	3.02	[36]
Salt hydrate	22.6-30.7	122.3	0.54	1.08	-	1100	2.31	1.34	[37]
SP-22	18-22	150	0.5	0.5	1400	1500	2	2	[38]
Eutectic PCMs									
Eutectic	22	130.2	-	-	-	-	-	-	[39]
Eutectic	14.2	98.21	-	-	-	-	-	-	[39]
Eutectic	21	155	-	-	-	-	-	-	[40]
Eutectic	24	147.7	-	-	-	-	-	-	[41]
Eutectic	25.5-27	203.8	-	-	-	-	-	-	[42]

Evaluating the thermophysical properties of PCMs is essential to ensure their suitability for specific building applications. Differential Scanning Calorimetry (DSC) is the most commonly employed and effective method for this purpose. DSC precisely identifies key properties such as melting and solidification points, enthalpy values, overall heat storage capacity, and specific heat. Additionally, PCM manufacturers and suppliers typically supply technical data sheets detailing these thermophysical properties, validated across multiple thermal cycles. Selecting the appropriate PCM also requires careful consideration of local climate conditions, particularly in areas experiencing significant weather fluctuations. Furthermore, careful planning and precise

installation are vital to prevent common PCM issues such as material segregation and subcooling, which can severely limit their performance and practical use [43].

- *Chemical properties:* no segregation, interaction with the encapsulating material, irradiative, nonflammable, noncorrosive, nonexplosive, and stable phase transition cycles throughout long service life.

- *Other:* widely available, inexpensive, eco-friendly, and recyclable.

1.6.2. Incorporation Techniques

PCMs are incorporated into building envelope elements by one of the following techniques.

- *Direct incorporation:* the simplest and most cost-effective method of incorporating PCM into building materials involves directly mixing the PCM, either in powder or liquid form, into common construction mixtures, such as gypsum mortar, cement mortar, or concrete. This straightforward technique requires minimal expertise and can be easily carried out without specialized equipment [44].

However, this direct integration method comes with notable drawbacks. One significant issue is PCM leakage during its melting phase. If the PCM used is flammable, this leakage can lead to incompatibility with building materials and increase fire risks. Furthermore, mixing PCM directly into building materials, especially when the PCM is in a liquid state, can negatively affect the mechanical properties of the finished structural components. Specifically, the introduction of liquid PCM into mixtures can disrupt the proper water-to-material ratio, resulting in weakened structural integrity, particularly at elevated temperatures [45].

- *Immersion technique:* the immersion technique involves soaking porous building materials in liquid PCM, which is then absorbed into the material by capillary action. Despite its simplicity, this approach has several notable drawbacks when used in concrete structures. Key concerns include PCM leakage during melting, potential incompatibility with structural materials, and an increased risk of corrosion in embedded steel reinforcement bars [46].

- *Encapsulation technique:* encapsulation is an effective solution to the problem of PCM leakage and plays a key role in enhancing the material's compatibility with building components. By enclosing the PCM within a protective barrier, this method prevents direct exposure to the environment and significantly reduces the risk of leakage. More than just a containment strategy, encapsulation also increases the heat transfer surface area, which improves thermal conductivity and, in turn, maximizes the PCM’s energy storage performance [22].

There are two main encapsulation approaches: macro-encapsulation and micro-encapsulation. In macro-encapsulation, PCMs are contained within larger structures such as tubes, shells, panels, or plates. Micro-encapsulation, on the other hand, involves coating the PCM with a fine polymer shell, creating microscopic capsules that can be embedded into building materials, as shown in Fig. 1.6 [47,48].

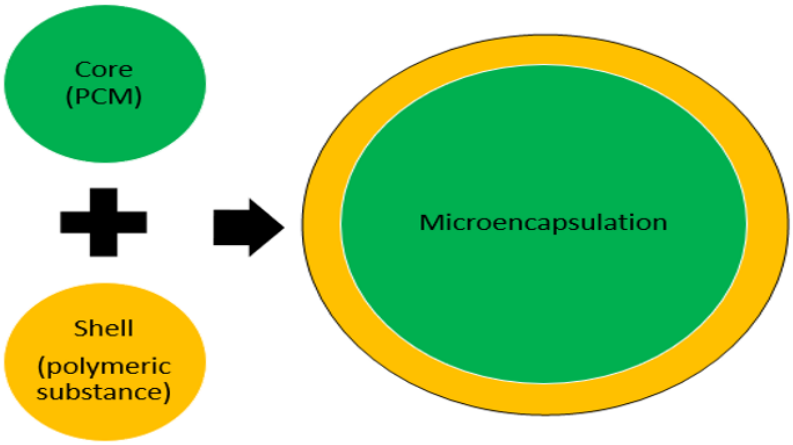

Fig. 1.6: *Micro-encapsulation technique*

Regardless of the method, the choice of encapsulating material is crucial. It must prevent leakage, preserve the PCM's thermal properties, avoid chemical reactions with the PCM, and remain stable under thermal and mechanical stress. It should also accommodate any volume changes that occur during phase transitions while maintaining structural integrity and thermal performance over time [49,50]. Materials like aluminum, copper, and stainless steel are commonly used in macro-encapsulation systems due to their excellent thermal conductivity, structural strength, and long-term compatibility with building materials [51]. Examples of these macro-encapsulation designs are illustrated in Fig. 1.7.

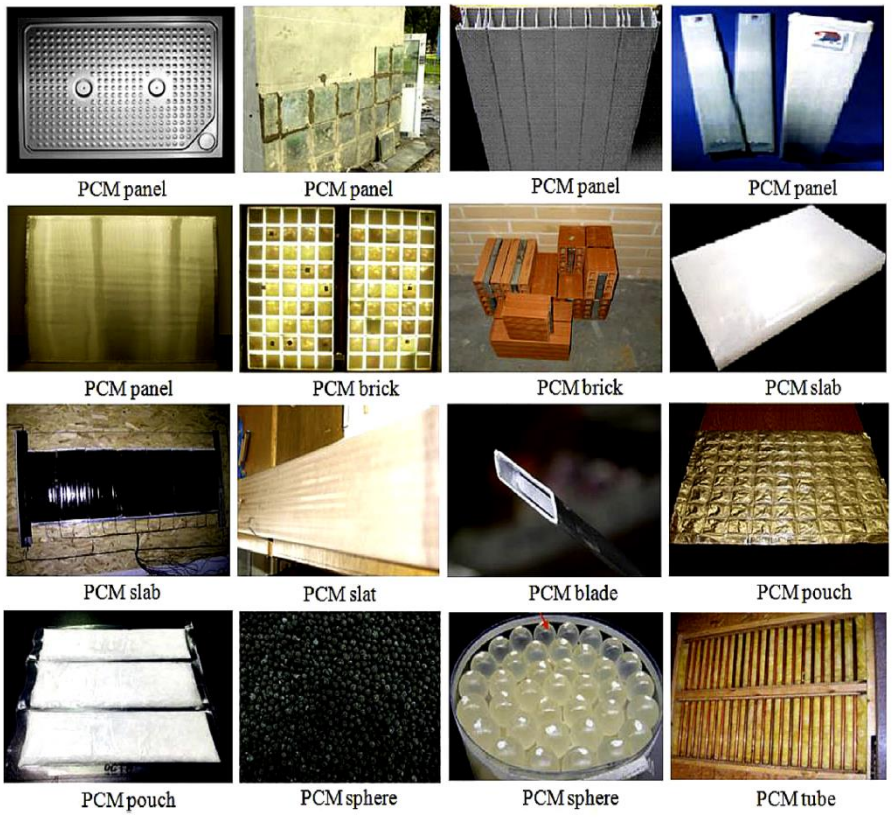

Fig. 1.7: *Macro-encapsulation forms used in building envelopes* [52]

- *Shape-stabilized technique:* in the shape-stabilized approach, the PCM is incorporated into a self-supporting solid network (e.g., cross-linked polymer matrix or a rigid conductive framework) that maintains structural integrity during melting and solidification. Leakage is suppressed because the solid skeleton mechanically confines the PCM and the composite remains dimensionally stable even when a large fraction of PCM is liquid. Depending on the matrix, shape-stabilized PCMs can also improve effective thermal conductivity and show stable performance over repeated thermal cycles, which is attractive for building components that must retain mechanical integrit [53,54].

- *Form-stable PCM composites:* in the form-stabilized approach, the PCM is typically impregnated into a porous support (e.g., porous minerals, lightweight aggregates, or other porous carriers). When the PCM melts, it is retained primarily by capillary forces and adsorption within the pore structure, which limits leakage under normal operating conditions. The PCM content and leakage resistance are governed by pore volume, pore-size distribution, and PCM–support wettability; therefore, performance depends strongly on the selected carrier and impregnation method. Form-stabilized composites are widely used in building materials due to their practical manufacturability, although the achievable PCM fraction and mechanical strength can be constrained by the carrier properties [55].

1.6.3. Parameters Affecting the Performance of PCM in Building Envelopes

The thermal performance of PCMs is influenced by a wide range of factors. To achieve optimal results, it's essential to carefully consider and manage these parameters throughout the design and application process [56]. The most critical of these influencing factors are outlined and discussed in the following sections.

- *Melting temperature:* is one of the most critical factors influencing the performance of PCMs, as it directly affects both the charging (heat absorption) and discharging (heat release) phases. For effective integration into building systems, the melting temperature must align with the thermal demands of the specific application and climate.

In colder seasons, PCM should have a lower melting point to take advantage of limited solar radiation and enhance heating efficiency. Conversely, during the summer, a higher melting point is preferable to minimize heat transfer into the building and reduce cooling loads.

According to Researchers [57], the ideal melting temperature varies depending on the application, for domestic water heating, the optimal range is 29 [°C] to 60 [°C]. For indoor thermal comfort, the recommended range falls between 22 [°C] and 28 [°C]. For cooling-oriented applications, PCMs with melting points of 21 [°C] or lower are most effective. Table 1.3 provides an overview of the operational melting temperatures for several commercially available PCMs commonly used in building envelope systems.

Table 1.3: *Operational melting temperature of commercially available PCMs* [58]

PCM	PCMs operational melting temperature from the manufacturer's datasheet [°C]	Manufacturer
RT-21HC	21	Rubitherm
RT-22HC	22	Rubitherm
RT-25HC	25	Rubitherm
RT-27	27	Rubitherm
Purer Temp 23	23	Entropy Solutions
Micronal DS5040X	23	BASF
Micronal DS5008X	25	BASF
MPCM24D	24	BASF
Micronal DS5038X	25	Microteklabs
MacroPCM28	28	Microteklabs
MacroPCM24	24	Microteklabs

- *PCM thickness:* the thickness of the PCM layer within a building envelope plays a crucial role in determining how much thermal energy can be stored during phase transitions. When only a thin layer or small volume of PCM is used, such as in efforts to reduce summer cooling loads, it tends to absorb a limited amount of heat and reaches its melting point quickly, becoming fully liquid in a short time. This limits its effectiveness in maintaining thermal balance. In contrast, a thicker or higher volume PCM layer can absorb significantly more heat during the charging phase, slowing down heat transfer through the building component and enhancing thermal performance. However, simply increasing the amount isn't always the best solution; if the PCM volume is not optimized, it can lead to inefficiency or unnecessary material use.

As a result, determining the right PCM volume is essential for achieving reliable performance. The required PCM volume can be calculated from $V_{PCM} = \frac{m_{PCM}}{\rho_{PCM}}$, where m [kg] is the mass of PCM and ρ [kg/m^3] is the density of PCM.

The overall heat storage capacity of the PCM, E_{latent} [kJ], can be determined by Eq. (1.1) [59] as follows:

$$E_{latent} = n \times m \times H, \qquad (1.1)$$

where n is the number of cycles during the day, m [kg] is the mass of PCM, and H [kJ/kg] is the total energy exchange of PCM enthalpy content.

- *PCM position:* the position of the PCM layer within a building element is a key factor that influences its effectiveness and depends largely on the building's geographic location and whether the goal is to reduce heating or cooling demand. Several studies have emphasized that positioning the PCM layer closer to the heat source leads to better thermal performance [60]. In climates where cooling is the priority, this typically means placing the PCM toward the outer surface of the building envelope, where it can absorb solar heat before it penetrates the interior. Conversely, in heating-dominant climates, placing the PCM closer to the interior helps retain and slowly release stored heat into the occupied space [61]. Some research also suggests that positioning the PCM within the middle layer of a building component can yield consistent thermal performance throughout the year, especially in mixed climates [62]. Ultimately, the ideal location of the PCM layer is not only climate dependent, but also closely linked to the PCMs melting temperature, as it must align with the heat exposure level at its position to maximize phase change activity and energy efficiency.

1.6.4. Classification of PCM-Incorporated Buildings

The literature highlights several effective strategies for integrating PCMs into building components. In most cases, PCMs are either added as a separate layer or incorporated during the construction phase. This integration has led to notable performance improvements across various parts of the building envelope, including roofs, external walls, floors, and windows. Among these elements, roofs and external walls have received the most research attention. This is largely because they constitute the largest surface areas exposed to the external environment and are most affected by weather fluctuations. As a result, they contribute significantly to unwanted heat gains in summer and heat losses in winter, making them ideal targets for PCM integration.

By contrast, floors and windows have been less frequently studied in PCM applications. Floors, which are generally in contact with stable ground temperatures and less exposed to direct environmental conditions, tend to have a smaller impact on a building's overall thermal load. Nonetheless, some researchers have explored how PCM-enhanced flooring systems can contribute to improved indoor thermal comfort and energy savings, particularly in combination with radiant heating or cooling systems [63]. In the case of windows, PCM has been incorporated into frames and glazing cavities in several experimental designs. However, widespread adoption has been limited due to challenges such as material leakage and reduced transparency in glazed panels issues that compromise both aesthetics and function [64].

Given the significant thermal influence of external walls and roofs, most recent studies have focused on PCM applications in these areas. The following section presents a review of up-to-date research exploring PCM integration within various building materials and envelope configurations.

- *PCM incorporated in concrete:* concrete is one of the most widely used construction materials around the world, and incorporating PCMs into concrete has shown strong potential for enhancing indoor thermal comfort and improving energy efficiency in both heating and cooling

applications. By leveraging the thermal storage properties of PCMs, concrete elements can moderate temperature fluctuations and reduce overall energy demand.

However, integrating PCMs into concrete, particularly through micro-encapsulation, also presents some challenges. These include fire risks due to the polymeric encapsulation materials, a decrease in mechanical strength, and the poor low thermal conductivity of many PCMs [65]. To address these concerns and better understand the behavior of PCM-concrete systems, an experimental study using $Sr(OH)_2 \cdot 8H_2O$, a strontium-based PCM powder known for its high latent heat capacity [66]. DSC confirmed its desirable thermal properties. Their results showed a 15-21 % reduction in heat transfer through the concrete and only a minor loss in compressive strength. Moreover, the inclusion of PCM helped reduce thermal strain and cracks within the concrete matrix. In a long-term study, researchers investigated the durability of PCM-integrated concrete over 10 years. They tested two experimental chambers, one with 5 wt.% PCM and one without built-in 2005 using a consistent methodology. Despite long exposure to natural conditions, the thermal response remained consistent, and no significant difference in compressive strength was observed, suggesting the long-term stability of PCM-concrete composites [67]. Nevertheless, direct or immersion-based PCM integration can lead to problems such as subcooling, segregation, and leakage, especially under certain environmental conditions. The alkaline nature of concrete and the risk of steel reinforcement corrosion further limit the types of PCMs that can be safely used in structural applications [68]. Mortar-based systems offer an alternative approach, showing significant improvements in thermal comfort and energy efficiency when enhanced with micro-encapsulated PCM. Researchers developed and tested two such composites Micronal 5038X and Micronal 5040X, with melting points of 25 [°C] and 23 [°C], respectively, through both experimental methods and COMSOL Multiphysics simulations under the climate of Sicily, Italy [69]. They identified an optimal melting point of 27 [°C] and found that Micronal 5038X exhibited higher latent heat than its counterpart. The study also showed that adding 15 wt.% PCM to the mortar mixture reduced indoor surface temperatures and improved thermal comfort by approximately 15 % compared to standard cement mortar, according to ASHRAE comfort criteria.

These findings underline both the promise and complexity of using PCMs in concrete and mortar systems, highlighting the importance of material selection, structural compatibility, and long-term performance testing.

- *PCM-layer incorporated in building components:* in building applications, PCMs can be added as a separate layer within the construction and can function in either a passive or active mode. This method allows for the integration of a significant amount of PCM without compromising the mechanical integrity of structural components. One of its major advantages is the flexibility to introduce thermal energy storage without altering the building's load-bearing properties.

Researchers explored this strategy by simulating the performance of PCM boards embedded within walls under five different climate zones in China using the EnergyPlus modeling tool. Their analysis focused on energy savings and CO_2 emission reductions, accounting for both PCM type

and thickness. The results showed that PCM integration in warm-climate buildings could reduce wall-related energy consumption by 6 % and CO_2 emissions by about 1 %. Importantly, the positioning of the PCM layer made a noticeable difference placing the PCM inside the insulation layer resulted in an additional 1 % to 7 % energy savings compared to placing it on the outside of the insulation [70]. Moreover, in regions with hot and extreme climates, increasing the thickness of the PCM layer contributed to an additional 2 % to 6 % reduction in energy use. Further exploring the benefits of layered PCM systems, another study conducted a numerical simulation of a dual-layer PCM wall system under five different climatic conditions in Iran. In their model, PCMs with different melting points were arranged in sequence, with the lower melting temperature PCM placed closest to the interior. Using EnergyPlus, the study found that this approach extended the thermal comfort period from 63 % to 75 % in semi-arid winter climates, and from 73 % to 93 % in dry climates [71]. The research group introduced a hybrid system combining a perlite-based composite PCM wallboard and a solar heating system connected through capillary tubes. Installed within the interior wall of a test room, as illustrated in Fig. 1.8, this setup was evaluated over three winter days in Tianjin, China. Compared to a reference room without PCM, the hybrid system reduced daily heating energy consumption by 44.16 %. The study concluded that such hybrid systems not only significantly improve energy efficiency, but also help to maintain indoor thermal comfort during the heating season [72].

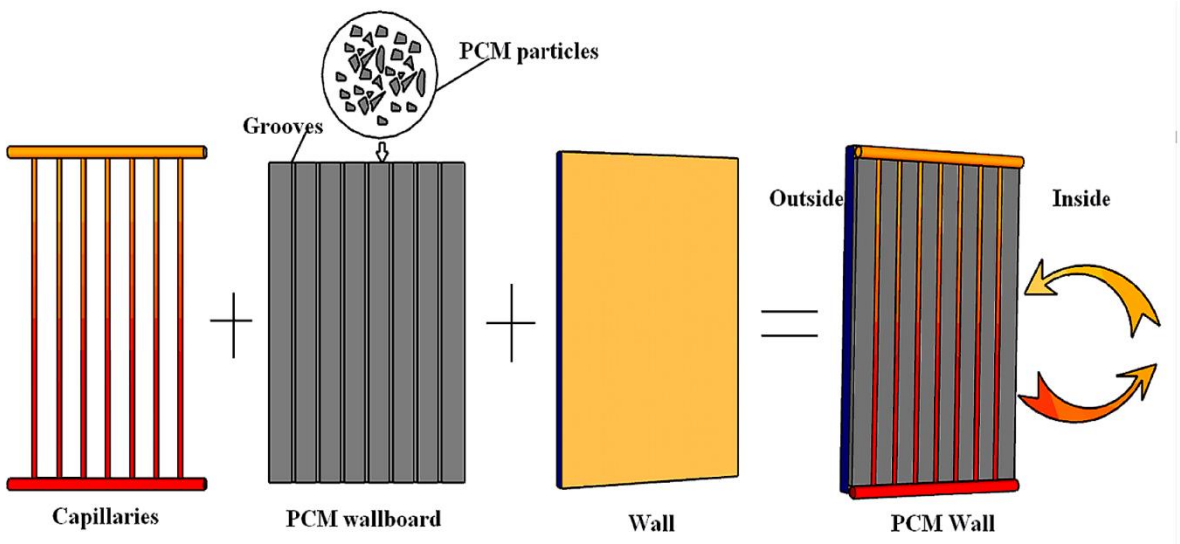

***Fig. 1.8**: Proposed hybrid PCM wall design* [72]

1.7. Outline of the Thesis

In Chapter 2, new insights are presented into the numerical modeling of PCMs for thermal energy storage. By simulating the melting behavior of RT-27 using ANSYS Fluent under realistic convective heating conditions, the chapter uncovers detailed thermal behavior patterns such as the transition from conduction to convection-dominated heat transfer. The results validate the effectiveness of CFD tools in capturing the complex phase change dynamics, offering a precise

framework for PCM design in energy-efficient buildings. In Chapter 3, original findings emerge from a comprehensive parametric optimization of PCM integration into building envelopes. By evaluating different positions, thicknesses, and melting temperatures of PCM layers, the study identifies optimal configurations that significantly reduce heat transfer. The results not only demonstrate the sensitivity of thermal performance to these parameters, but also establish a practical methodology for customizing PCM use based on local climatic conditions, with a focus on buildings in Miskolc, Hungary. In Chapter 4, the research breaks new ground by systematically evaluating the thermal impact of various PCM capsule geometries (cuboid, cylindrical, and prismatic) within building materials. The simulations reveal that capsule shape plays a critical role in heat storage and release efficiency. Novel insights are provided into how geometry affects phase transition rates and overall energy performance, guiding the future design of encapsulated PCM systems for optimal building integration. In Chapter 5, the thesis introduces a novel integration of PCMs into traditional Flemish bond brick walls (architectural method) previously underexplored from a thermal efficiency perspective. The study reveals that Flemish bond structures alone can reduce heat transfer by 6 %, and when combined with PCM, the reduction improves to 21 %. These results highlight a pioneering approach that fuses historical building techniques with cutting-edge energy storage materials, advancing sustainable construction while preserving architectural aesthetics.

2. MODELING AND SIMULATION OF PHASE CHANGE MATERIALS IN BUILDING ENVELOPES

In this chapter, PCMs are examined for their critical role in thermal energy storage systems. The chapter focuses on numerical modeling of PCMs, with particular emphasis on using ANSYS Fluent to simulate the melting process. The primary objective is to model the thermal behavior of RT-27 PCM under convective heating conditions using computational fluid dynamics (CFD). The simulation captures the shift from conduction-dominated heat transfer in the early stages to natural convection as the melting progresses. Key variables analyzed include temperature distribution, liquid fraction, density variation, and velocity fields over time. Through this numerical study, the chapter demonstrates that CFD is a reliable and accurate tool for simulating phase change processes and for optimizing the design of PCM-based thermal energy storage systems in building applications.

2.1. Overview of PCM Thermal Modeling

Numerous studies have investigated heat transfer mechanisms in PCMs integrated into building envelopes. These investigations often involve analytical models, numerical simulations, and CFD to capture the complex thermal behavior of PCMs. CFD has proven particularly valuable in advancing the engineering design of thermal energy storage systems, offering a powerful toolset for performance analysis and system optimization. By simulating the detailed flow and thermal fields, CFD enables designers to enhance energy efficiency while also reducing development time and costs through virtual prototyping.

The thermal behavior of PCMs during a phase transition also referred to as a phase change, is typically described using a partial differential equation (PDE). This equation can be solved either analytically or numerically, depending on the complexity of the system. However, analytical solutions are often limited due to the presence of nonlinear phase front interfaces, irregular geometries, and non-standard boundary conditions. Only a few simplified one-dimensional (1D) models have been analytically solved, and these are generally restricted to basic geometries and uniform conditions. The nonlinearity introduced by the moving phase boundary, which is influenced by the latent heat absorbed or released at the interface, presents a significant challenge in numerical modeling as well.

Despite these difficulties, two main approaches are commonly used to analyze heat transfer in solid-liquid PCM systems.

- *The enthalpy-based method* is one of the most widely used approaches for modeling phase change in PCMs, primarily because it does not require explicit tracking of the solid-liquid interface. In this method, the latent heat associated with the phase transition is incorporated directly into the energy equation through a total enthalpy term. One of the main advantages of this formulation is that it eliminates the need to define boundary conditions at the phase interface, allowing the model to handle the transition more flexibly.

The governing equation can be determined by Eq. (2.1), which remains mathematically similar to that of a single-phase system, which simplifies the computational process. Phase change occurs within a defined mushy zone (a region in which both solid and liquid phases coexist) resulting in a smoother, more realistic transition between states. The total enthalpy includes both sensible and latent heat, where the latent component is determined by the product of the liquid fraction and the latent heat of fusion. The liquid fraction varies continuously from zero to one, depending on the temperature range between the solidus and liquidus points.

$$\frac{\partial}{\partial t}(\rho H) + \nabla.(\rho v H) = (k \nabla T) + S, \qquad (2.1)$$

where H [J/ kg] is the enthalpy of the material, ρ [kg/ m^3] is the density of the material, T [°C] is the temperature, k [W/mK] is the thermal conductivity, v [m/s] is the velocity of the fluid, S is the source term.

This method offers a convenient and stable framework for simulating the thermal behavior of PCMs, particularly in complex systems where interface tracking and non-linear boundary conditions can complicate traditional numerical approaches. As a result, it has become a preferred strategy in computational modeling of PCM-integrated building components.

- *The temperature-based method:* approaches phase-change modeling by using temperature as the individual dependent variable. In this formulation, the solid-liquid interface can be explicitly tracked, allowing for the energy conservation equations to be defined separately for the solid and liquid phases. This separation provides a more precise description of the thermal behavior during the phase transition.

By independently solving the energy equations for each phase, this method enables accurate determination of the phase boundary location and heat transfer characteristics. Such precision makes the temperature-based approach particularly suitable for problems where interface tracking is critical. The mathematical representation of this method is typically described by Eq. (2.2), which governs the energy conservation in each phase domain.

$$\frac{\partial T_S}{\partial n}.k_s = \frac{\partial T_L}{\partial n}.k_L + \rho.H.k.v_n\,, \qquad (2.2)$$

where T_S [°C] is the solidus temperatures of PCM, T_L [°C] is the liquids temperature of PCM, k_s [W/mK] is the thermal conductivity of solid phase, k_L [W/mK] is the thermal conductivity of liquid phase, n is the unit normal vector to the interface, v_n is the normal component of the velocity of the interface, H [J/kg] is the enthalpy of material.

2.2. CFD Analysis

In recent years, a variety of modeling and simulation techniques have been employed to evaluate the thermal performance of PCMs and the energy savings achieved through their integration into building components. These methods range from laboratory-scale experiments used to validate simulation tools to whole-building simulations that assess real-world performance. To model PCM behavior accurately, researchers frequently rely on several well-established computational tools, including EnergyPlus [70], ANSYS Fluent [73], COMSOL Multiphysics [74], TRYNSYS [75], MATLAB software [76], ABAQUSTM solver [77] DIANA-finite element analysis [78].

Most researchers use the building component as a 1D convection, an unsteady state without an internal heat source, to model the heat behavior of PCM-incorporated buildings. However, Eq. (2.3) [79], can be used to determine the thermal behavior of the composite wall that contains the PCM layer.

$$\frac{\partial T}{\partial t} = \alpha \frac{\partial^2 T}{\partial x^2}, \tag{2.3}$$

where T [°C] is the temperature of the element, t [s] is the time, x [m] is the element thickness, and α [m^2/s] is the thermal diffusivity [ratio of the material thermal conductivity to its density and specific heat ($k/\rho\, c$)]. Eq. (2.3) can be changed to Eq. (2.4) [80], to account for the PCM melting and solidification processes.

$$\frac{\partial T}{\partial t} = \alpha \frac{\partial^2 T}{\partial x^2} - \frac{L_H}{C_p}\frac{\partial f}{\partial t}, \tag{2.4}$$

where L_H [kJ] is the latent heat of fusion, C_p [kJ/kgK] is the specific heat at constant pressure, and f is the liquid fraction (ratio of the melted PCM during phase transition).

The liquid fraction ranges from 0 to 1, as shown in Eq. (2.5)

$$f = \begin{cases} 0 & if\ T < T_S(Solidification) \\ \dfrac{T - T_S}{T_L - T_S} & if\ T_S < T < T_L(Mushy\ zone) \\ 1 & if\ T > T_L(Melting) \end{cases}, \tag{2.5}$$

where T_L [°C] is the liquidus temperature of PCM and T_S [°C] is the solidus temperature of PCM.

Eq. (2.4) is provided as a simplified formulation commonly used in wall heat-conduction models, where latent heat is represented through the liquid fraction f. In this dissertation, Eq. (2.4) is not solved directly. Instead, the numerical simulations are performed in ANSYS Fluent using the enthalpy-porosity melting/solidification model as we will see next.

Engineering challenges related to phase change phenomena have been successfully addressed using the Fluent module in ANSYS Workbench [81], which includes a dedicated model capable of simulating a wide range of melting and solidification scenarios. This tool can resolve phase transitions that occur either over a specific temperature range or at a single melting point, making

it suitable for various PCM-related applications. The modeling process begins with a geometric definition and meshing of physical problems using ANSYS's mesh generation tools. Once the geometry is meshed, boundary layers and zone types are specified. The mesh is then exported to Fluent Solver, where simulations are carried out. To ensure that the results are numerically stable and grid-independent, simulations are typically run with various grid sizes and time step values. While finer grids and smaller time steps generally yield more accurate results, they are also favored for faster computational convergence in transient simulations. ANSYS Fluent employs the enthalpy-porosity method to simulate melting and solidification processes, as illustrated in Fig. 2.1.

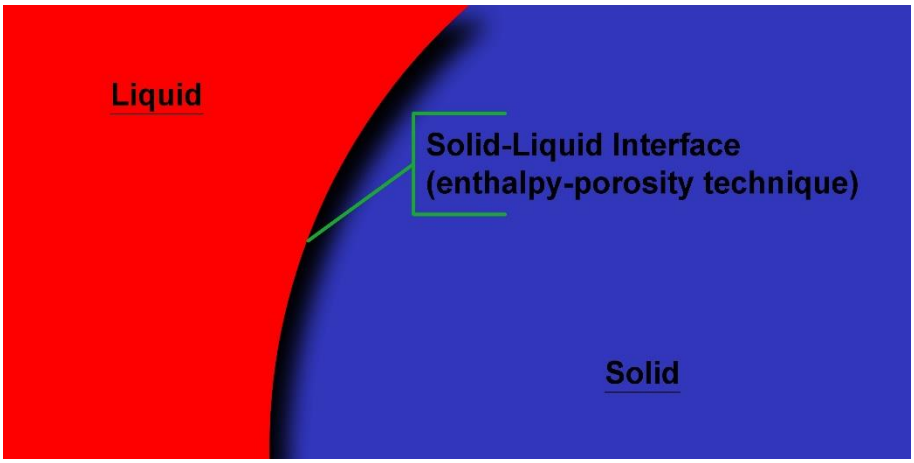

Fig. 2.1: *Enthalpy porosity method*

This method does not explicitly track the moving phase boundary. Instead, it assigns a liquid fraction to each cell in the PCM domain, representing the volume percentage of liquid in that cell. This fraction is calculated iteratively using the enthalpy balance equation. The liquid fraction ranges from 0 to 1, with 0 indicating a fully solid state and 1 indicating a fully liquid state. The phase transition region is modeled as a mushy zone. Within this mushy zone, the porosity decreases continuously from 1 to 0, mimicking the behavior of a pseudo-porous medium [82]. As solidification progresses, both porosity and velocity in the affected cells drop to zero, reflecting the cessation of fluid motion in the solid phase.

The energy equation is written as it is shown in Eq. (2.6).

$$\frac{\partial}{\partial t}(\rho H) + \nabla.(\rho v H) = (k \nabla T) + S\,, \qquad (2.6)$$

where H [J/ kg] is the enthalpy of the material, ρ [kg/ m^3] is the density of the material, T [°C] is the temperature, k [W/mK] is the thermal conductivity, v [m/s] is the velocity of the fluid, S is the source term. The sum of the sensible heat and the latent heat is employed to calculate the material's enthalpy [82].

$$H = h + \Delta H\,, \qquad (2.7)$$

where h [J/kg] is the sensible heat, ΔH [J/kg] is the latent heat content, where:

$$h = h_{ref} + \int_{T_{ref}}^{T} C_p \times dT, \qquad (2.8)$$

where h_{ref} [J/kg] is the reference enthalpy, T_{ref} [°C] is the reference temperature, C_p [J/kg°C] is the specific heat at a constant pressure of PCM.

The latent heat content can be written in terms of the latent heat of material as shown in Eq. (2.8).

$$\Delta H = f \times L\,, \qquad (2.9)$$

the latent heat content can vary between zero (for a solid) and L (for a liquid).

The momentum equation is written as it is shown in Eq. (2.10).

$$\rho\left(\frac{\partial v}{\partial t} + v.\nabla v\right) = -\nabla p + \mu\nabla^2 v + \rho g + S\,, \qquad (2.10)$$

where ρ [kg/m^3] is the density, p [Pa] is the pressure, μ [Pa.s] is the dynamic viscosity, ρg is the buoyancy.

PCM density was specified as a temperature-dependent property using a piecewise-linear function in ANSYS Fluent. So the continuity equation is written as it is shown in Eq. (2.11).

$$\frac{\partial \rho}{\partial t} + \nabla.(\rho v) = 0\,, \qquad (2.11)$$

The Fluent software offers two primary solver types: the pressure-based solver and the coupled density-based solver. For simulating melting and solidification problems, only the pressure-based solver is applicable, as illustrated in Fig. 2.2.

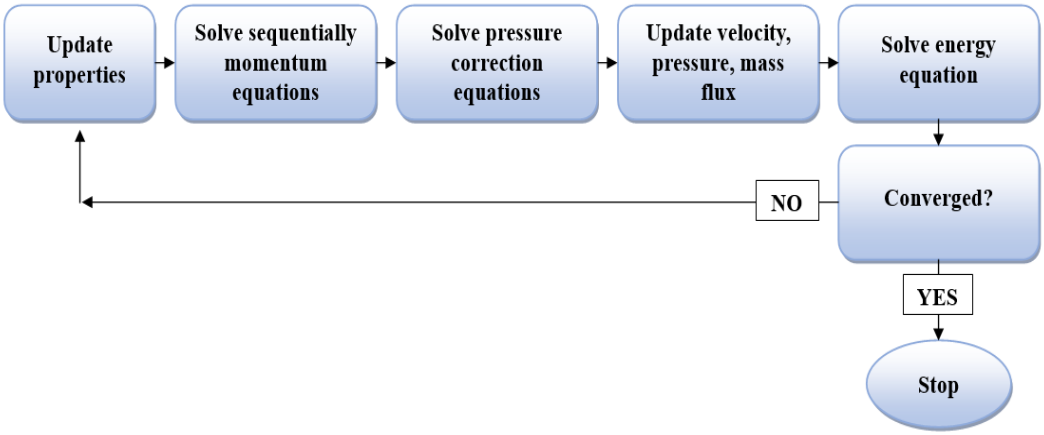

Fig. 2.2: *Pressure-based flow chart*

To handle convection terms during simulation, Fluent provides several discretization schemes. Among these, the first-order upwind, power law, and second-order upwind methods are most commonly used in phase change applications. An overview of the complete solution strategy, including the flow of steps from initialization to convergence, is presented in Fig. 2.3. Additional details on solver settings, initialization procedures, and discretization techniques are provided in [81].

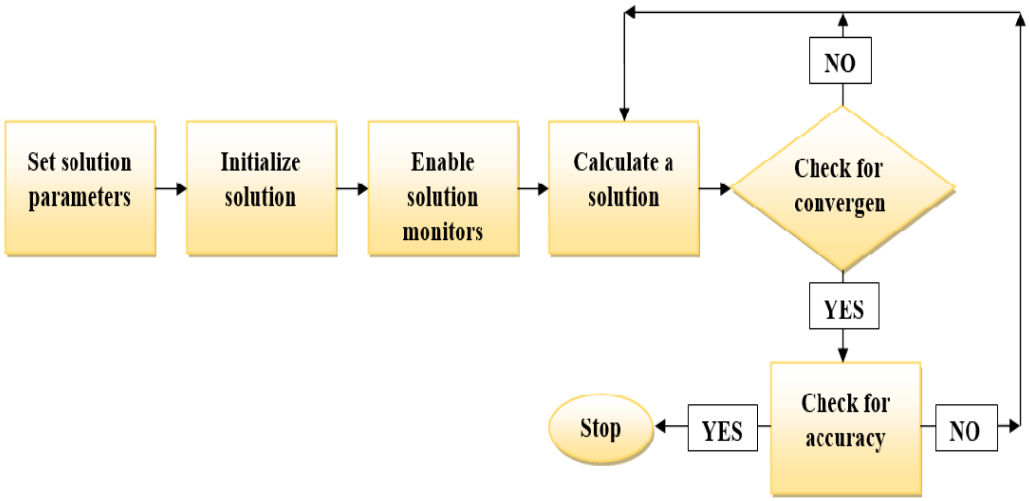

Fig. 2.3: *Fluent solution flow chart*

In phase change simulations, the thermophysical properties of materials (such as density, thermal conductivity, specific heat capacity, and viscosity) may vary with temperature or depend on the material's chemical composition. Fluent accommodates this by allowing these properties to be defined in several ways: as constant values, as temperature-dependent functions (using polynomial, piecewise-linear, or piecewise-polynomial formats), or through User-Defined Functions (UDFs) written in custom code to describe complex behaviors.

In the case of PCMs, properties like density and viscosity are often modeled as temperature-dependent, governed by empirical or semi-empirical correlations. Accurately capturing these variations is essential for reliable modeling of phase change processes, particularly in systems where the transition occurs over a temperature range or where fluid flow significantly affects thermal performance.

2.3. Physical and Numerical Model

The melting process of the PCM was simulated using the melting and solidification model available in ANSYS Fluent. This model is based on the enthalpy-porosity method, which is widely used for representing phase change phenomena in computational simulations. The approach allows for the phase transition to occur within a mushy zone and eliminates the need for explicit tracking of the solid-liquid interface.

2.3.1. Physical model

In this study, an organic PCM known as RT-27, produced by Rubitherm GmbH, was selected for the simulations. RT-27 is well-suited for thermal storage applications due to its stable thermal characteristics and moderate melting temperature. The thermophysical properties of RT-27 used in the simulation are summarized in Table 2.1.

Table 2.1: *Thermophysical properties of RT-27, based on Rubitherm GmbH* [83]

Property	Phase	Value
Density [kg/m^3]	solid phase	880 at 15 [°C]
	liquid phase	760 at 40 [°C]
Dynamic viscosity [N.s/m^2]	liquid phase	0.02
Specific heat [J/kgK]	both phases	2000
Thermal conductivity [W/mK]	both phases	0.2
Latent heat [J/kg]	-	189000
Solidus temperature [°C]	-	24.5
Liquidus temperature [°C]	-	26.5

2.3.2. Model Characterization and Mesh Generation

The geometric model used for simulating the PCM zone is shown in Fig. 2.4. The model consists of a two-dimensional rectangular domain, measuring 10 [mm] in width and 200 [mm] in height, which represents the region occupied by the PCM.

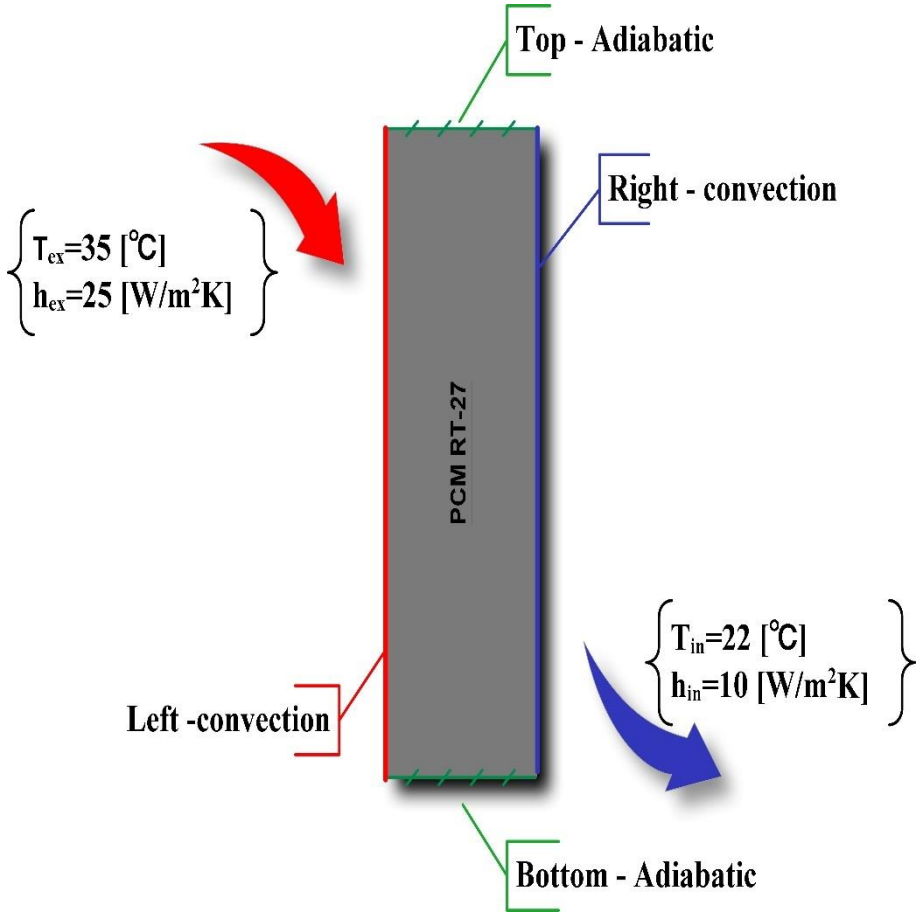

Fig. 2.4: *Schematic of the model*

The boundary conditions for the PCM simulation domain are defined as follows: The top and bottom surfaces of the PCM zone are treated as adiabatic, meaning there is no heat flux across these boundaries q=0 [W/m^2]. The left boundary is exposed to an external convective environment, characterized by a heat transfer coefficient of h_{ex}=25 [W/m^{2}K] and an ambient temperature of T_{ex}=35 [°C]. On the right boundary, convection is also applied, but with a lower heat transfer coefficient of h_{in}=10 [W/m^{2}K] and an internal air temperature of T_{in}=22 [°C]. These conditions are used to simulate the thermal behavior of the PCM as it undergoes a phase transition under different heating and cooling effects from either side. The simulations were conducted using ANSYS Fluent, which solves the governing equations using the finite volume method. An important part of the pre-processing stage is selecting an appropriate mesh size to ensure solution accuracy and numerical stability. As illustrated in Fig. 2.5, the meshed model consists of 12,375 elements and 12,616 nodes.

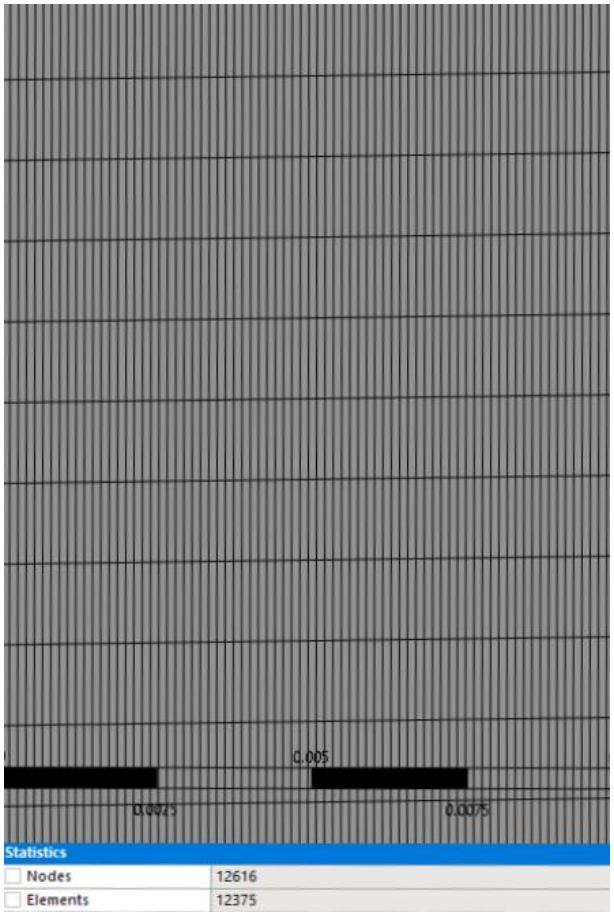

Fig. 2.5: *Schematic of the meshed PCM zone*

2.3.3. Assumptions and Simulation Description

The numerical modeling was carried out under the following assumptions:

- The melting process is transient and modeled in two dimensions.
- The flow of PCM in its liquid phase is considered incompressible, non-Newtonian, and turbulent.

- The PCM exhibits a piecewise linear variation in density during the phase transition.
- There is no internal heat generation within the PCM domain.

For the numerical solution, the second-order upwind scheme was employed to discretize the momentum equations, while the first-order upwind scheme was used for the energy equation. The SIMPLE algorithm was used to couple pressure and velocity, and PRESTO was applied for pressure interpolation. All simulations were conducted using the standard solver in ANSYS Fluent. Convergence criteria for the continuity, momentum, and energy equations were set to residuals of 10^{-5}, 10^{-8}, and 10^{-10}, respectively. A time step of 0.1 seconds was used, with 10 iterations performed at each time step to ensure solution accuracy and temporal stability.

2.4. Numerical Results

A numerical analysis was performed to investigate the melting behavior of RT-27 within a rectangular domain measuring 10 [mm] in width and 200 [mm] in height. The PCM was subjected to convective heating from the left and right boundaries, while the top and bottom boundaries were treated as adiabatic. This configuration replicates a simplified building envelope condition to observe heat transfer during phase change.

The simulation was conducted over a 360 [min] melting cycle, with results recorded at 30 [min] intervals to track the transient thermal response of the PCM. The findings are presented through contour plots showing the spatial distribution of key physical parameters, including liquid fraction, temperature, density, and velocity, at selected time steps throughout the simulation.

The following results, as well as the numerical model conducted for this study, were thoroughly validated through comparison with established numerical and experimental research found in the literature [73, 84-86]. Several previously published studies reported similar trends in melting behavior, including the initiation of phase change at the heated boundary, the evolution of the liquid fraction over time, and the influence of natural convection on the melting front. The strong agreement between the present findings and those of earlier investigations provides confidence in the accuracy, consistency, and reliability of the simulation approach and modeling assumptions adopted in this work.

2.4.1. Liquid-Fraction Contours

The evolution of the liquid fraction during the melting process is illustrated in Fig. 2.6, where the progression of the phase-change front over time is visible. In these contour plots, red regions represent fully liquid PCM (liquid-fraction f=1), while blue areas indicate fully solid PCM (f=0). The transition zone between these extremes is referred to as the mushy zone, where both solid and liquid phases coexist. This zone represents the moving melting front. At the early stage of melting, particularly within the first 30 [min], the melting interface remains nearly parallel to the left wall, suggesting that heat conduction is the dominant mode of heat transfer. As the process continues and reaches 60 [min], the melted PCM, having a higher temperature and lower density, begins to rise due to buoyancy effects and creates circulation patterns that enhance convective heat transfer.

This behavior leads to a more dynamic interface, with the top of the PCM chamber melting within the first 60 [min] and approximately half of the PCM volume transitioning to the liquid phase by 90 [min].

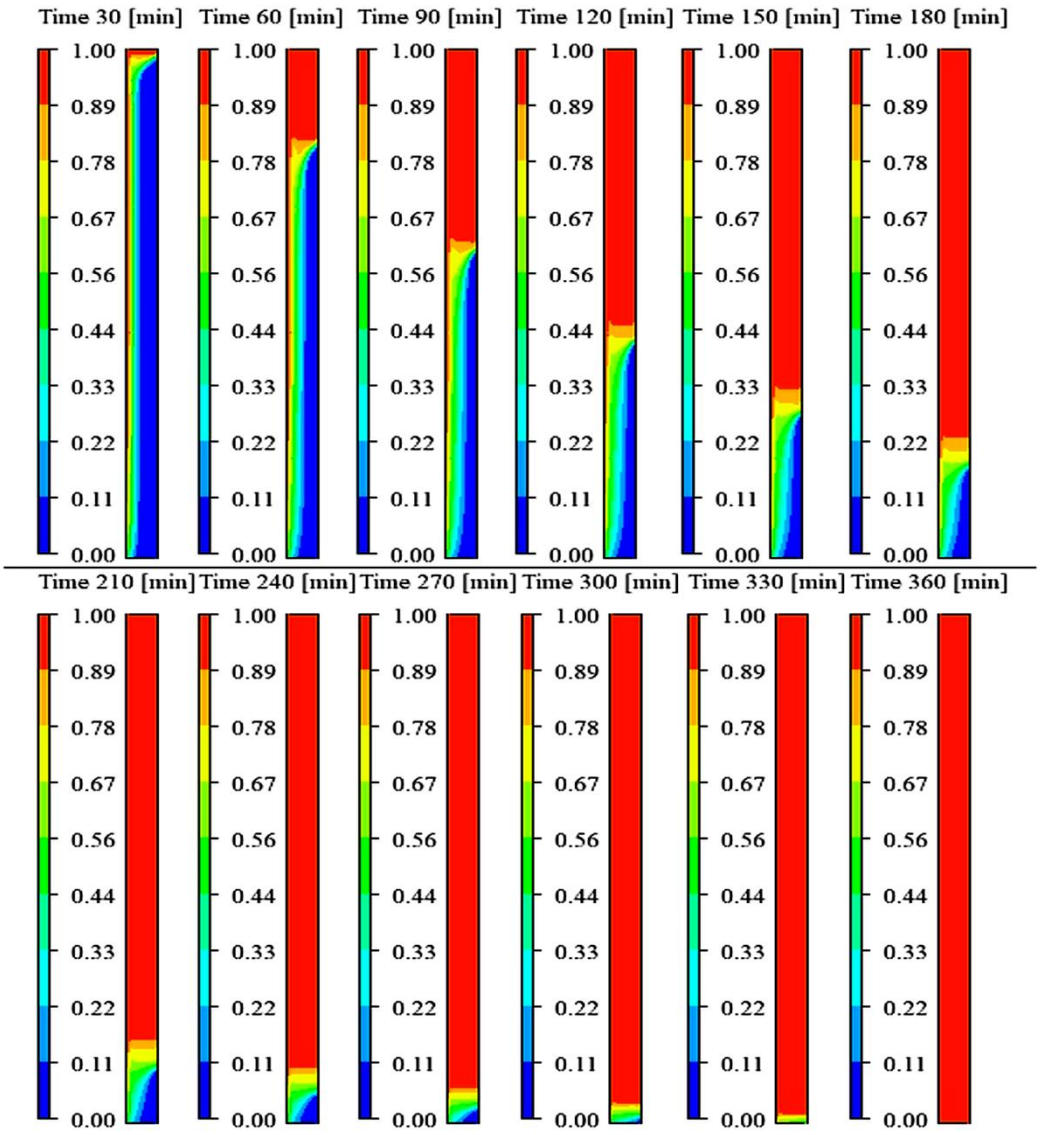

Fig. 2.6: *Liquid-fraction contours*

The change in the overall melting fraction over time is presented in Fig. 2.7. At the beginning of the simulation t=0 [min], the PCM is entirely in a solid state, corresponding to a melting fraction of 0 %. As the simulation progresses, the melting fraction increases steadily due to the continuous heat input. At 30 [min], the melting fraction reaches 23%, increasing to 42 % at 60 [min] and 57 % at 90 [min]. By 120 [min], it rises to 69 % and continues to increase to 78 % at 150 [min], 85 % at 180 [min], and 90 % at 210 [min]. Further heating results in 93 % melting at 240 [min], 96 % at 270 [min], 98 % at 300 [min], 99 % at 330 [min], and finally, full melting is achieved at 360 [min] with a melting fraction of 100 %.

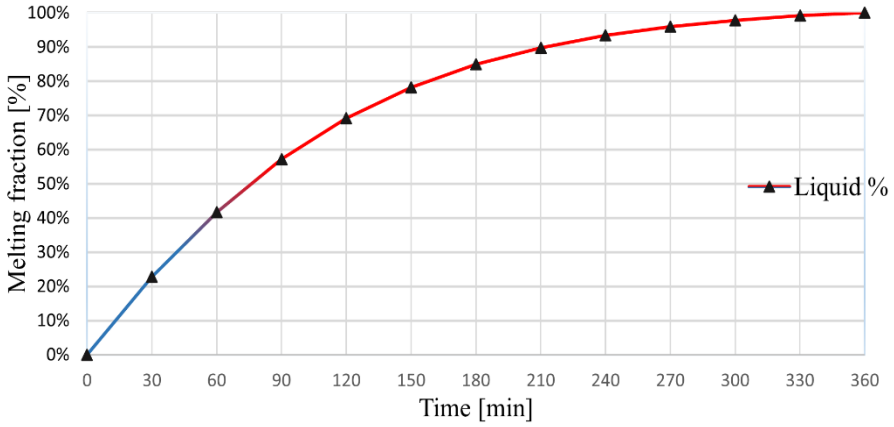

Fig. 2.7: *Melting fraction changing over time*

2.4.2. Temperature Contours

The temperature distribution within the PCM domain and its evolution over time is presented in Fig. 2.8, with contour plots shown at regular 30 [min] intervals throughout the 360 [min] simulation. At the beginning, middle, and end of the melting process, the maximum recorded temperatures were approximately 27.5 [°C], 32.7 [°C], and 33.4 [°C], respectively. As indicated by the comparison between Figs. 2.6 and 2.8, melting begins when the local temperature reaches approximately 24.5 [°C], which corresponds to the onset of phase transition for RT-27.

In the contour plots, blue regions represent low-temperature zones, which largely coincide with the solid phase of the PCM, as confirmed by the liquid fraction distributions in Fig. 2.6. After around 60 [min], a distinct red zone begins to emerge near the left wall, indicating localized regions of higher temperature. This zone continues to expand as a result of convective currents and turbulence within the liquid PCM, which promotes heat transfer deeper into the material. By the end of the simulation, at 360 [min], the entire PCM domain has transitioned into the liquid phase. As a result, the temperature field becomes more uniform, with clearly defined isothermal zones. This occurs because once the melting is complete and the PCM is fully liquid, the thermal properties stabilize, and the heat distribution tends to equalize, as visually evident in the final contour of Fig. 2.8.

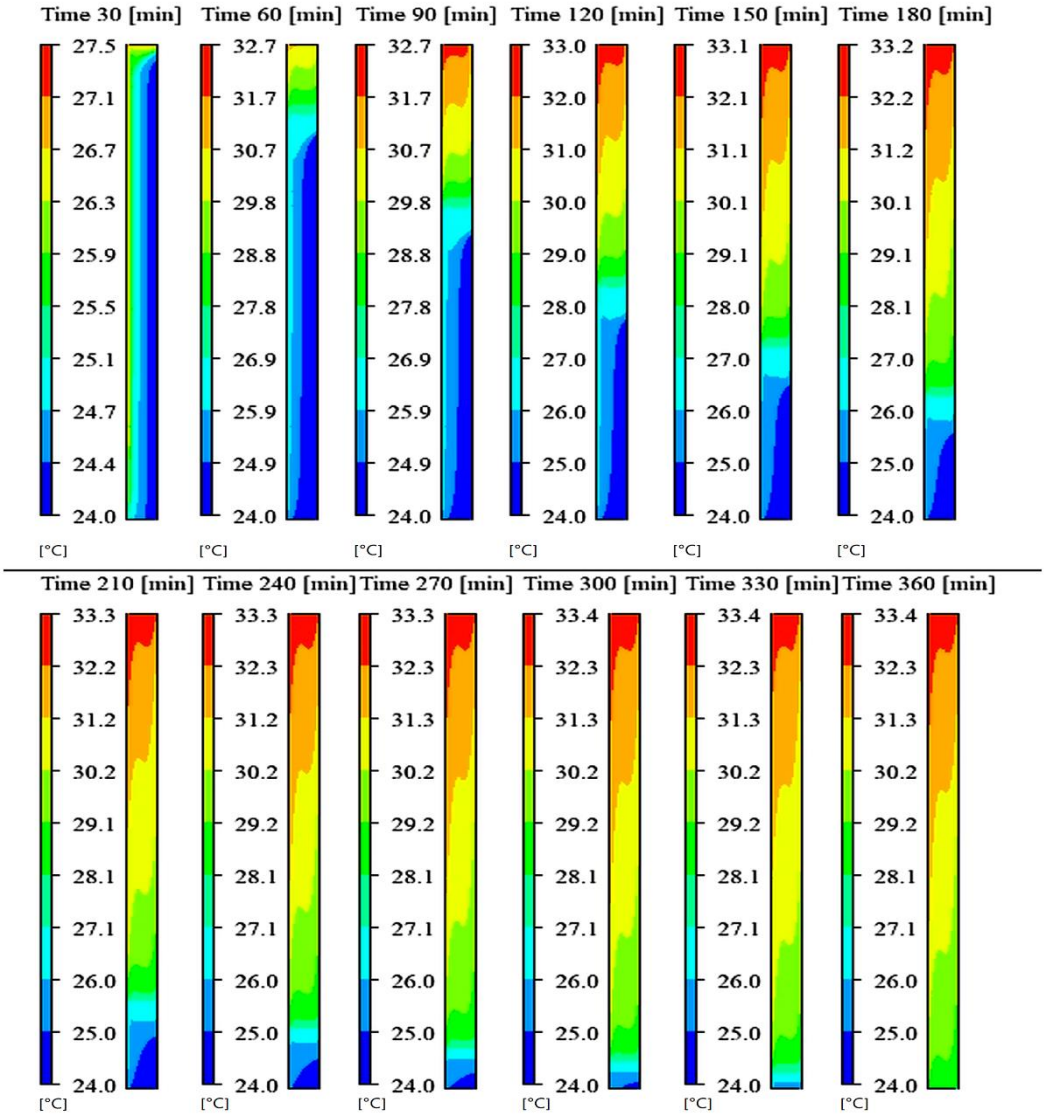

Fig. 2.8: *Temperature contours*

2.4.3. Density Contours

The evolution of density contours within the PCM domain over time is illustrated in Fig. 2.9, with results displayed at 30 [min] intervals throughout the melting process. As PCM undergoes heating, its density decreases with rising temperature, reflecting the inherent temperature-dependent behavior of the material. As a result, the less dense, warmer PCM tends to rise toward the upper region of the domain due to buoyancy forces, creating a distinct zone of low-density fluid, which is represented in blue in the contour plots. This vertical density stratification becomes more pronounced as the phase transition progresses, with continuous circulation reinforcing the accumulation of lower-density PCM in the upper layers. Toward the end of the melting process, the entire PCM domain reaches a thermally uniform liquid state, and the density distribution

stabilizes. At the final simulation time of 360 [min], the PCM's density becomes constant across the domain, reaching approximately 780 [kg/m^3], which corresponds to the fully melted phase.

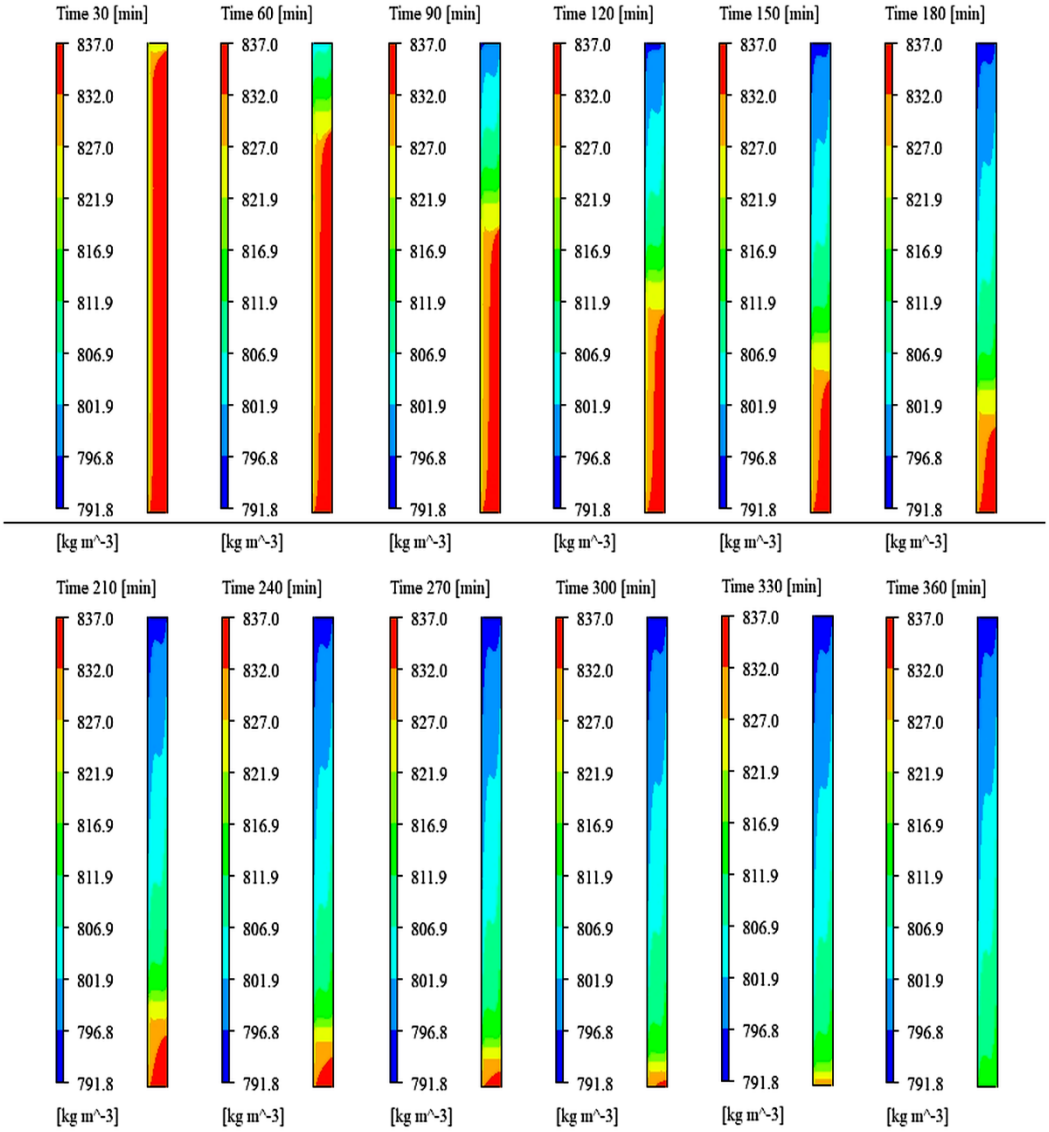

Fig. 2.9: *Density contours*

2.4.4. Velocity Contours

The velocity contours and their temporal evolution throughout the melting process are presented in Fig. 2.10, with intervals taken at 30 [min]. The regions of the highest fluid velocity, indicated in orange, are primarily located near the left and right boundaries of the PCM domain. These zones correspond to areas of intense thermal gradients and rising liquid PCM, where buoyant flow is most active due to localized heating. As the melting progresses and the PCM transitions entirely into the liquid phase, the temperature and density within the domain begin to stabilize. Once PCM is fully melted, the thermal gradients diminish significantly, resulting in the elimination of buoyancy-driven flow. Consequently, at the end of the melting cycle 360 [min], the

fluid motion ceases, and the velocity across the entire domain approaches very low value, indicating that the PCM has reached a quasi-steady state.

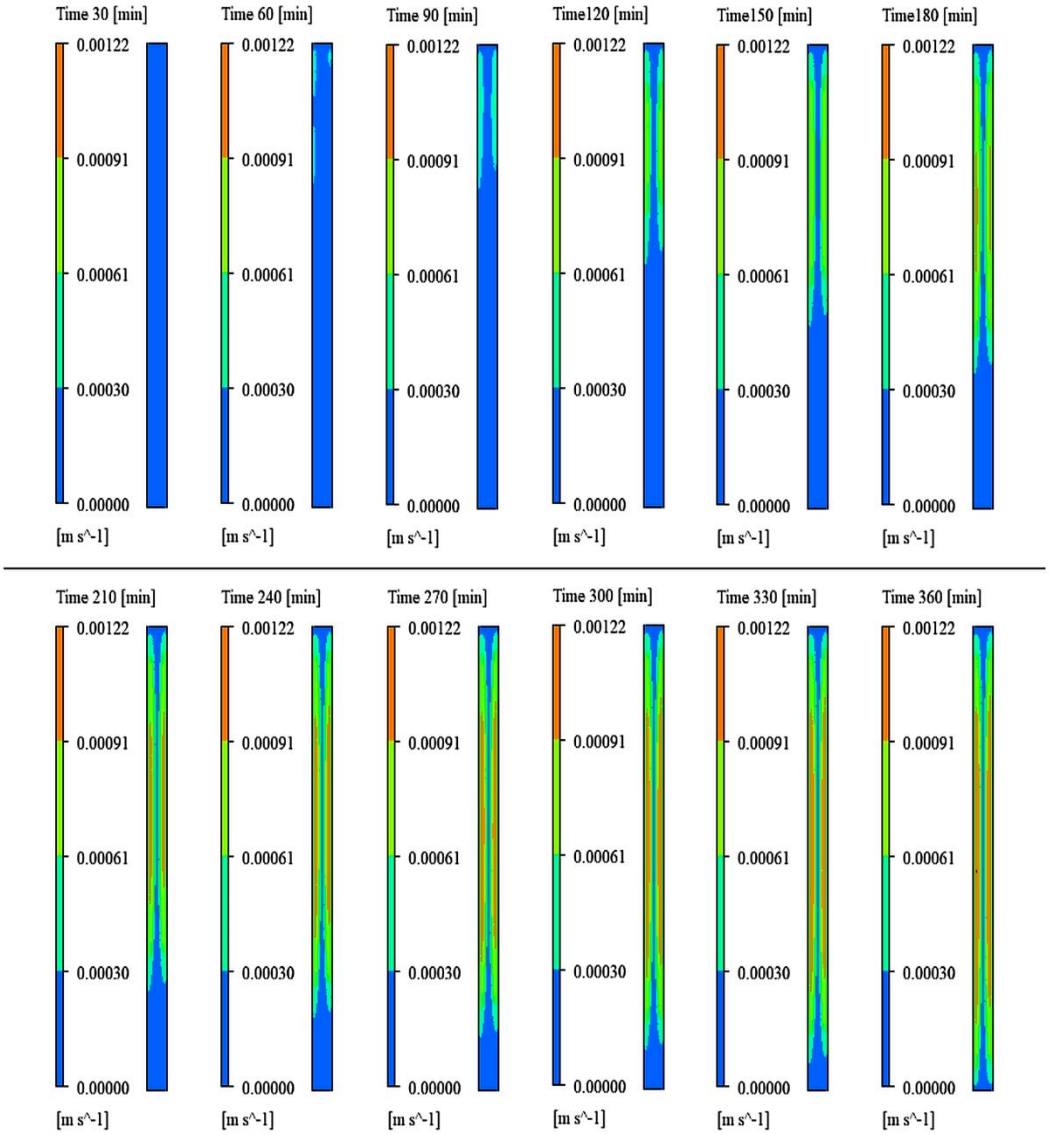

Fig. 2.10: *Velocity contours*

2.5. Summary of This Chapter

This chapter has provided a detailed exploration of PCMs used in thermal energy storage applications, focusing particularly on their classification, thermal characteristics, and methods of numerical simulation. A central theme of the chapter was the implementation of CFD specifically, the use of ANSYS Fluent software as a powerful and practical tool for modeling PCM behavior under various thermal conditions. The chapter outlined how CFD not only delivers highly accurate simulations of transient thermal processes, but also offers engineers and researchers effective means for design optimization, cost reduction, and efficiency improvement in latent heat storage (LHS) systems.

The chapter began with an overview of PCM thermal modeling and a significant portion of the chapter was dedicated to modeling and simulation of PCM melting behavior using ANSYS Fluent. The enthalpy-porosity method was introduced as the foundation for simulating the phase transition, where the melting front is represented as a mushy zone without requiring explicit tracking. The melting process of RT-27, an organic PCM, was analyzed in a vertically oriented rectangular domain under convective heating conditions. The study employed fine meshing and carefully selected time steps to ensure numerical stability, emphasizing the importance of pre-processing and solver settings in transient heat transfer simulations. The simulation results revealed distinct thermal and dynamic patterns throughout the melting cycle. During the initial 0-30 [min], heat transfer occurred predominantly by conduction, as the thermal energy gradually penetrated the solid PCM. As the temperature increased and part of the PCM entered the liquid phase, natural convection began to dominate, accelerating the melting rate, particularly in the middle and later stages of the process. A clear density gradient developed due to temperature differences, leading to buoyancy-driven flow that enhanced the thermal mixing within the PCM zone. Furthermore, it was observed that melting begins at the top of the domain and proceeds downward, a behavior attributed to the vertical orientation of the heating and the nature of the PCM's density change with temperature. As the melting progressed, velocity contours confirmed the presence of convective cells near the walls, which gradually dissipated as the PCM fully liquefied. By the end of the 360 [min] cycle, the entire domain had reached a thermally stable state, with uniform temperature and density distributions and very low velocity (quasi-steady).

The chapter concludes by affirming that ANSYS Fluent is a capable and reliable platform for simulating PCM-based thermal storage systems. However, the successful application depends on several key factors, including accurate material properties, appropriate meshing strategies, time step management, and the correct implementation of boundary conditions. The findings of this study not only validate the simulation methodology through comparison with existing literature, but also provide practical guidance for future modeling efforts involving PCM integration into energy-efficient building systems.

3. OPTIMIZATION OF PARAMETERS INFLUENCING PCM PERFORMANCE INTEGRATED IN BUILDING ENVELOPES

In this chapter, a detailed parametric investigation was conducted to evaluate and optimize the key factors that influence the thermal performance of PCMs when integrated into building envelopes. Integrating PCMs into construction layers helps to maintain thermal comfort during hot summer days. However, the efficacy of PCM-based systems is highly dependent on several design parameters, the position of the PCM layer, its thickness, and its melting temperature. If not carefully considered, these variables can limit the intended thermal storage and regulatory performance of PCM systems. Therefore, this chapter is dedicated to analyzing and optimizing these critical parameters to ensure maximum energy efficiency and effective heat management.

This chapter focuses on a building envelope typical of Miskolc, Hungary, which consists of 3 [cm] cement, 15 [cm] brick, and 2 [cm] plaster layers. Using this configuration as a reference model, the research aims to answer a key question: To what extent do PCM position, thickness, and melting temperature influence the reduction of heat transfer through the wall? Through numerical simulations using ANSYS Fluent, the study examines how variations in these parameters affect the building's thermal behavior under local climatic conditions.

PCMs, when combined with passive latent heat thermal energy storage, offer a promising solution to address the growing energy demands of modern buildings. The results of this investigation show that melting temperature and enthalpy are particularly influential in determining the PCMs effectiveness. Furthermore, the findings reveal that it is possible to define an optimal PCM layer position within the wall assembly. This position is closely tied to both the thermal properties of the PCM and the environmental conditions it is exposed to. By identifying optimal parameter combinations, this chapter provides practical insights for enhancing the performance of PCM-integrated building envelopes, contributing to more energy-efficient and climate-responsive building design.

3.1. Model Characteristics

A visual representation of the simulated external wall assembly is presented in Fig. 3.1, reflecting the typical construction practices used in buildings located in Miskolc, Hungary, where this study is based. The wall model consists of three distinct layers: 3 [cm] of cement, 15 [cm] of brick, and 2 [cm] of plaster, resulting in a total wall thickness of 20 [cm], excluding any PCM layer. The height of the wall section used in the simulation is also 20 [cm]. The thermophysical

properties of the construction materials incorporated in the simulation are summarized in Table 3.1.

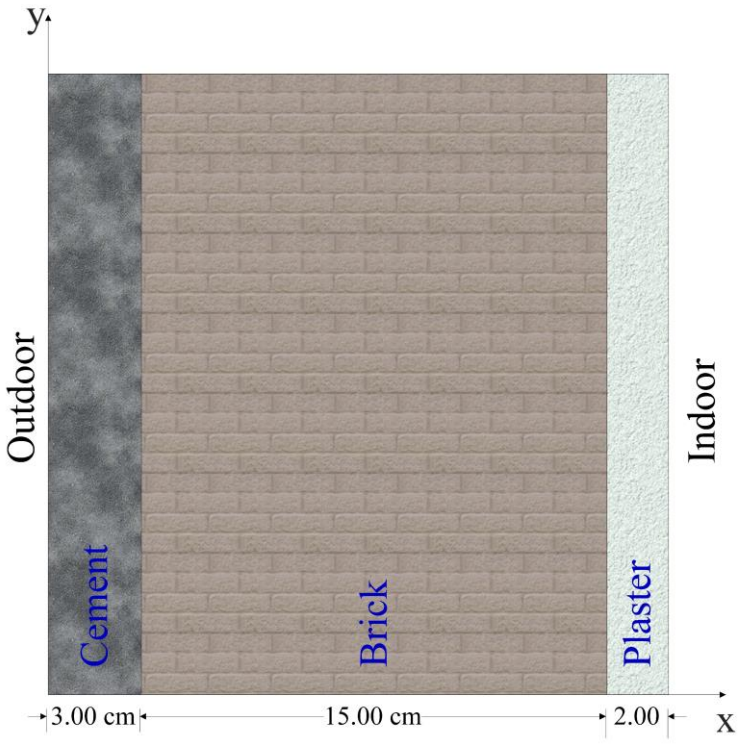

Fig. 3.1: *Wall schematic without PCM*

Table 3.1: *Properties of building envelope materials* [87]

Property	Cement	Brick	Plaster
Density [kg/m^3]	2300	1460	1680
Specific heat [J/kgK]	2000	880	1085
Thermal conductivity [W/mK]	1.4	1.3	0.22

To accurately simulate the PCM-integrated wall system, several assumptions were made to simplify and control the modeling process. First, it was assumed that the top and bottom surfaces of the wall were adequately insulated, thereby preventing any heat loss through those boundaries. Second, all layers of the wall assembly, including plaster, brick, cement, and the PCM were considered uniform in structure and thermophysical properties. Additionally, the convection effects within the liquid phase of the PCM were included in the model, while the PCM remained embedded in a solid matrix during phase transition.

To evaluate the influence of PCM thickness on thermal performance, PCM layers of 1 [cm], 3 [cm], and 5 [cm] were introduced into the wall envelope. Moreover, to assess the effect of layer position, the PCM was positioned in four different locations within the wall structure. The properties of the PCMs used in the simulation are detailed in Table 3.2.

Table 3.2: *Thermo-physical properties of PCM* [83]

Property	**Phase**	**Organic PCM**		**Inorganic PCM**	
		RT-27	RT-21	SP-25E2	SP-21EK
Density [kg/m^3]	Solid [°C]	880 at 15	880 at 15	1600 at 15	1600 at 15
	Liquid [°C]	760 at 40	770 at 25	1500 at 35	1500 at 35
Specific heat [J/kgK]	Both phases	2000	2000	2000	2000
Thermal conductivity [W/mK]	Both phases	0.2	0.2	0.5	0.5
Latent heat [J/kg]	-	189000	165000	180000	170000
Solidus temperature [°C]	-	24.5	19	24	20
Liquidus temperature [°C]	-	26.5	24	26	22

In this study, the indoor air temperature was maintained at a constant value of 22 [°C], representing a typical thermal comfort condition for occupants [88]. For all wall simulations, the convective heat transfer coefficients were set at 25 [W/m^{2}K] on the outdoor surface and 10 [W/m^{2}K] on the indoor surface, following established thermal modeling standards [89]. Additionally, the top and bottom surfaces of the wall were considered adiabatic with a heat flux of q=0 [W/m^2], ensuring that no heat transfer occurred through these boundaries. The ambient outdoor temperature used in the simulations corresponds to the average hourly data recorded in Miskolc, Hungary, during three days in mid-July, as illustrated in Fig. 3.2. The temperature profile was averaged over the years 2020 to 2023 to provide a representative external thermal condition for the simulation [90]. To ensure computational efficiency and numerical stability in this transient thermal simulation, a time step Δt of 10 [sec] was selected. This value allowed the solution to converge reliably within 10 iterations per time step, providing a balance between accuracy and runtime performance.

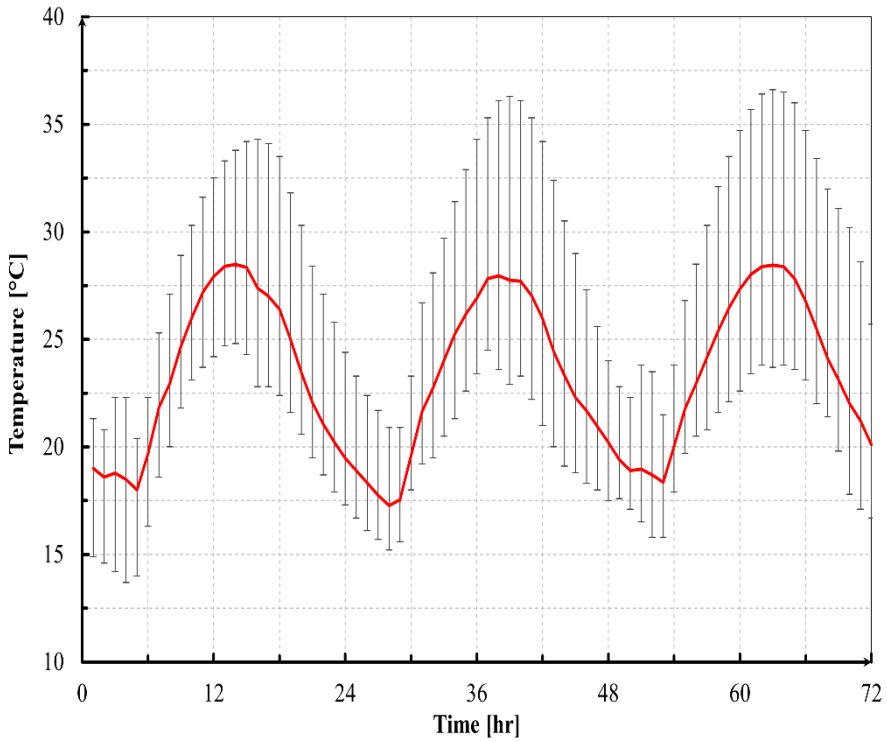

Fig. 3.2: *Mean temperature variations over time in July for Miskolc, Hungary*

The Fourier equation determines the heat transfer flux, considering the initial temperature variation inside the wall, as can be seen in Fig. 3.3 [12].

$$q = \frac{(T_{ex} - T_{in})}{\frac{1}{h_{ex}} + \frac{\delta_1}{k_1} + \frac{\delta_2}{k_2} + \frac{\delta_3}{k_3} + \frac{\delta_4}{k_4} + \frac{1}{h_{in}}}, \qquad (1.1)$$

where T_{ex} [°C] is the outdoor temperature, T_{in} [°C] is the indoor temperature k_i [W/mK], i=1,2,3,4 is the thermal conductivity for each section, δ_i [m], i=1,2,3,4 is the thickness for each section.

However, to evaluate the temperature at the interfaces between the wall layers for calculating the temperature gradient and heat transfer through the multilayer wall, utilize the following equations:

$$T_1 = T_{in} + \ddot{q}\left(\frac{\delta_1}{k_1} + \frac{\delta_2}{k_2} + \frac{\delta_3}{k_3} + \frac{\delta_4}{k_4} + \frac{1}{h_{in}}\right), \qquad (3.2)$$

$$T_2 = T_{in} + \ddot{q}\left(\frac{\delta_2}{k_2} + \frac{\delta_3}{k_3} + \frac{\delta_4}{k_4} + \frac{1}{h_{in}}\right), \qquad (3.3)$$

$$T_3 = T_{in} + \ddot{q}\left(\frac{\delta_3}{k_3} + \frac{\delta_4}{k_4} + \frac{1}{h_{in}}\right), \qquad (3.4)$$

$$T_4 = T_{in} + \ddot{q}\left(\frac{\delta_4}{k_4} + \frac{1}{h_{in}}\right), \qquad (3.5)$$

$$T_5 = T_{in} + \frac{\ddot{q}}{h_{in}} \qquad (3.6)$$

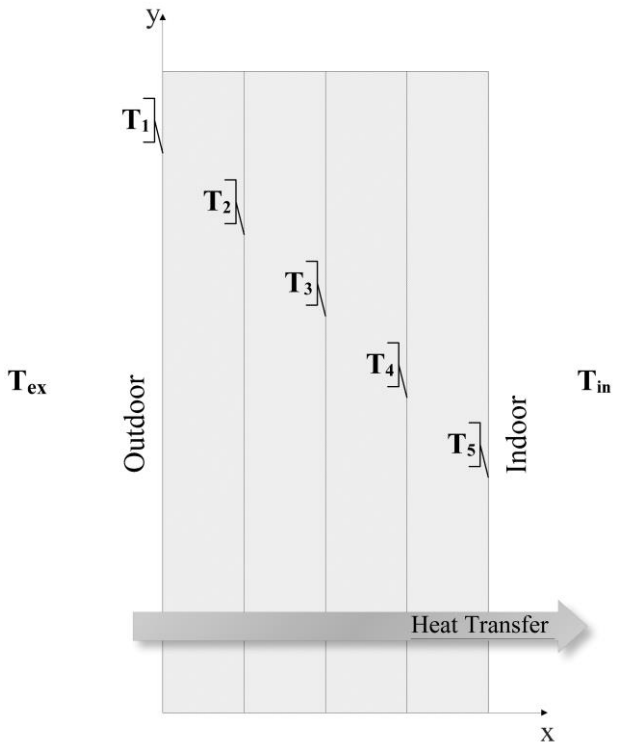

Fig. 3.3: *Wall sections*

3.2. Validation

The numerical approach adopted in this study was validated using experimental results reported by A. Pasupathy et al. [23]. In their work, a test room with dimensions $1.22 \times 1.22 \times 2.44$ [m^3] was constructed to evaluate the thermal performance of PCM panels installed on the roof. The phase change material used in their study was an inorganic salt hydrate mixture composed of 48% $CaCl_2$, 4.3 % NaCl, 0.4 % KCl, and 47.3 % H_2O. To isolate the effect of the PCM panel, all walls except the ceiling were insulated with 6 [mm] thick plywood.

During the experiment, the indoor temperature was maintained at a constant 27 [°C], with convective heat transfer coefficients of 1 [W/m^2K] on the interior surface and 5 [W/m^2K] on the exterior. Fig. 3.4 presents the temperature variations observed on the underside of the ceiling, both experimentally and numerically, alongside the corresponding ambient temperature profile for comparison.

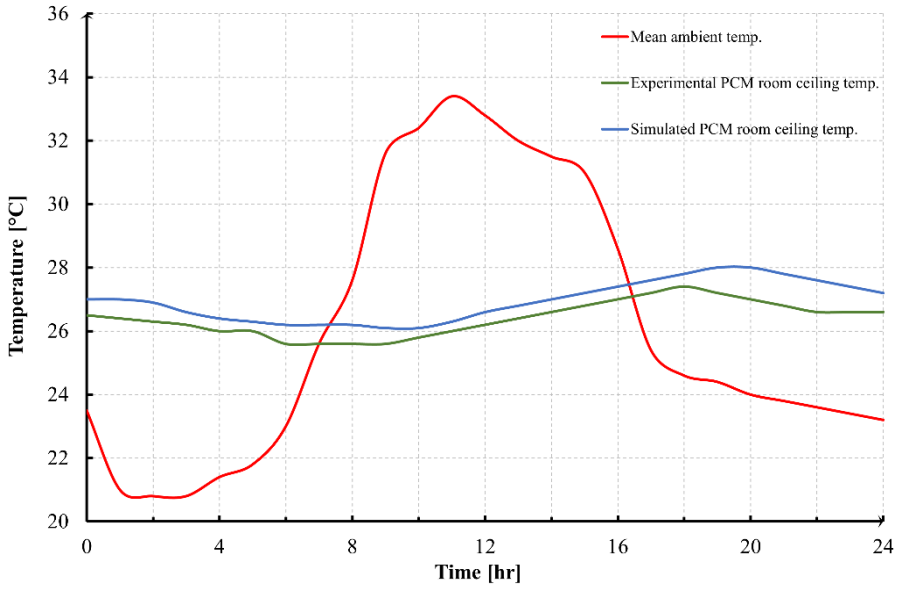

Fig. 3.4: *Evaluating numerical results compared to prior experimental outcomes under consistent ambient temperature conditions*

As shown in Fig. 3.4, the simulated roof temperature profile closely follows the experimental data across a 24 [hr] cycle. Both curves demonstrate consistent trends, with only minor deviations observed throughout the day. The experimental PCM room ceiling temperature peaks slightly lower than the simulated values, with a maximum difference of approximately 0.6 [°C], which falls within an acceptable error margin for building energy simulations. Importantly, the simulation also captures the delayed response of the PCM layer to rising ambient temperatures, a key indicator of effective latent heat absorption. Both the experimental and numerical curves show a thermal lag of several hours behind the peak ambient temperature, highlighting the PCM's role in thermal damping and peak load shifting. This close agreement between the two profiles validates the robustness and accuracy of the simulation method, confirming its suitability for analyzing and optimizing PCM integration in building envelopes. The ability of the numerical model to reproduce both the thermal inertia and attenuation effects of PCM panels underscores its effectiveness for predictive design and thermal performance assessments in future studies.

3.3. Numerical Results

3.3.1. Effect of Integrating PCM in the Building Envelope

This study analyzes the effect of integrating 1 [cm] of RT-27 PCM into the building envelope by comparing the inner surface temperature of a wall with and without PCM. As shown in Fig. 3.5, the wall with PCM demonstrates noticeably reduced temperature fluctuations compared to the non-PCM case. The PCM layer acts as a thermal buffer, absorbing heat during peak external conditions and releasing it when temperatures drop, thereby stabilizing the surface temperature.

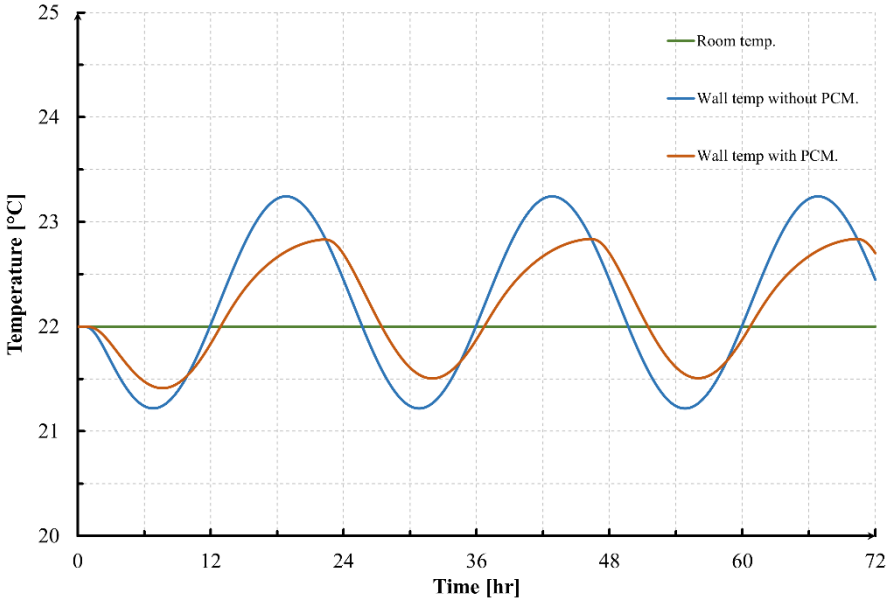

Fig. 3.5: *Indoor surface temperature distribution with and without PCM (RT-27)*

Over the observed 72 [hr] period, the wall without PCM shows temperature swings between approximately 21 [°C] and 23.4 [°C], while the PCM-integrated wall maintains a narrower range of about 21.4 [°C] to 23 [°C]. This reduction in amplitude reflects the latent heat absorption during melting and subsequent delayed heat release during solidification. The thermal lag introduced by the PCM not only reduces the peak temperature, but also smooths the curve, delaying heat flow toward the indoor environment. This effect directly contributes to energy savings. Heat transfer calculations showed that the total thermal gain into the conditioned space decreased from 2.25 [W] to 1.74 [W], corresponding to a 23 % reduction. By moderating the wall's interior surface temperature and narrowing the thermal gradient between the wall and indoor air, the PCM reduces the cooling demand and improves overall thermal comfort.

3.3.2. Effect of Relocating PCM in the Building Envelope

The numerical analysis presented in the previous section was specifically applied to the wall configuration depicted in Fig. 3.6 (b), where the PCM layer was positioned between the brick and cement, placing it near the exterior surface of the building envelope. This section explores the effect of PCM placement at four distinct positions within the wall assembly, aiming to assess its impact on the overall heat transfer rate through the wall, as illustrated in Fig. 3.6.

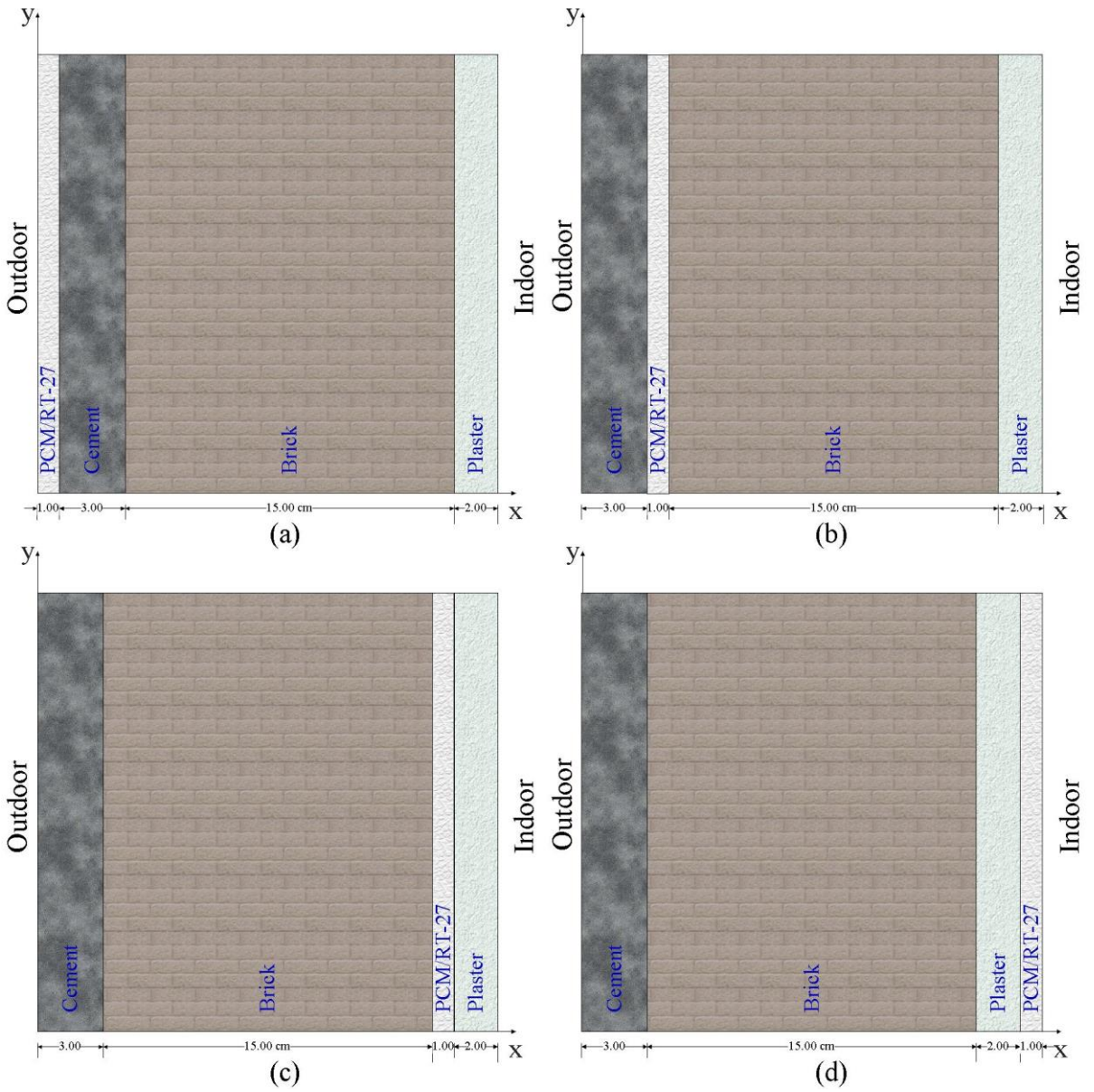

Fig. 3.6: *Schematic of building envelope with PCM*

The four evaluated PCM locations are as follows:

a) Externally mounted, on the outermost surface of the building envelope.

b) Near the exterior, embedded between the cement and bricklayers.

c) Near the interior, placed between the brick and plaster layers.

d) Directly on the interior surface, forming the innermost layer of the envelope.

In each configuration, a 1 [cm] thick layer of RT-27 PCM was incorporated. As shown in Fig. 3.7, the position of PCM within the wall significantly influences heat transfer.

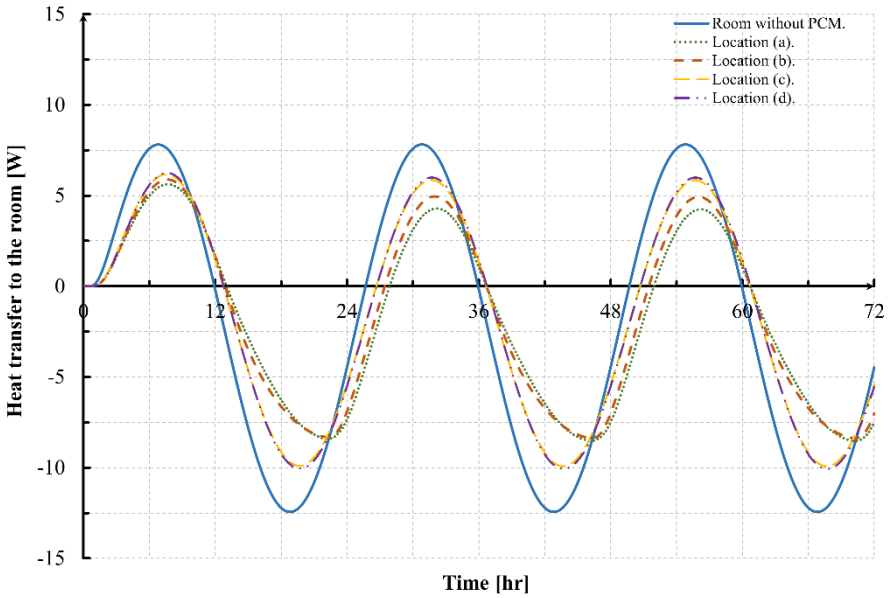

Fig. 3.7: *Heat transmission into the room when the PCM is relocated*

The data presented in Table 3.2 indicate that placing PCM closer to the exterior surface yields the greatest reduction in thermal transmission. This is due to the PCM absorbing a substantial portion of the incoming heat flux before it penetrates deeper into the wall.

Table 3.2: *Total heat flux to the room when the PCM is relocated*

Location	Heat flux to the room [W]		Reduction [%]
	Building envelope without PCM	Building envelope with PCM	
a)	2.25	1.90	15
b)	2.25	1.74	23
c)	2.25	1.86	17
d)	2.25	1.86	17

Based on these findings, subsequent investigations in this study focused primarily on the configuration where PCM is located near the exterior, as it consistently demonstrated the most effective thermal regulation performance.

3.3.3. Effect of PCM Thickness on the Building Envelope

Based on the findings of the previous section, position (b) where the PCM layer is placed between the cement and brick, was identified as the most effective configuration for reducing heat transmission. Building on this result, the thickness of the PCM (RT-27) was varied systematically, starting from 1 [cm], then increasing to 3 [cm], and finally to 5 [cm], as illustrated in Fig. 3.8.

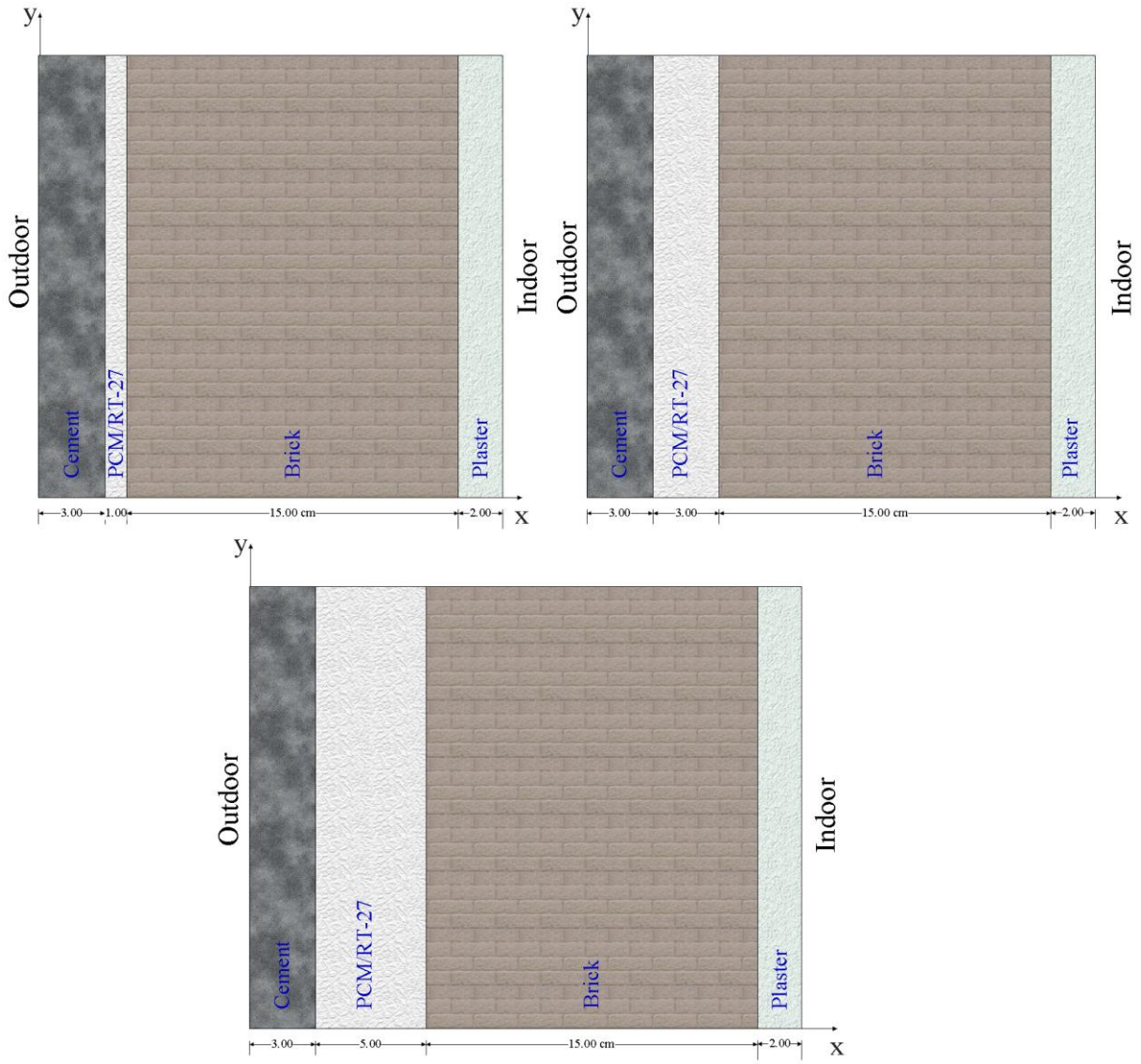

Fig. 3.8: *Schematic of building envelope with multi-thickness PCM*

The simulations revealed that the amount of thermal energy stored within the PCM increases significantly with greater thickness. This enhanced storage capacity allows the PCM to absorb more heat, thereby reducing the net energy transferred to the indoor space. As a result, the thermal buffering effect becomes more pronounced, especially under conditions of fluctuating external temperatures. Fig. 3.9 illustrates the temperature distribution on the interior surface of the wall for the three PCM thicknesses. Temperature fluctuations on the inner surface decrease as PCM thickness increases, demonstrating a stronger damping effect. This trend indicates that a thicker PCM layer provides improved thermal inertia, delaying and minimizing heat flow into the conditioned space.

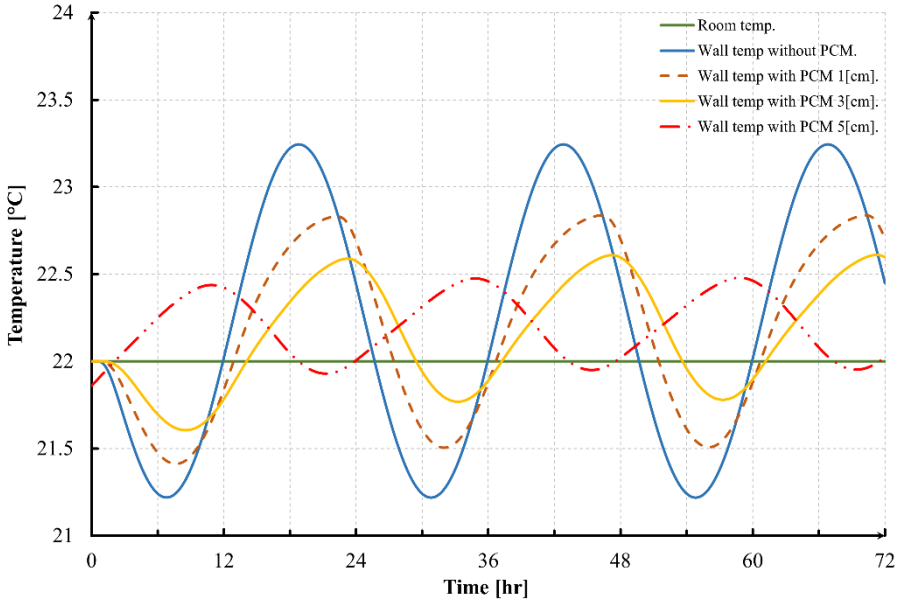

Fig. 3.9: *Indoor surface temperature distribution with different thicknesses of PCM (RT-27)*

Furthermore, since heat flux is directly influenced by the temperature gradient, increasing the PCM thickness results in a progressive reduction in heat transfer to the room. The corresponding total heat transmission values for each thickness configuration are summarized in Table 3.3, clearly showing that thicker PCM layers yield better thermal insulation performance.

Table 3.3: *Total amount of heat flux to the room when changing the thickness of the PCM*

Thickness [cm]	**Heat flux to the room [W]**		**Reduction [%]**
	Building envelope without PCM	**Building envelope with PCM**	
1	2.25	1.74	23
3	2.25	1.47	34
5	2.25	1.30	42

3.3.4. Effect of PCM Thermophysical Properties

This section evaluates the impact of using different PCM types on the thermal performance of the building envelope. Since each PCM possesses unique thermophysical properties, such as melting temperature, latent heat capacity, and thermal conductivity, variations in these characteristics result in differences in the amount of material melted and, consequently, in the total thermal energy stored. Fig. 3.10 presents the indoor surface temperature distribution for walls incorporating various PCM types under identical boundary conditions. As expected, the temperature fluctuations differ among the PCMs, reflecting their individual heat absorption and storage capacities. The total heat transferred to the room for each PCM type is summarized in Table 3.4.

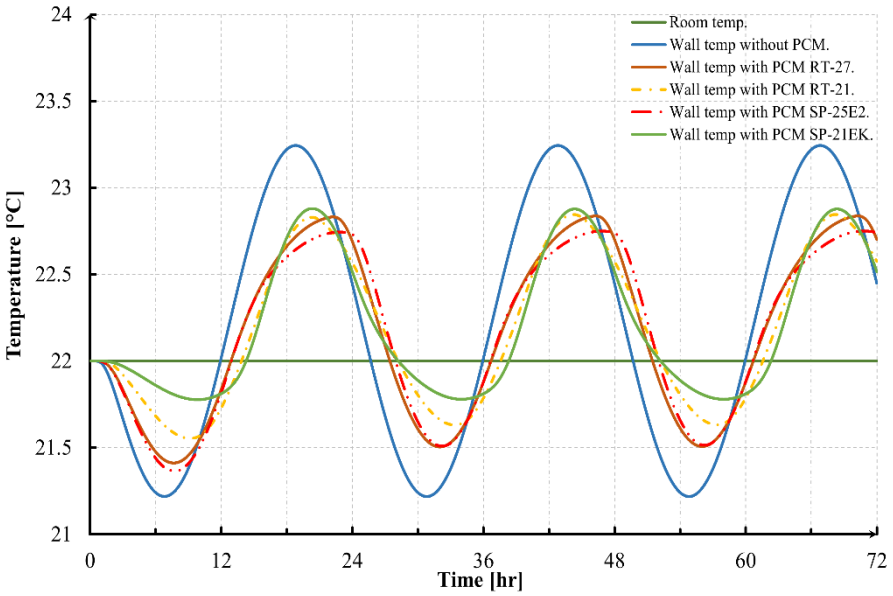

Fig. 3.10: *Indoor surface temperature distribution with different types of PCM*

Table 3.4: *Total amount of heat flux to the room for different types of PCM*

PCM type	Heat flux to the room [W]		Reduction [%]
	Building envelope without PCM	Building envelope with PCM	
RT-27	2.25	1.74	23
RT-21	2.25	1.82	19
SP-25E2	2.25	1.67	26
SP-21EK	2.25	2.09	7

Among the tested materials, SP-25E2 demonstrated the lowest total heat transfer. Since the PCM volume is fixed, this improved performance is primarily associated with its higher volumetric latent storage capacity ρL_H (linked to higher density), while the melting temperature range further affects how effectively this storage is activated under the wall thermal load.

3.4. Summary of This Chapter

This chapter presented a comprehensive numerical investigation into the optimization of key parameters affecting the thermal performance of PCMs when integrated into building envelopes. The study focused on a representative wall configuration typical of Miskolc, Hungary, composed of 3 [cm] cement, 15 [cm] brick, and 2 [cm] plaster layers. Using validated CFD simulations, the chapter explored the impact of PCM layer position, thickness, and material properties on reducing indoor heat gain and enhancing thermal comfort.

The analysis began by examining the effect of PCM placement at four distinct positions within the wall assembly. Results showed that positioning the PCM closer to the exterior surface significantly enhanced its thermal buffering capacity and led to the greatest reduction in heat

transmission. This configuration was selected for further parametric analysis. Next, the influence of PCM thickness was assessed using RT-27. Increasing the PCM layer from 1 [cm] to 5 [cm] resulted in greater energy storage, lower interior surface temperature fluctuations, and a measurable reduction in total heat transfer to the indoor space. The study also evaluated the performance of different PCM types, demonstrating that thermal properties particularly melting temperature and thermal conductivity play a decisive role in effectiveness. Among the tested materials, SP-25E2 achieved the lowest overall heat transmission, confirming the importance of matching PCM properties to the climate and application. From the simulation results, several key conclusions were drawn:

- Incorporating PCMs into wall assemblies reduces heat transfer and improves thermal stability.
- Temperature fluctuations at the indoor surface are significantly dampened by PCM integration.
- Thermal conductivity influences performance through a dual role, lower k can reduce instantaneous conduction, while higher k can enhance PCM charging/discharging, therefore, the net heat flux reduction depends on the combined PCM properties and operating conditions rather than conductivity alone.
- Optimal performance is achieved when the PCM is placed near the outer surface of the wall, where it intercepts and absorbs incoming heat early.
- Increasing PCM thickness allows for higher thermal energy storage within the envelope, further enhancing performance.

Overall, this chapter highlights the critical role of design variables in PCM-based envelope systems and provides practical insights for energy-efficient building strategies in moderate continental climates like that of Miskolc.

4. Optimization of PCM Capsule Shape for Enhanced Building Envelopes

In this chapter, the focus shifts to the geometric optimization of macro-encapsulated PCMs, intending to enhance thermal performance in building envelopes. While earlier chapters addressed the influence of PCM location, thickness, and thermal properties, the shape and encapsulation of PCMs play an important role in determining the efficiency of heat absorption, storage, and release within building systems.

For practical and long-term use in building materials, PCMs must be encapsulated to prevent leakage, ensure safety, and maintain structural integration. Encapsulation involves enclosing the PCM within a protective shell, which not only prevents leakage during phase transitions, but also isolates the PCM from environmental conditions. To function effectively in thermal storage systems, the encapsulation material must meet several criteria: it must prevent leakage, retain the PCM thermal characteristics, avoid chemical interactions with the PCM, remain structurally stable under operating conditions, and be compatible with the construction material in which it is embedded [91]. Furthermore, the shape of the capsule significantly impacts the surface area-to-volume ratio, heat transfer efficiency, and rate of phase transition.

This chapter explores a range of capsule geometries by embedding them within standard wall assemblies. Using CFD based on the finite volume method, the simulations analyze thermal performance during heating, melting, and solidification cycles. The walls are modeled under realistic environmental conditions relevant to Miskolc, Hungary. By comparing the thermal behavior, melting time, heat flux, and energy storage capacity across different shapes, this chapter seeks to identify the optimal capsule geometry for PCM integration. The findings offer valuable design insights for improving thermal energy storage systems and promoting energy-efficient, passive building solutions.

4.1. Model Characteristics

To evaluate the thermal performance of PCM capsules integrated into building envelopes, RT-27 (paraffin wax) the same organic phase change material used in the previous chapter was selected. This material, produced by Rubitherm, was chosen not only for consistency across simulation stages, but also because of its excellent thermal properties and proven suitability for moderate continental climates like that of Miskolc, Hungary. RT-27 exhibits a high latent heat storage capacity, stable phase change near a constant temperature, no supercooling, and chemical

inertness, all of which contribute to long-term thermal stability and performance in building applications.

The simulation model was based on a brick wall assembly, representative of common masonry construction found in Miskolc. This selection ensures that the wall's thermal characteristics reflect local construction practices, enabling a realistic assessment of PCM integration under region-specific environmental conditions. The indoor temperature was fixed at 22 [°C], aligning with thermal comfort guidelines [88]. Boundary conditions included convective heat transfer coefficients of 25 [W/m^{2}K] for the external surface and 10 [W/m^{2}K] for the internal surface [89]. The top and bottom surfaces of the wall were considered adiabatic, with a heat flux of q=0 [W/m^2]. To replicate realistic outdoor thermal loading, a three-day ambient temperature profile for mid-July in Miskolc was applied. This profile was developed using average hourly temperatures from 2020 to 2023, retrieved from free open-source weather [90].

4.2. Samples Geometry

A total of eleven PCM-embedded samples and one reference (non-PCM) block were systematically evaluated to investigate the influence of capsule geometry on thermal performance. Each sample was filled with RT-27 paraffin wax, selected for its reliable latent heat storage properties and consistent melting behavior. To ensure comparability across all configurations, the total volume of each test block was standardized at 1500 [cm^3].

The study explored a range of encapsulation geometries to examine how shape affects heat transfer dynamics within the wall system. The tested capsule configurations included:

- *Cuboid-shaped capsules:* Five samples, shown in Fig. 4.1 (a-e), were constructed with cuboidal geometry. This shape offers a simple, orthogonal structure suitable for analyzing heat conduction along three perpendicular axes, providing insight into directional heat flow behavior.

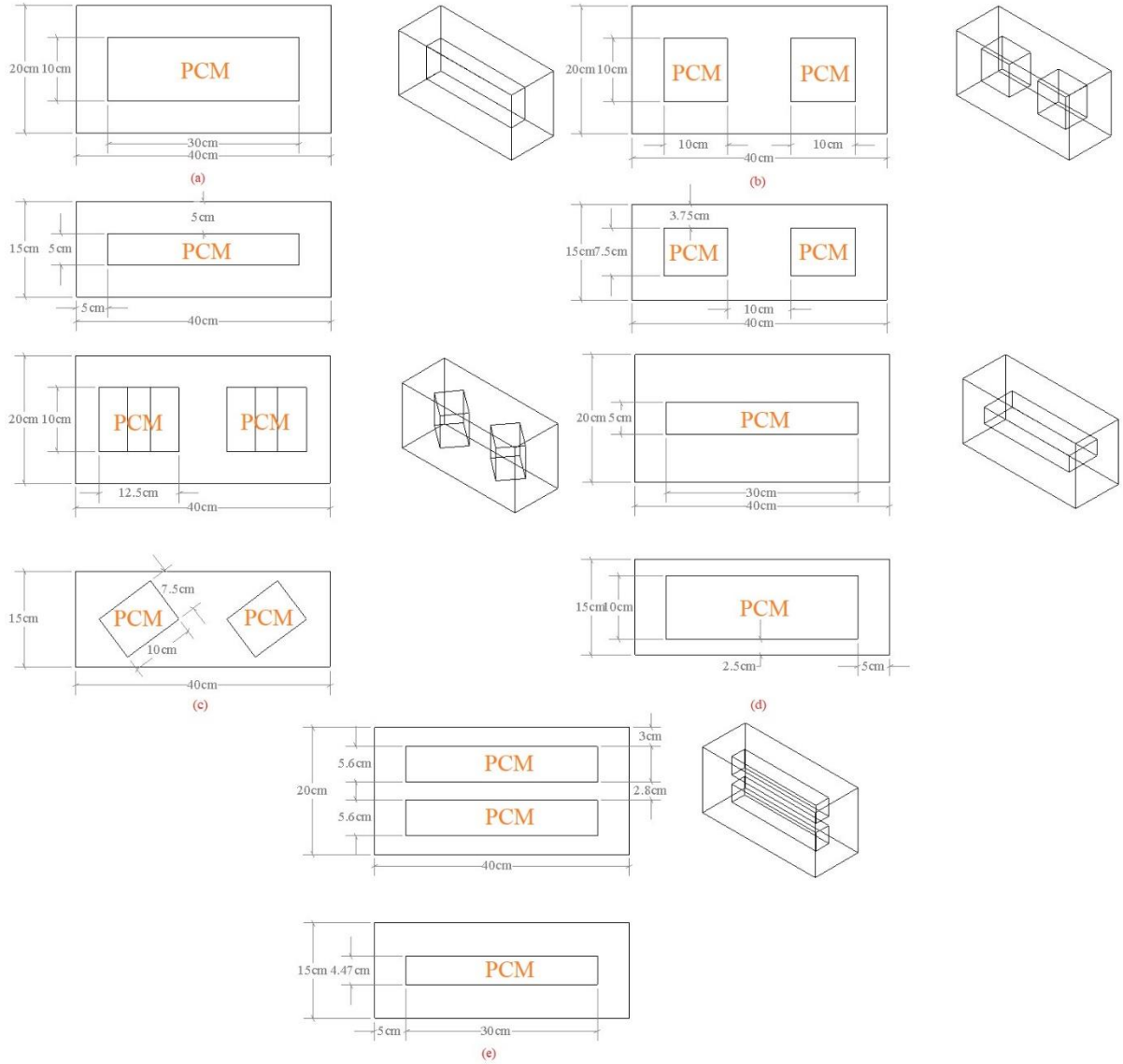

Fig. 4.1: *Cuboids technical sketches: (a) cuboid capsule, (b) two vertical cuboid capsules, (c) two cuboid 90° tilted capsules, (d) cuboid inverted capsule, and (e) two horizontal cuboid capsules*

- *Cylinder-shaped capsules:* Three cylindrical samples, illustrated in Fig. 4.2 (a-c), were used to study radial and axial heat conduction. The cylindrical shape enables analysis of the influence of curved surfaces on thermal distribution and melting uniformity.

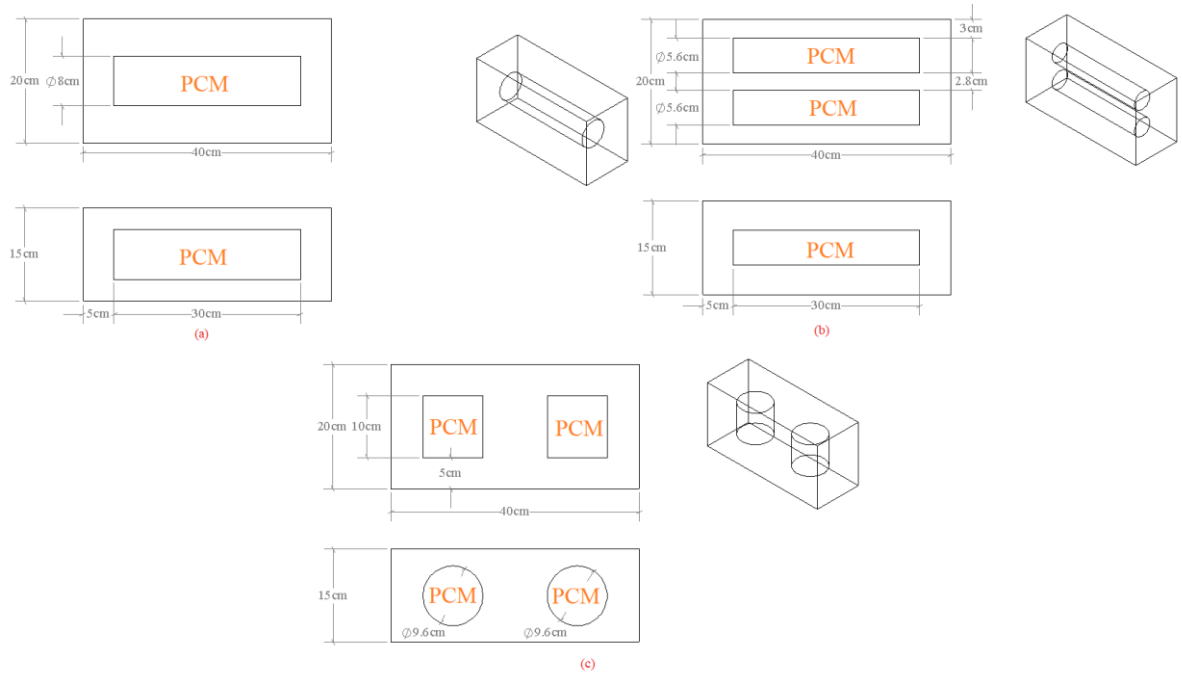

Fig. 4.2: *Cylinders technical sketches: (a) horizontal cylindrical capsule, (b) two horizontal cylindrical capsules, and (c) two vertical cylindrical capsules*

- *Prism-shaped capsules:* As depicted in Fig. 4.3 (a-c), three samples were designed with prismatic geometry, characterized by triangular cross-sections extruded into a 3D form. Prismatic capsules offer advantages in terms of structural integration, packing efficiency, and potentially enhanced heat transfer due to varied surface area exposure.

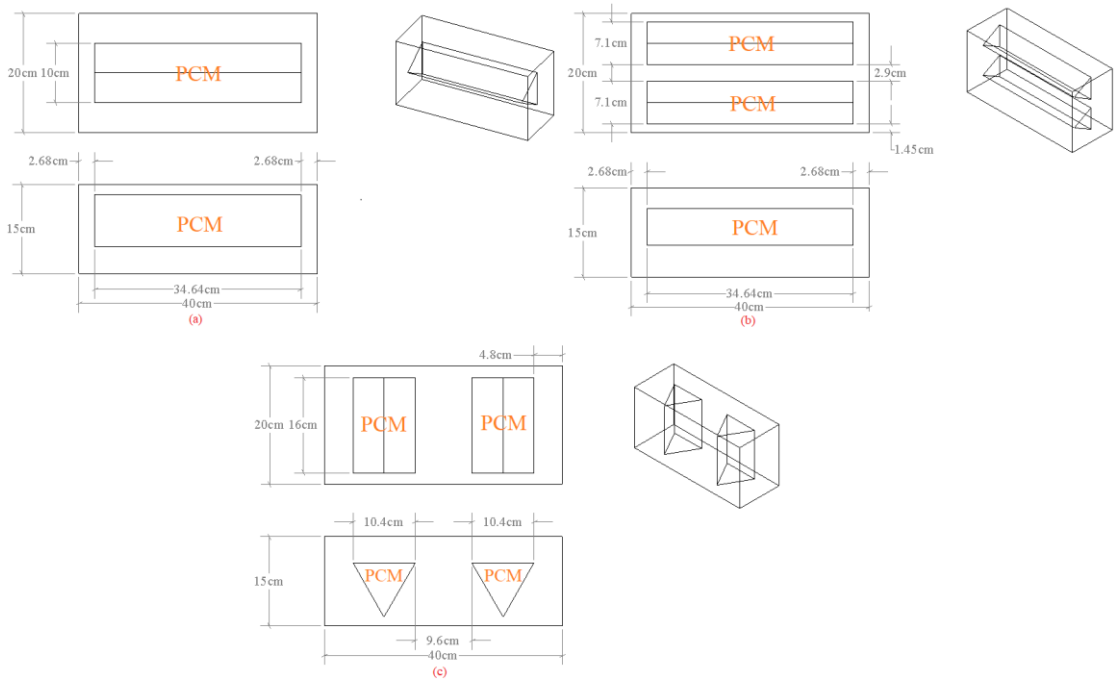

Fig. 4.3: *Prisms technical sketches: (a) horizontal prismatic capsule, (b) two horizontal prismatic capsules, and (c) two vertical prismatic capsules*

By incorporating these distinct geometric forms, the study enables a comprehensive evaluation of the relationship between capsule shape and thermal performance. Understanding this relationship is critical for the optimization of PCM systems in building envelopes, where geometry significantly affects heat absorption rate, phase transition efficiency, and structural adaptability.

4.3. Validation and Independence of Mesh Grid

4.3.1. Validation

To ensure the reliability of the numerical approach adopted in this chapter, validation was conducted by referencing the experimental results of A. Pasupathy et al. [23], whose study involved assessing the thermal behavior of PCM panels integrated into a test room roof. Although the PCM used in their experiment was an inorganic salt hydrate, and the current study utilizes RT-27 paraffin wax, the fundamental thermal responses such as temperature attenuation and delayed peak loads serve as robust benchmarks for comparison.

In their setup, Pasupathy et al. maintained constant indoor temperatures and monitored temperature fluctuations at the PCM ceiling interface over a 24 [hr] period. The simulated results in the present study were aligned with this framework and compared accordingly. The thermal response captured by the simulation in this work mirrored the experimental trends with a maximum deviation of approximately 0.6 [°C] within acceptable tolerances for building energy simulations. Moreover, the numerical model successfully reproduced key dynamic features such as thermal lag and damping, characteristic of phase change behavior. The PCM layer's ability to delay and flatten temperature peaks, as shown in both experimental and simulated curves, reinforces the model's capacity to predict PCM-driven performance in building applications. This comparative validation confirms that the methodology employed here is sufficiently accurate for the subsequent analysis of PCM capsule geometry and its impact on thermal efficiency.

4.3.2. Independence of Mesh Grid

To ensure reliable and accurate numerical results, a mesh independence analysis was conducted. In CFD simulations, the computational domain is discretized into finite control volumes, or cells, through a meshing process. In this study, structured hexahedral cells were generated using ANSYS Meshing. While a finer mesh generally improves solution accuracy, it also significantly increases computational demand. Hence, it is important to identify a mesh density beyond which further refinement yields negligible changes in results (a condition known as mesh independence).

Seven mesh configurations with increasing node counts were evaluated, focusing on their impact on the wall's indoor surface temperature. As shown in Fig. 4.4, a substantial rise in temperature accuracy was observed as the number of nodes increased, particularly up to approximately 45,000 nodes. Beyond this threshold, the indoor surface temperature remained nearly constant, indicating that the simulation results were no longer sensitive to further mesh refinement. Consequently, a mesh with 45,000 nodes was selected as the optimal balance between computational efficiency and numerical accuracy for all subsequent simulations in this study.

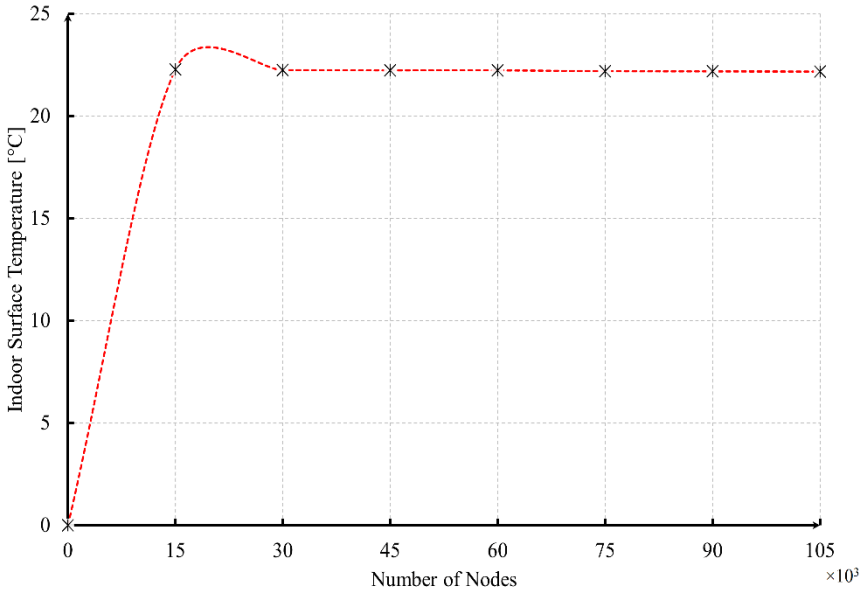

Fig. 4.4: *Variations of indoor surface temperature at different grid sizes*

4.4. Numerical Results

4.4.1. Effect of Incorporating Cuboid-Shaped Capsules

In this section, the thermal performance of cuboid-shaped PCM capsules embedded within a wall structure was systematically analyzed. Five geometric configurations were examined to determine how their shapes influence indoor surface temperatures and overall heat transfer into the room.

The incorporation of PCM capsules into cuboid geometries offers several notable benefits. The cuboid structure presents a higher surface area-to-volume ratio, which facilitates more efficient heat exchange during the melting and solidification processes. Cuboids promote a more uniform phase transition across the volume of PCM, reducing the risk of localized overheating or undercooling. Their flat surfaces and modular shape also allow for improved integration into structural components, such as walls or panels. Fig. 4.5 (a-e) shows the time-dependent indoor surface temperatures for the wall integrated with different cuboid-shaped PCM capsules, alongside a reference wall without PCM. In each case, the PCM-embedded configurations demonstrate reduced temperature fluctuations, confirming their ability to absorb heat and regulate interior surface temperature. Among these, the capsule labeled cuboid shape (a) exhibits the most consistent thermal moderation.

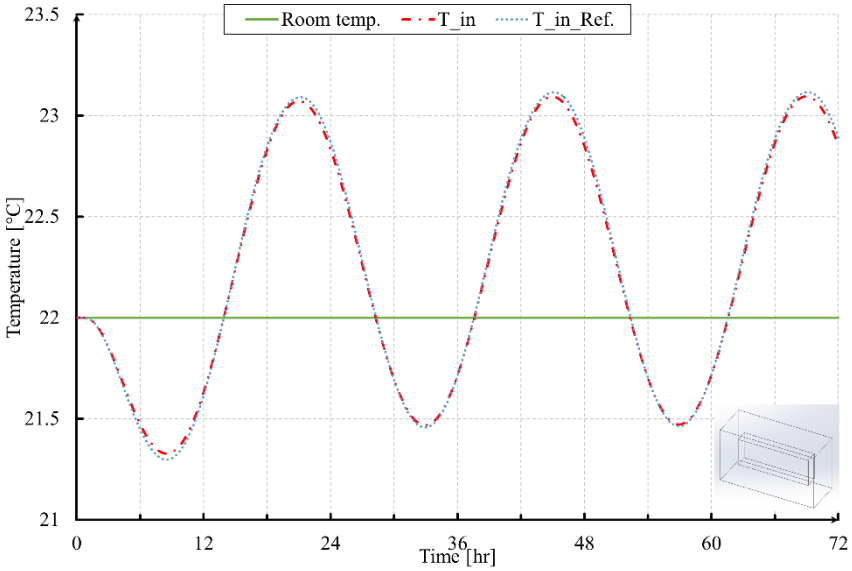

Fig. 4.5(a): *Indoor surface temperature distribution with cuboid capsule*

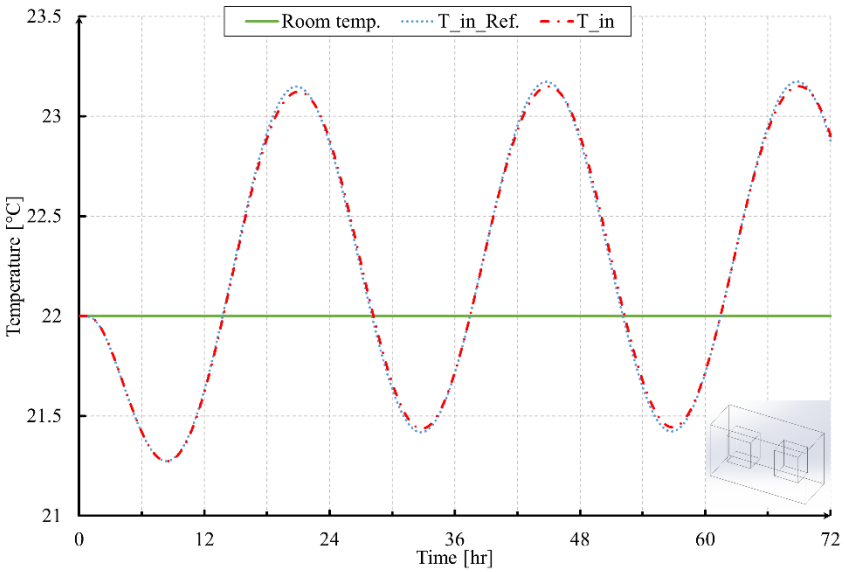

Fig. 4.5(b): *Indoor surface temperature distribution with two vertical cuboid capsules*

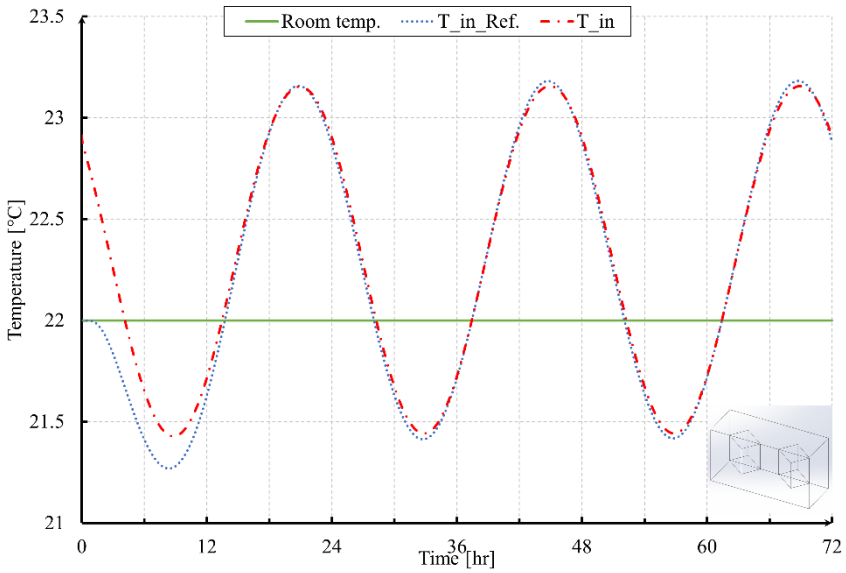

Fig. 4.5(c): *Indoor surface temperature distribution with two cuboid 90° tilted capsules*

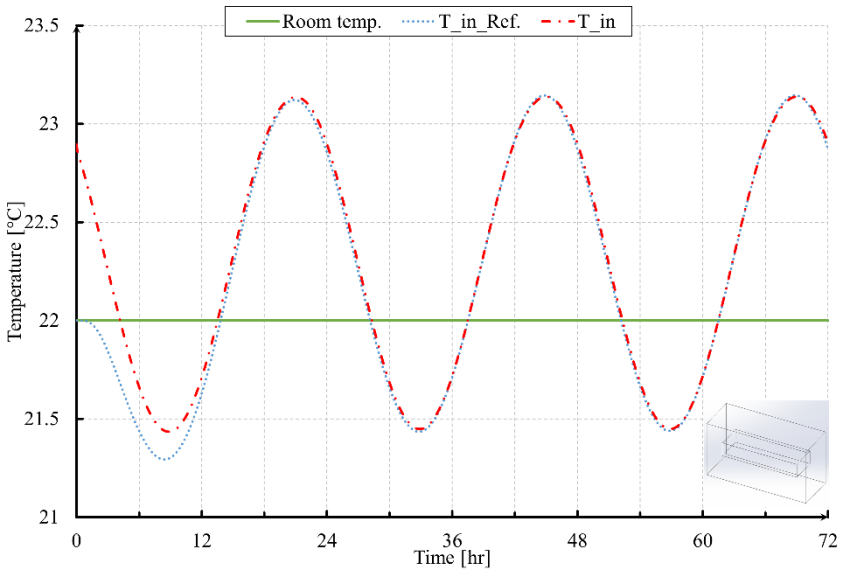

Fig. 4.5(d): *Indoor surface temperature distribution with cuboid inverted capsule*

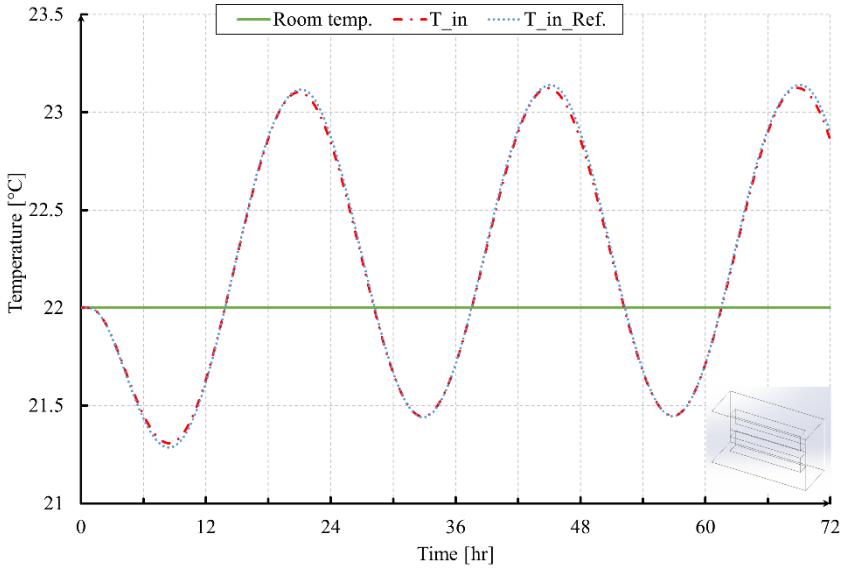

Fig. 4.5(e): *Indoor surface temperature distribution with two horizontal cuboid capsules*

This thermal buffering is quantitatively supported by the total heat transfer values shown in Fig. 4.6. Compared to the non-PCM reference wall, the cuboid capsules achieved varying degrees of energy reduction. Notably, cuboid shape (a) produced the highest reduction in heat transmission up to 37 % followed closely by shapes (b) and (e), which reduced heat flow by 35 % and 36 %, respectively. Conversely, shapes (c) and (d) yielded lower reductions, around 8 % and 9 %, suggesting that shape optimization plays a critical role in enhancing thermal efficiency.

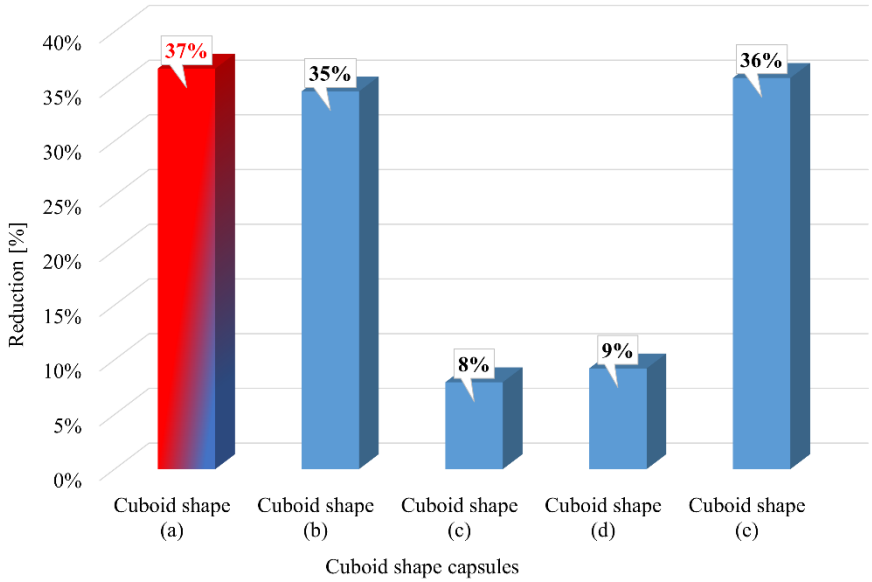

Fig. 4.6: *Total amount of heat transfer reduction to the room for different cuboid capsules*

Overall, the findings underscore the importance of geometric design in PCM encapsulation. Strategically shaped cuboid capsules significantly enhance thermal performance, reduce indoor heat gains, and contribute to improved energy efficiency in building envelopes.

4.4.2. Effect of Incorporating Cylinder-Shaped Capsules

Optimizing the geometry of PCM capsules can significantly influence thermal performance because capsule shape affects the available heat-transfer area, characteristic conduction length, and the charging/discharging rate of the PCM. In this study, cylindrical capsules provide a practical geometry for integration into hollow-brick cavities and can promote more uniform heat transfer around the capsule perimeter, depending on the selected dimensions and placement. However, the thermal advantage of any capsule shape is not inherent; it depends on the specific surface-area-to-volume ratio and geometric constraints of the wall system. In addition to thermal considerations, cylindrical capsules can offer good mechanical stability under load and are relatively straightforward to manufacture and integrate into building components.

In this study, the impact of embedding PCM within cylindrical capsules was analyzed. Fig. 4.7(a-c) shows the temporal variation in indoor surface temperature for walls embedded with three distinct cylindrical capsule designs. Across all configurations, the incorporation of PCM led to noticeably lower temperature fluctuations compared to the reference wall without PCM. This thermal dampening effect is attributed to PCM acting as a latent heat sink, absorbing excess thermal energy during peak conditions and releasing it during cooler periods. As a result, the indoor surface remains more stable and closer to the comfort temperature range.

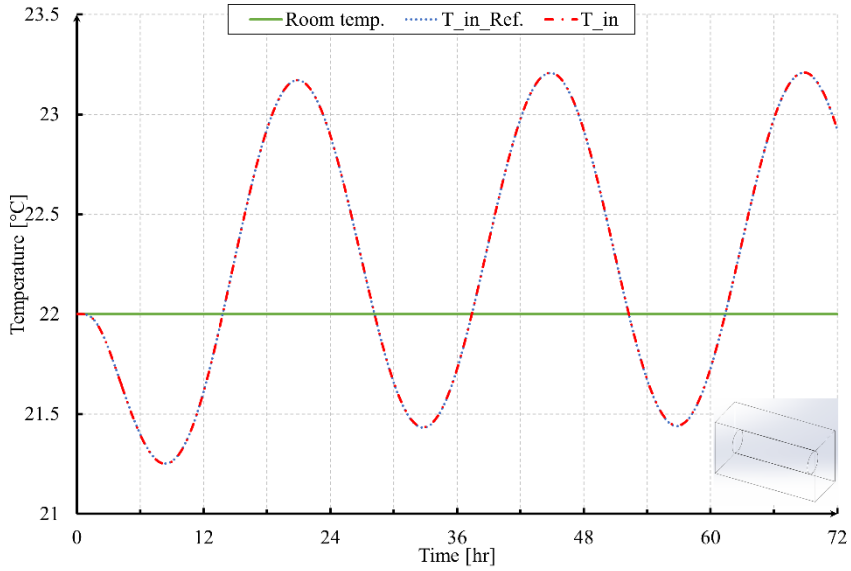

Fig. 4.7(a): *Indoor surface temperature distribution with horizontal cylindrical capsule*

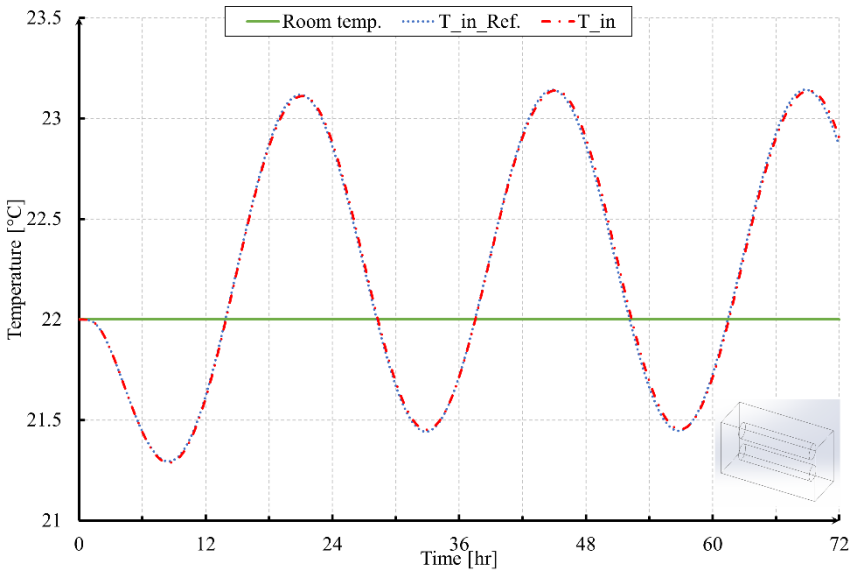

Fig. 4.7(b): *Indoor surface temperature distribution with two horizontal cylindrical capsules*

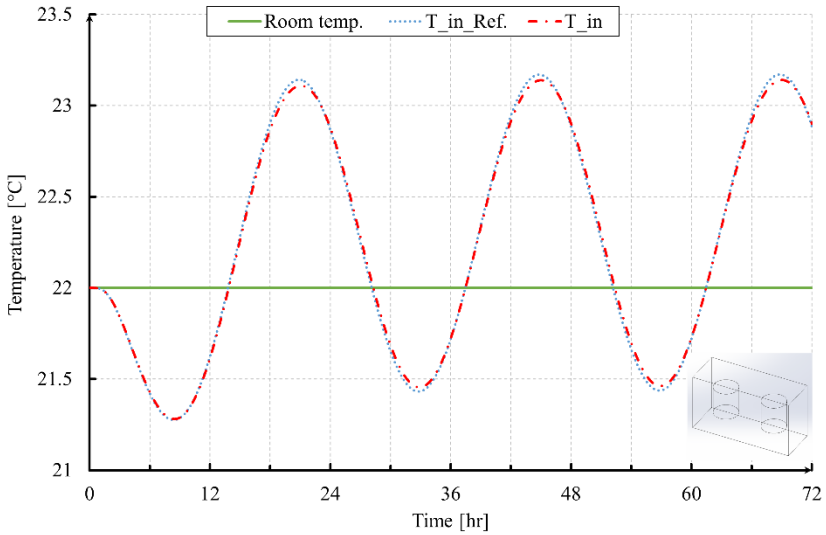

Fig. 4.7(c): *Indoor surface temperature distribution with two vertical cylindrical capsules*

The effectiveness of each cylindrical capsule shape is further quantified in Fig. 4.8, which presents the percentage reduction in heat transfer to the room. Among the three configurations studied, the cylindrical capsule (b) demonstrated the highest thermal performance, achieving a 35.85 % reduction in heat transfer. This indicates that, beyond just geometry, the spatial distribution and volume-to-surface ratio of the PCM capsule significantly influence the extent of energy absorption and the resulting indoor temperature stabilization.

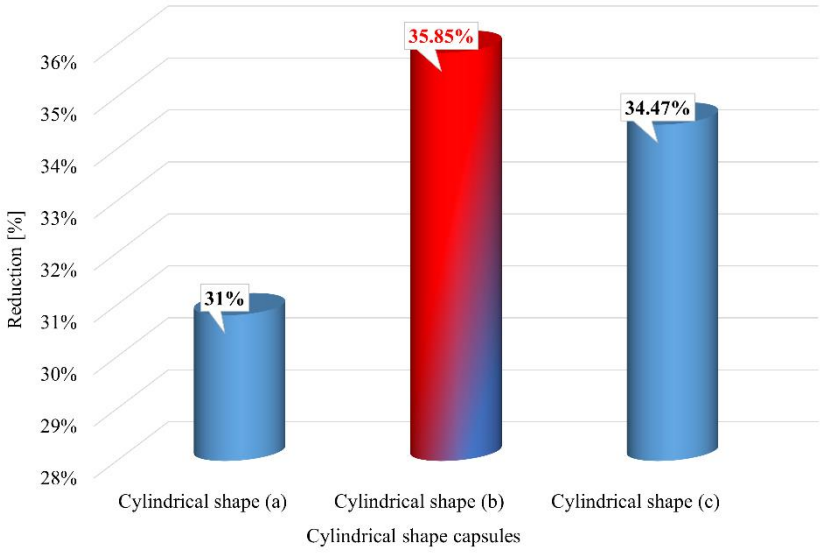

Fig. 4.8: *Total amount of heat transfer reduction to the room for different cylindrical capsules*

These results confirm that cylindrical capsules particularly optimized configurations like (b) are effective in reducing peak thermal loads, thus enhancing the energy efficiency of PCM-integrated building envelopes.

4.4.3. Effect of Incorporating Prism-Shaped Capsules

Prismatic capsules can improve thermal response due to geometric effects (e.g., surface-area-to-volume ratio and heat transfer area), while the PCM volume is kept constant at 1500 cm^3 across all cases. Enhanced thermal conductivity and more uniform phase transitions are promoted by extended surface contact, which contributes to consistent temperature regulation. Moreover, their compatibility with modular and structural designs makes them especially suitable for integration into building materials. However, prismatic capsules can pose manufacturing challenges due to their complex shapes and sharp edges, potentially complicating encapsulation processes. Despite these limitations, they are ideal for applications demanding high energy storage efficiency and precise thermal control.

This study explored the influence of PCM encapsulated in prismatic shapes on indoor surface temperatures. Fig. 4.9 (a-c) presents the temperature fluctuations across walls integrated with different prism-shaped capsules. Compared to walls without PCM, the temperature oscillations within PCM-integrated walls are significantly reduced, highlighting the heat-sink effect of the PCM, which limits energy transmission from outside to inside surfaces.

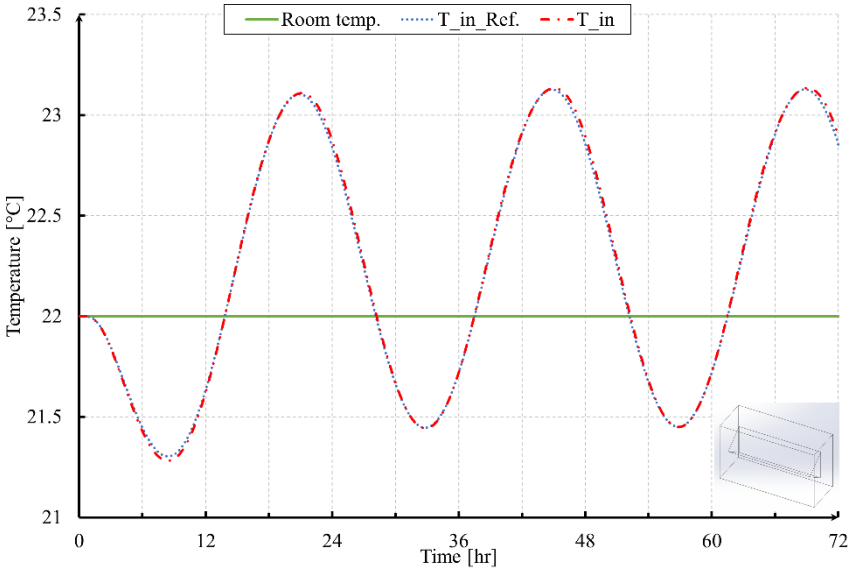

Fig. 4.9(a): *Indoor surface temperature distribution with horizontal prismatic capsule*

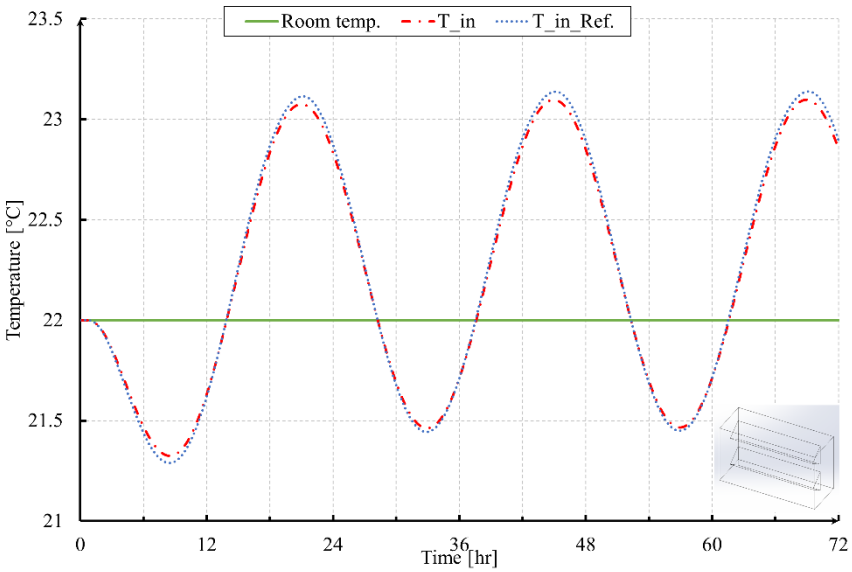

Fig. 4.9(b): *Indoor surface temperature distribution with two horizontal prismatic capsules*

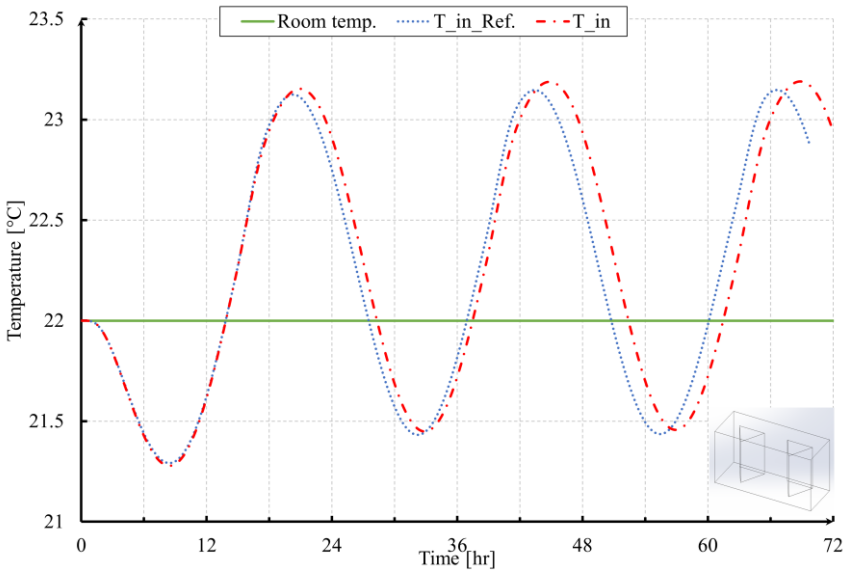

Fig. 4.9(c): *Indoor surface temperature distribution with two vertical prismatic capsules*

Fig. 4.10 compares the total heat transfer to the room for each prismatic configuration. Among the examined designs, prism-shaped capsule (b) yielded the greatest reduction in thermal energy transmission, demonstrating its superior effectiveness in mitigating heat flow into the interior space.

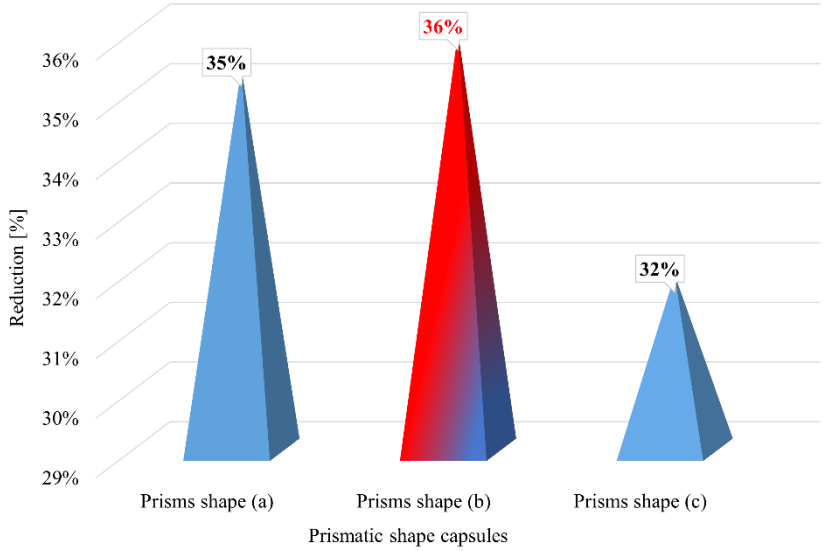

Fig. 4.10: *Total amount of heat transfer reduction to the room for different prismatic capsules*

4.5. Summary of This Chapter

This chapter focused on optimizing the geometric configuration of PCM capsules embedded within building envelopes to enhance thermal performance. Using RT-27 paraffin wax selected for its favorable thermal characteristics and suitability for Miskolc's climate, the study evaluated how different capsule shapes influence energy storage and heat transfer in building walls.

Three primary capsule shapes were examined: cuboid, cylindrical, and prismatic, each offering distinct thermal and structural advantages. Cuboid-shaped capsules demonstrated superior heat transmission reduction, achieving the highest performance in limiting indoor temperature fluctuations. Their flat surfaces promote uniform phase transitions and make them structurally compatible with modular wall components, while also being cost-effective and easy to manufacture. Cylindrical capsules offered good mechanical stability and directional heat flow, making them well-suited for integration into hollow or tubular masonry systems. These shapes also exhibited strong thermal damping with moderate energy savings, particularly with optimal configurations. Prismatic capsules, despite being more complex and costly to manufacture, excelled in applications requiring space efficiency and controlled heat release. Their enhanced packing density and consistent thermal behavior made them ideal for high-performance energy regulation needs.

Across all tests, numerical simulations confirmed that incorporating PCM in various optimized capsule shapes effectively reduced heat transmission into the indoor environment, thereby lowering energy loads. Among the designs studied, cuboid capsule (a) achieved the greatest heat transfer reduction, as shown in Fig. 4.11 highlighting the importance of geometric optimization in PCM applications.

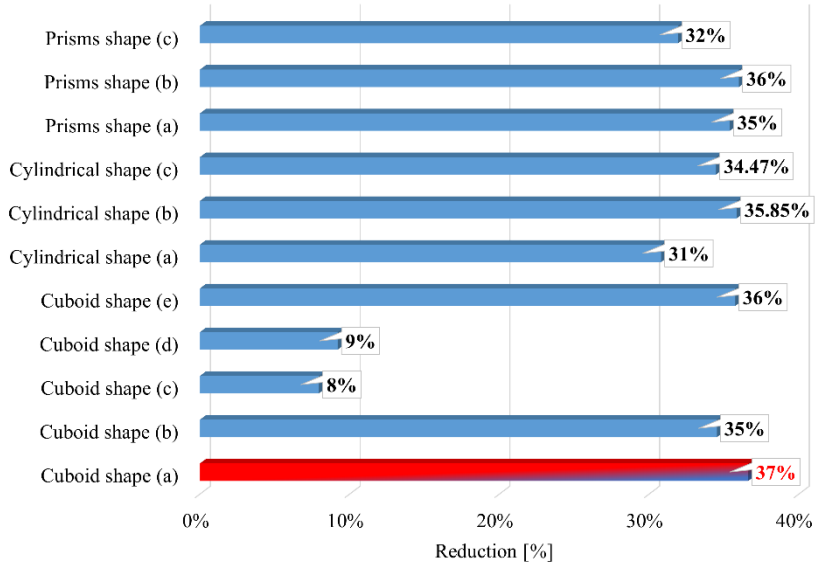

Fig. 4.11: *Total amount of heat transfer reduction to the room for different capsules*

Ultimately, the chapter concludes that capsule shape selection should be based on the specific thermal, spatial, and economic requirements of the application. Cuboid designs are optimal for cost-effective thermal regulation, cylindrical shapes serve well in directed systems, and prismatic forms are ideal where space utilization and thermal uniformity are critical.

5. COMBINING AESTHETICS AND EFFICIENCY PCM APPLICATIONS IN FLEMISH BOND WALLS

In this chapter, the focus shifts to the integration of PCMs into Flemish bond brick walls, a strategy that combines architectural tradition with modern energy efficiency solutions. Bricks have long served as both structural and decorative elements in building envelopes, with Flemish bond patterns offering a distinctive aesthetic characterized by alternating headers and stretchers. While this design enhances the visual appeal of facades, its influence on thermal performance remains underexplored in academic literature.

To address this gap, the chapter investigates how incorporating PCMs into Flemish bond walls can enhance their thermal behavior, offering both passive thermal regulation and reduced energy demands. PCMs are well-suited for LHS systems, where they absorb excess heat during peak temperature periods and release it when temperatures drop, thus maintaining a stable indoor environment. This capability is particularly relevant in the context of increasing energy consumption and the need for sustainable building practices. The study employs numerical simulations to assess heat transfer dynamics and temperature regulation in Flemish bond walls integrated with RT-27 PCM, focusing on a real-world climate scenario in Miskolc, Hungary. The results demonstrate that while Flemish bond structures alone reduce energy transfer by 6 %, the addition of PCM enhances this reduction to 21 %, thanks to their latent heat storage potential. This dual effect highlights the synergy between traditional construction methods and advanced thermal materials. By combining the aesthetic value of Flemish bond architecture with the thermal efficiency of PCM technology, this chapter underscores a novel approach to sustainable building design. It provides insight into how energy performance and visual form can be simultaneously optimized, offering a compelling solution for energy-conscious architecture without sacrificing heritage or aesthetics.

5.1. Model Characteristics

To simulate the structural and thermal behavior of exterior walls typical of Miskolc, Hungary, a brick block with dimensions of 40×20×15 [cm] was selected as the reference model. This block typifies the masonry commonly employed in regional construction, making it an ideal candidate for representing the real-world thermal properties and performance of local building envelopes. By choosing a widely used material configuration, the study ensures that simulation results reflect realistic climatic conditions and construction practices, allowing for a reliable evaluation of thermal behavior and energy efficiency.

The thermal performance of two Flemish bond-configured samples and one standard reference block was systematically analyzed. The samples were geometrically arranged to reflect the structure of a Flemish bond wall, as depicted in Fig. 5.1 (a-c). A Flemish bond is characterized by alternating headers and stretchers in each course, with headers of one course aligned centrally over the stretchers of the course below. Every alternate course begins with a header at the corner. While aesthetically pleasing and structurally sound, Flemish bonds require greater masonry skill and precision, making them more challenging to construct.

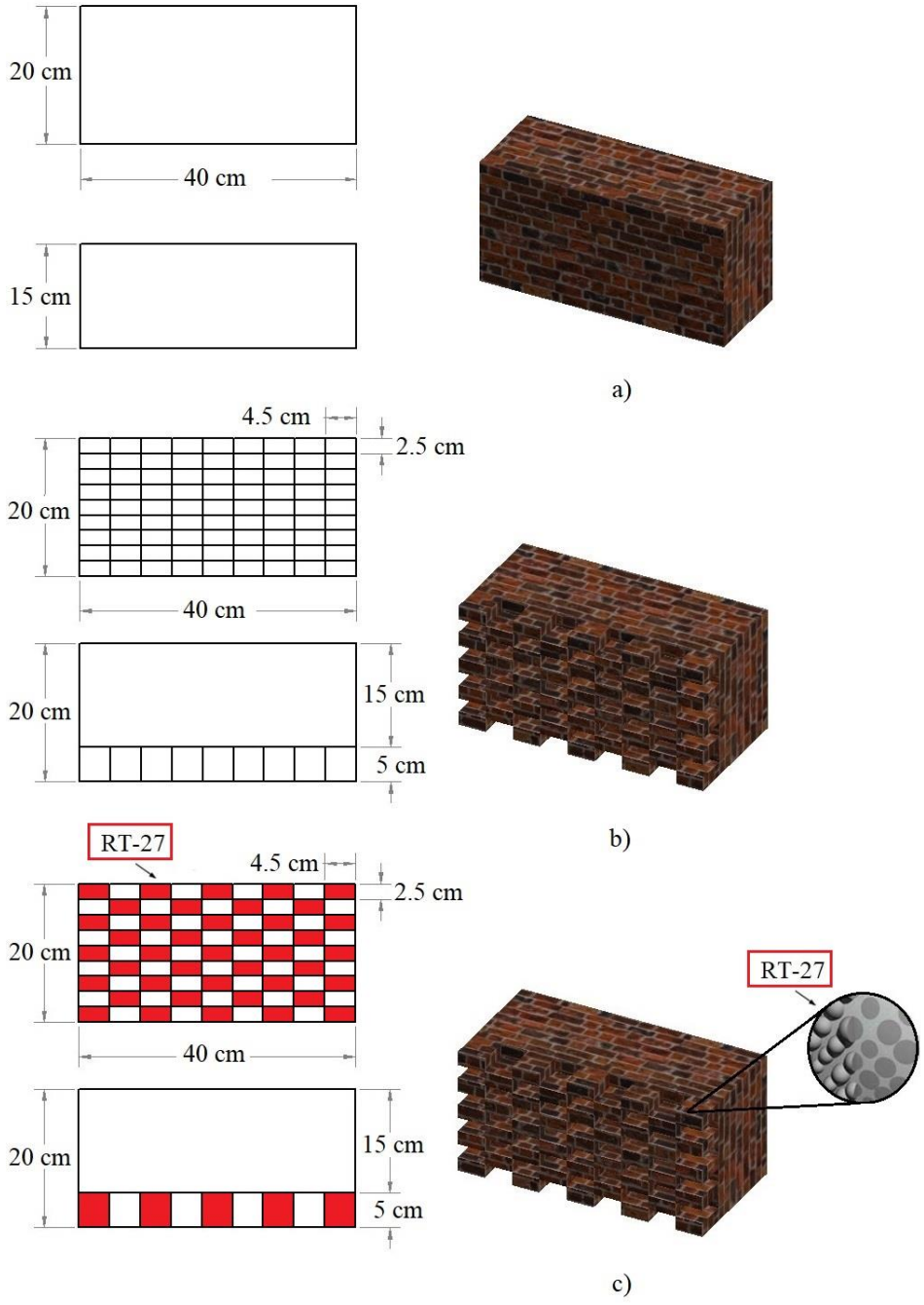

Fig. 5.1: *a) Schematic view of brick block, b) Schematic view of brick block with Flemish bond, c) Schematic view of brick block (Flemish bond) integrated with PCM*

In the simulation setup, the indoor temperature was held constant at T_{in}= 22 [°C], consistent with thermal comfort standards [88]. Convective heat transfer coefficients were set at h_{ex}= 25 [W/m^{2}K] for the external surface and h_{in}= 10 [W/m^{2}K] for the internal surface [89]. The top and bottom surfaces of the wall were assumed to be insulated, with a heat flux of q= 0 [W/m^2], to focus the analysis on horizontal heat transfer through the wall assembly. The ambient outdoor temperature variation was recorded over three days in mid-July for the city of Miskolc. The average outdoor temperature during this timeframe was calculated using data from 2020 to 2023 [90], providing a representative thermal profile for simulating building envelope performance under summer peak conditions.

5.2. Validation and Independence of Mesh Grid

To ensure the accuracy and credibility of the numerical simulations performed in this study, both validation and mesh independence analyses were conducted. Although the focus of this chapter differs from earlier analyses by addressing Flemish bond wall geometries, the core computational model was cross-validated against experimental data provided by A. Pasupathy et al. [23]. Their research, which investigated the thermal performance of PCM panels in a controlled test room environment, offers a benchmark for validating the numerical model's ability to capture key thermal dynamics such as temperature delay, attenuation, and heat transfer reduction due to latent heat effects. Despite differences in structural layout and PCM type, the numerical results in this chapter exhibit a similar trend in temperature stabilization and thermal lag behavior, indicating that the model reliably captures the influence of PCMs in dynamic thermal environments. This cross-validation offers confidence in extending the numerical framework to more complex wall configurations like the Flemish bond structure.

Furthermore, a mesh independence study was conducted to verify that the numerical outcomes are not sensitive to mesh size, particularly considering the intricate geometry of the Flemish bond arrangement. Hexahedral elements were employed in the meshing process using ANSYS Meshing, and simulations were run on seven progressively finer mesh grids. The key parameter evaluated for independence was the indoor surface temperature, which serves as a direct indicator of the wall's thermal response. Results showed that beyond approximately 45,000 nodes, the variation in temperature outcomes became negligible, suggesting that further mesh refinement would not significantly impact accuracy, but would instead increase computational cost. Therefore, the selected mesh configuration strikes an effective balance between precision and efficiency, ensuring robust simulation outcomes throughout the analysis of the PCM-enhanced Flemish bond walls.

5.3. Numerical Results

5.3.1. Effect of Incorporating Flemish Bond in the Building Envelope

This section explores the thermal implications of integrating the Flemish bond brick arrangement into the external wall design. The Flemish bond, courser alternating headers, and

stretchers in each course are not only an aesthetic architectural feature, but also introduce structural complexity that can influence thermal performance. To assess this, a comparative numerical simulation was performed using a standard brick wall configuration and one enhanced with a Flemish bond pattern. Fig. 5.2 presents the temperature profiles on the indoor surface of the wall over a 72 [hr] period under typical summer weather conditions in Miskolc, Hungary. The green line denotes the constant indoor room temperature of 22 [°C], while the blue dashed curve represents the temperature profile of a wall without the Flemish bond, and the orange curve indicates the temperature response of the wall incorporating the Flemish bond. It is evident from the figure that the wall with the Flemish bond exhibits a smoother temperature fluctuation with visibly reduced peaks and troughs. This highlights the Flemish bond's capacity to act as a thermal buffer, dampening the temperature swings that result from outdoor thermal loading.

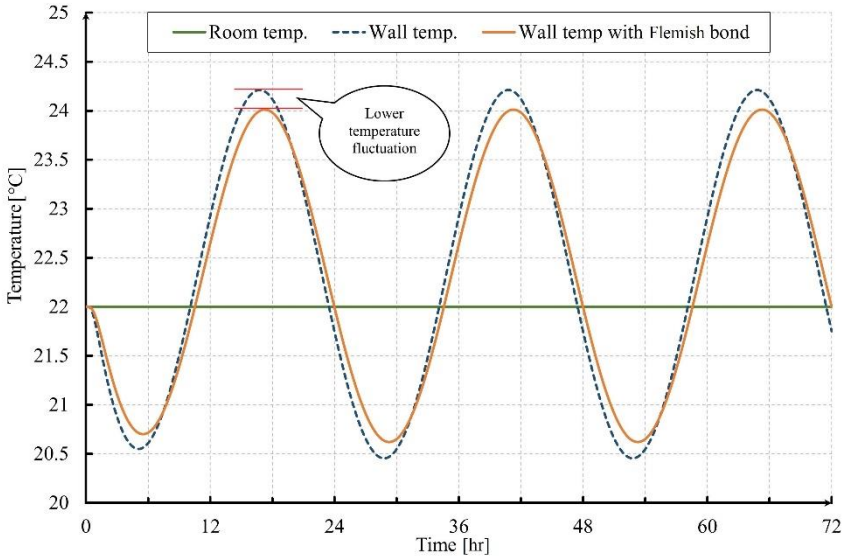

Fig. 5.2: *Indoor surface temperature distribution with Flemish bond*

The reduced thermal amplitude can be attributed to the geometry of the Flemish bond, which introduces additional layers of mass and internal voids that delay the progression of heat waves through the wall. As a result, the indoor surface experiences less dramatic changes in temperature over time, which contributes to enhanced thermal comfort and greater energy efficiency. Specifically, the highest indoor wall temperature in the standard wall approaches 24.3 [°C], whereas, in the Flemish bond wall, it remains closer to 24 [°C], a subtle but important improvement that reduces cooling loads. The quantitative evaluation confirms this thermal benefit. The total heat transmitted into the interior space was calculated as 3.56 [W] for the conventional wall, while the wall with the Flemish bond configuration recorded a reduced value of 3.33 [W]. This corresponds to a 6 % reduction in heat gain, demonstrating the potential of the Flemish bond not only as an architectural design choice, but also as a passive thermal management strategy. In conclusion, the incorporation of a Flemish bond into building envelopes enhances the thermal performance of walls by moderating temperature fluctuations and decreasing the amount of heat transmitted into interior spaces. This result suggests that geometric features associated with the

Flemish bond configuration can contribute to reduced heat transfer, separating pattern effects from thickness/thermal-mass effects will be addressed in future work.

5.3.2. Effect of Incorporating PCM in Flemish Bond

The computations conducted in the previous section were explicitly applied to the wall illustrated in Fig. 5.1(a), where a Flemish bond was incorporated into the building's exterior envelope. In this context, the Flemish bond design was utilized on the outer surface of the wall. This architectural choice not only enhances the aesthetic appeal, but also impacts the wall's structural integrity and thermal performance. This section further investigates the effect of integrating PCM into the same wall configuration. Embedding PCM within a Flemish bond structure enhances the thermal inertia of the wall and provides a buffering effect against ambient temperature fluctuations. As shown in Fig. 5.3, the wall with the combined use of the Flemish bond and PCM demonstrates significantly lower fluctuations in indoor surface temperature compared to the reference wall and the wall with the Flemish bond only. The red dotted curve, representing the wall with both Flemish bond and PCM, exhibits a flatter thermal response with reduced peaks and valleys, indicating a more stable and controlled indoor thermal environment. This dampening effect is a direct result of PCMs latent heat storage behavior, which smooths out the temperature variations by absorbing thermal energy during warmer periods and releasing it during cooler phases.

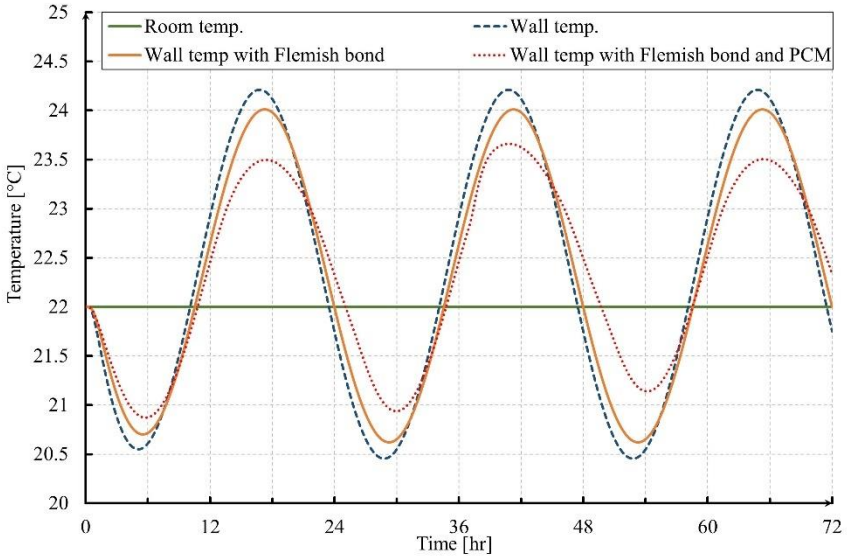

Fig. 5.3: *Indoor surface temperature distribution with Flemish bond and phase change material*

Fig. 5.4 provides further evidence of improved performance by presenting the heat transfer to the room over time. The graph indicates that the integration of PCM reduces both the maximum and minimum magnitudes of heat transfer into the room. The reference wall shows the highest amplitude in heat flux, while the wall incorporating the Flemish bond and PCM exhibits the most moderated curve, with the lowest peak values. This suggests a substantial reduction in the cooling and heating loads, as PCM buffers against rapid energy exchange. The total heat transmitted into

the interior space was calculated for the wall with the Flemish bond with PCM configuration recorded a reduced value of 2.82 [W].

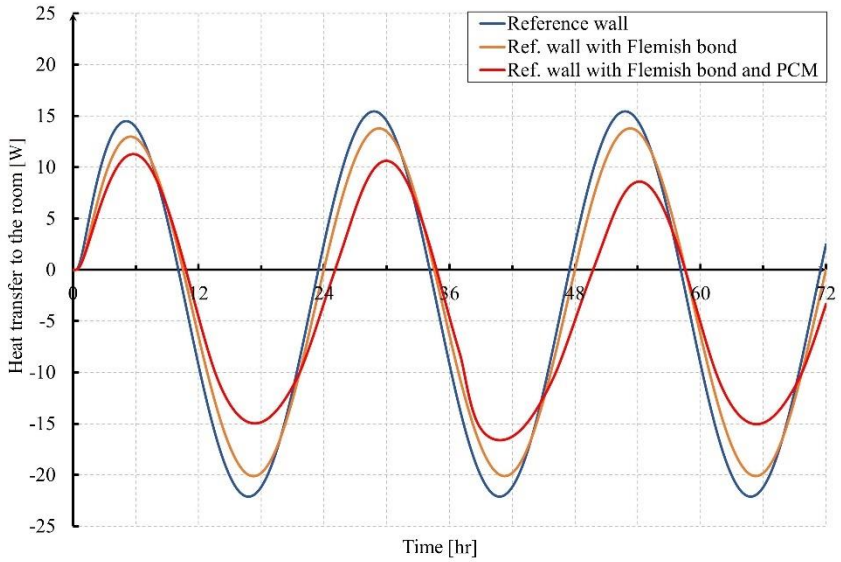

Fig. 5.4: *Heat transfers to the room when the phase change material is incorporated in the Flemish bond*

Quantitatively, while the Flemish bond alone reduced heat transfer by approximately 6 %, the addition of PCM pushed this reduction up to 21 %. These results confirm that the combination of architectural detailing (Flemish bond) with advanced thermal energy storage (PCM) not only improves the aesthetic and structural properties of the building envelope, but also provides a highly effective passive thermal regulation strategy. The findings highlight the synergy between passive design and material innovation, offering a promising direction for sustainable building solutions in climates such as that of Miskolc, Hungary.

5.4. Summary of This Chapter

This chapter presented a detailed numerical investigation into the thermal and energy performance of Flemish bond masonry walls, with and without the integration of PCM. Traditionally appreciated for their architectural aesthetics and historical use in masonry, Flemish bond walls were analyzed in this study not only for their structural benefits, but also for their thermal behavior in the context of energy-efficient building design.

Simulations using representative climatic data from Miskolc, Hungary, demonstrated that the Flemish bond wall configuration on its own contributed to a 6 % reduction in heat transfer to the indoor environment compared to a standard reference wall. This improvement is attributed to the increased mass and layered pattern of the Flemish bond, which inherently moderates temperature fluctuations by acting as a passive thermal buffer. The innovative focus of the chapter was the integration of RT-27 paraffin wax PCM into the Flemish bond configuration. When incorporated, the PCM capitalized on its latent heat storage capability, absorbing excess thermal energy during high external temperatures and releasing it during cooler periods. This dual function of storage

and release significantly improved thermal stability, reducing temperature fluctuations across the wall's indoor surface.

As shown in Fig. 5.3 and Fig. 5.4, the wall with both Flemish bond and PCM experienced markedly lower peak temperatures and smoother heat flux patterns over a 72 [hr] period. Most notably, as illustrated in Fig. 5.5, the total reduction in heat transfer reached 21 %, underscoring the synergistic impact of combining the thermal mass benefits of the Flemish bond with the dynamic energy buffering properties of PCM.

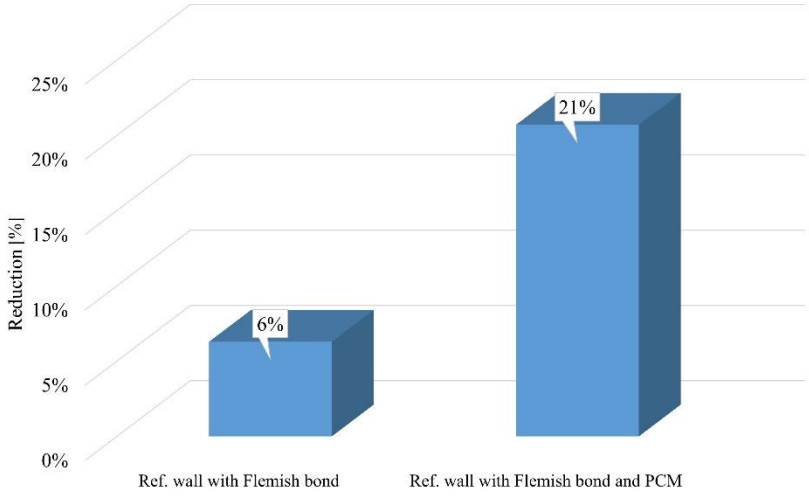

Fig. 5.5: *Total amount of heat transfer reduction to the room for different building envelope designs*

These findings not only validate the role of PCMs in enhancing building envelope performance, but also propose a novel use case: leveraging the geometric and aesthetic structure of traditional masonry patterns to augment energy efficiency. The integration of PCM into Flemish bond structures introduces a compelling path forward in sustainable architecture, preserving historical design while meeting modern energy performance demands.

6. THESES – NEW SCIENTIFIC RESULTS

T1. I developed and validated a reliable CFD-based approach to simulate the melting of RT-27 PCM under convective heating conditions. I implemented the model in ANSYS Fluent using the enthalpy–porosity method and established a reproducible workflow that addresses key numerical aspects, including mesh generation, boundary conditions, and solver settings. Using this framework, I analyzed the transition from conduction-dominated to convection-dominated heat transfer during melting and quantified the influence of buoyancy-driven flow and thermal stratification on the charging process. This work provides a practical simulation methodology for optimizing PCM integration in building energy systems. *Publications* (1-3).

T2. I systematically analyzed the effect of PCM layer positioning within building envelopes under realistic environmental conditions. Using CFD simulations, I showed that placing the PCM layer closer to the exterior surface can enhance wall thermal performance and reduce heat transfer to the indoor space by up to 23%. This result provides practical, climate-specific guidance for optimal PCM placement in wall assemblies and supports improved passive thermal regulation in building design. *Publications* (1,4).

T3. I investigated how PCM layer thickness influences the thermal performance of PCM-enhanced walls within the tested range 1–5 cm. I found that increasing thickness increases latent storage capacity and thermal inertia and reduces temperature fluctuations; within the investigated range, the maximum heat-transfer reduction (up to 42%) was achieved at 5 cm. This result provides practical guidance for thickness selection in the examined range and highlights that further increases may exhibit diminishing returns and must be balanced against construction constraints. *Publications* (1,4).

T4. I compared the performance of multiple PCM materials for building-envelope applications by evaluating how their thermophysical properties influence wall heat transfer. Under the tested conditions, I identified SP-25E2 as the best-performing PCM among the selected candidates, achieving up to a 26% reduction in heat transfer. Based on these results, I formulated practical material-selection guidance that links PCM characteristics (especially melting range and volumetric storage potential) to the climatic loading and wall requirements for effective PCM integration in energy-efficient construction. *Publications* (1,4).

T5. I systematically analyzed how PCM capsule geometry affects the thermal performance of building envelopes. Using CFD simulations, I compared cuboid, cylindrical, and prismatic capsule configurations under realistic climatic boundary conditions and quantified their impact on indoor-side heat transfer and temperature regulation. Under the fixed study constraints (same wall and boundary conditions, and a constant PCM quantity), I found that the capsule configuration, through its geometry and the resulting PCM distribution-contact area within the wall, significantly influences PCM charging/discharging behavior and overall

heat transfer reduction. In the tested cases, cuboid capsules produced the largest reduction (up to 37%), followed by cylindrical capsules (≈36%) and prismatic capsules (up to 35.85%), depending on space utilization and constructability constraints. Based on these results, I proposed practical configuration recommendations and established a validated simulation workflow for evaluating encapsulated PCM systems in building envelopes. *Publications* (1,5).

T6. I investigated, for the first time in this dissertation, the combined effect of integrating PCM into a Flemish-bond masonry wall to improve thermal performance under realistic climatic boundary conditions. I found that the tested Flemish-bond wall configuration reduces indoor-side heat transfer by approximately 6% compared with the reference wall. I further showed that embedding RT-27 PCM within the Flemish-bond cavities provides an additional performance gain, leading to a total heat transfer reduction of about 21% relative to the conventional wall assembly. This work also establishes a CFD-based workflow for simulating the transient thermal behavior of complex masonry PCM configurations and provides design insight into combining masonry detailing with latent thermal storage for passive temperature control. *Publications* (6).

ACKNOWLEDGEMENTS

First and foremost, I would like to express my deepest gratitude to the University of Miskolc for granting me the opportunity to pursue my doctoral studies and for providing the academic environment and resources essential for this research.

I am profoundly thankful to my supervisor, Dr. Béla Kovács, for his unwavering support, continuous guidance, and belief in my work. His expertise, constructive feedback, and encouragement have been instrumental in helping me navigate the complexities of this research and develop both academically and personally.

I would also like to express my sincere appreciation to my friend, Dr. Jad Aboud, for his invaluable guidance throughout this journey. His thoughtful advice and continuous encouragement have played a significant role in shaping the direction and outcome of this work.

I would also like to express my deepest appreciation to my family. Their unconditional love, sacrifices, and endless encouragement have been the cornerstone of everything I have achieved. To my parents, thank you for instilling in me the values of hard work, perseverance, and integrity. Your support, both emotionally and morally, has carried me through the most difficult moments of this journey. Your belief in my abilities gave me the strength to overcome obstacles and stay focused on my goals. To Maria, Amer, and Nay, thank you for your constant encouragement and for always being there when I needed reassurance or a reminder of what truly matters.

A special and heartfelt thanks to the greatest support in my life, Dr. Lilla Nánai. Her love, understanding, and constant encouragement have been my foundation, especially during the most challenging phases of this journey. Her unwavering belief in me, both personally and professionally, has been a true source of motivation, and her patience and support have made this achievement possible.

My gratitude extends to the faculty members, staff, and colleagues at the University of Miskolc, whose cooperation and support helped to create an inspiring and productive research environment.

To all those who supported me, directly or indirectly, your contributions have been invaluable. I am truly grateful for each person who played a part in this journey.

REFERENCES

[1] "The future of cooling opportunities for energy-efficient air conditioning together secure sustainable," *International Energy Agency*. [Online]. Available: https://www.iea.org/reports/the-future-of-cooling (last accessed Jun. 2025).

[2] "Global status report for buildings and construction 2019," *International Energy Agency*. [Online]. Available: https://www.iea.org/reports/global-status-report-for-buildings-and-construction-2019 (last accessed Jun. 2025).

[3] C. Far and H. Far, "Improving energy efficiency of existing residential buildings using effective thermal retrofit of building envelope," *Indoor and Built Environment*, vol. 28, no. 6, pp. 744-760, Jul. 2019. DOI: 10.1177/1420326X18794010.

[4] P. Lotfabadi and P. Hançer, "A comparative study of traditional and contemporary building envelope construction techniques in terms of thermal comfort and energy efficiency in hot and humid climates," *Sustainability*, vol. 11, no. 13, Jul. 2019. DOI: 10.3390/su11133582.

[5] H. Wang, W. Lu, Z. Wu, and G. Zhang, "Parametric analysis of applying PCM wallboards for energy saving in high-rise lightweight buildings in Shanghai," *Renew Energy*, vol. 145, pp. 52-64, Jan. 2020. DOI: 10.1016/j.renene.2019.05.124.

[6] R. A. Kishore, M. V. A. Bianchi, C. Booten, J. Vidal, and R. Jackson, "Optimizing PCM-integrated walls for potential energy savings in U.S. Buildings," *Energy Build*, vol. 226, Nov. 2020. DOI: 10.1016/j.enbuild.2020.110355.

[7] K. Saafi and N. Daouas, "Energy and cost efficiency of phase change materials integrated in building envelopes under Tunisia Mediterranean climate," *Energy*, vol. 187, Nov. 2019. DOI: 10.1016/j.energy.2019.115987.

[8] R. Ye, R. Huang, X. Fang, and Z. Zhang, "Simulative optimization on energy saving performance of phase change panels with different phase transition temperatures," *Sustain Cities Soc*, vol. 52, Jan. 2020. DOI: 10.1016/j.scs.2019.101833.

[9] M. Alam, P. X. W. Zou, J. Sanjayan, and S. Ramakrishnan, "Energy saving performance assessment and lessons learned from the operation of an active phase change materials system in a multi-storey building in Melbourne," *Appl Energy*, vol. 238, pp. 1582-1595, Mar. 2019. DOI: 10.1016/j.apenergy.2019.01.116.

[10] J. Shi, X. Huang, X. Guo, X Shan, Z Xu, X. Zhao, Z. Sun, W. Aftab, C. Qu, R. Yao, and R. Zou, "Experimental Investigation and Numerical Validation on the Energy-Saving Performance of A passive Phase Change Material Floor for A Real Scale Building," *ES Energy & Environment*, 2020. DOI: 10.30919/esee8c380.

[11] S. A. Nada, W. G. Alshaer, and R. M. Saleh, "Thermal characteristics and energy saving of charging/discharging processes of PCM in air free cooling with minimal temperature differences," *Alexandria Engineering Journal*, vol. 58, no. 4, pp. 1175-1190, Dec. 2019. DOI: 10.1016/j.aej.2019.10.002.

[12] B. Y. Yun, J. H. Park, S. Yang, S. Wi, and S. Kim, "Integrated analysis of the energy and economic efficiency of PCM as an indoor decoration element: Application to an apartment building," *Solar Energy*, vol. 196, pp. 437-447, Jan. 2020. DOI: 10.1016/j.solener.2019.12.006.

[13] M. Alizadeh and S. M. Sadrameli, "Indoor thermal comfort assessment using PCM based storage system integrated with ceiling fan ventilation: Experimental design and response surface approach," *Energy Build*, vol. 188, pp. 297-313, Apr. 2019. DOI: 10.1016/j.enbuild.2019.02.020.

[14] L. O. Afolabi, Z. M. Ariff, P. S. M. Megat-Yusoff, H. H. Al-Kayiem, A. I. Arogundade, and O. T. Afolabi-Owolabi, "Red-mud geopolymer composite encapsulated phase change material for thermal comfort in built-sector," *Solar Energy*, vol. 181, pp. 464-474, Mar. 2019. DOI: 10.1016/j.solener.2019.02.029.

[15] W. Zhang, Y. Wu, and J. K. Calautit, "A review on occupancy prediction through machine learning for enhancing energy efficiency, air quality and thermal comfort in the built environment," *Renewable and Sustainable Energy Reviews*, vol. 167, Oct. 2022. DOI: 10.1016/j.rser.2022.112704.

[16] Technology Roadmap Energy Efficient Building Envelopes, *International Energy Agency*. [Online]. Available: https://www.iea.org/reports/technology-roadmap-energy-efficient-building-envelopes (last accessed Jun. 2025).

[17] "An assessment of energy technologies and research opportunities chapter 5: increasing efficiency of building systems and technologies," *U.S Department of Energy*. [Online]. Available: https://www.energy.gov/articles/chapter-5-increasing-efficiency-buildings-systems-and-technologies (last accessed Jun. 2025).

[18] B. Lamrani, K. Johannes, and F. Kuznik, "Phase change materials integrated into building walls: An updated review," *Renewable and Sustainable Energy Reviews*, Apr. 2021. DOI: 10.1016/j.rser.2021.110751.

[19] V. V. Tyagi, A. K. Pandey, D. Buddhi, and R. Kothari, "Thermal performance assessment of encapsulated PCM based thermal management system to reduce peak

energy demand in buildings," *Energy Build*, vol. 117, pp. 44-52, Apr. 2016. DOI: 10.1016/j.enbuild.2016.01.042.

[20] K. Faraj, M. Khaled, J. Faraj, F. Hachem, and C. Castelain, "Phase change material thermal energy storage systems for cooling applications in buildings: A review," *Renewable and Sustainable Energy Reviews*, vol. 119, Mar. 2020. DOI: 10.1016/j.rser.2019.109579.

[21] A. Váz Sá, R. M. S. F. Almeida, H. Sousa, and J. M. P. Q. Delgado, "Numerical analysis of the energy improvement of plastering mortars with phase change materials," *Advances in Materials Science and Engineering*, 2014. DOI: 10.1155/2014/582536.

[22] S. S. Chandel and T. Agarwal, "Review of current state of research on energy storage, toxicity, health hazards and commercialization of phase changing materials," *Renewable and Sustainable Energy Reviews ,* Jan. 2017. DOI: 10.1016/j.rser.2016.09.070.

[23] A. Pasupathy, L. Athanasius, R. Velraj, and R. V. Seeniraj, "Experimental investigation and numerical simulation analysis on the thermal performance of a building roof incorporating phase change material (PCM) for thermal management," *Appl Therm Eng*, vol. 28, no. 5, pp. 556-565, Apr. 2008. DOI: 10.1016/j.applthermaleng.2007.04.016.

[24] F. S. Javadi, H. S. C. Metselaar, and P. Ganesan, "Performance improvement of solar thermal systems integrated with phase change materials (PCM), a review," *Solar Energy* , Aug. 2020. DOI: 10.1016/j.solener.2020.05.106.

[25] S. Bista, S. E. Hosseini, E. Owens, and G. Phillips, "Performance improvement and energy consumption reduction in refrigeration systems using phase change material (PCM)," *Applied Thermal Engineering,* Sep. 2018. DOI: 10.1016/j.applthermaleng.2018.07.068.

[26] Q. Mao and Y. Zhang, "Thermal energy storage performance of a three-PCM cascade tank in a high-temperature packed bed system," *Renew Energy*, vol. 152, pp. 110-119, Jun. 2020. DOI: 10.1016/j.renene.2020.01.051.

[27] A. Lecuona, J. I. Nogueira, R. Ventas, M. del C. Rodríguez-Hidalgo, and M. Legrand, "Solar cooker of the portable parabolic type incorporating heat storage based on PCM," *Appl Energy*, vol. 111, pp. 1136-1146, 2013. DOI: 10.1016/j.apenergy.2013.01.083.

[28] X. Hu and X. Gong, "Experimental study on the thermal response of PCM-based heat sink using structured porous material fabricated by 3D printing," *Case Studies in Thermal Engineering*, vol. 24, Apr. 2021. DOI: 10.1016/j.csite.2021.100844.

[29] X. Sun, J. Jovanovic, Y. Zhang, S. Fan, Y. Chu, Y. MO, and S. Liao, "Use of encapsulated phase change materials in lightweight building walls for annual thermal

regulation," *Energy*, vol. 180, pp. 858–872, Aug. 2019. DOI: 10.1016/j.energy.2019.05.112.

[30] B. Nghana and F. Tariku, "Phase change material's (PCM) impacts on the energy performance and thermal comfort of buildings in a mild climate," *Build Environ*, vol. 99, pp. 221-238, Apr. 2016. DOI: 10.1016/j.buildenv.2016.01.023.

[31] J. Koo, H. So, S. W. Hong, and H. Hong, "Effects of wallboard design parameters on the thermal storage in buildings," *Energy Build*, vol. 43, no. 8, pp. 1947-1951, Aug. 2011. DOI: 10.1016/j.enbuild.2011.03.038.

[32] F. Mehdaoui, M. Hazami, A. Messaouda, H. Taghouti, and A. A. Guizani, "Thermal testing and numerical simulation of PCM wall integrated inside a test cell on a small scale and subjected to the thermal stresses," *Renew Energy*, vol. 135, pp. 597-607, May 2019. DOI: 10.1016/j.renene.2018.12.029.

[33] E. Meng, H. Yu, and B. Zhou, "Study of the thermal behavior of the composite phase change material (PCM) room in summer and winter," *Appl Therm Eng*, vol. 126, pp. 212-225, 2017. DOI: 10.1016/j.applthermaleng.2017.07.110.

[34] A. Bontemps, M. Ahmad, K. Johanns, and H. Sallée, "Experimental and modelling study of twin cells with latent heat storage walls," *Energy Build*, vol. 43, no. 9, pp. 2456-2461, Sep. 2011. DOI: 10.1016/j.enbuild.2011.05.030.

[35] L. Yang, Y. Qiao, Y. Liu, X. Zhang, C. Zhang, and J. Liu, "A kind of PCMs-based lightweight wallboards: Artificial controlled condition experiments and thermal design method investigation," *Build Environ*, vol. 144, pp. 194-207, Oct. 2018. DOI: 10.1016/j.buildenv.2018.08.020.

[36] Z. X. Li, A. Al-Rashed, M. Rostamzadeh, R. Kalbasi, A. Shahsavar, and M. Afrand, "Heat transfer reduction in buildings by embedding phase change material in multi-layer walls: Effects of repositioning, thermophysical properties and thickness of PCM," *Energy Convers Manag*, vol. 195, pp. 43-56, Sep. 2019. DOI: 10.1016/j.enconman.2019.04.075.

[37] Y. Qiao, L. Yang, J. Bao, Y. Liu, and J. Liu, "Reduced-scale experiments on the thermal performance of phase change material wallboard in different climate conditions," *Build Environ*, vol. 160, Aug. 2019. DOI: 10.1016/j.buildenv.2019.106191.

[38] A. De Gracia, L. Navarro, A. Castell, Á. Ruiz-Pardo, S. Álvarez, and L. F. Cabeza, "Thermal analysis of a ventilated facade with PCM for cooling applications," *Energy Build*, vol. 65, pp. 508-515, 2013. DOI: 10.1016/j.enbuild.2013.06.032.

[39] R. Ye, C. Zhang, W. Sun, X. Fang, and Z. Zhang, "Novel wall panels containing $CaCl_2 \cdot 6H_2O$-$Mg(NO_3)_2 \cdot 6H_2O$/expanded graphite composites with different phase change temperatures for building energy savings," *Energy Build*, vol. 176, pp. 407–417, Oct. 2018. DOI: 10.1016/j.enbuild.2018.07.045.

[40] F. Kuznik, D. David, K. Johannes, and J. J. Roux, "A review on phase change materials integrated in building walls," *Renewable and Sustainable Energy Reviews*, 2011. DOI: 10.1016/j.rser.2010.08.019.

[41] L. F. Cabeza, A. Castell, C. Barreneche, A. De Gracia, and A. I. Fernandez, "Materials used as PCM in thermal energy storage in buildings: A review," *Renewable and Sustainable Energy Reviews,* vol. 15, no. 3, pp. 1675-1695, Apr. 2011. DOI: 10.1016/j.rser.2010.11.018.

[42] S. A. Memon, "Phase change materials integrated in building walls: A state of the art review," *Renewable and Sustainable Energy Reviews*, vol. 31, pp. 870-906, 2014. DOI: 10.1016/j.rser.2013.12.042.

[43] X. Bao, H. Yang, X. Xu, T. Xu, H. Cui, W. Tang, G. Sang, and W. Fung, "Development of a stable inorganic phase change material for thermal energy storage in buildings," *Solar Energy Materials and Solar Cells*, vol. 208, May 2020. DOI: 10.1016/j.solmat.2020.110420.

[44] S. Lu, Y. Li, X. Kong, B. Pang, Y. Chen, S. Zheng, and L. Sun, "A review of PCM energy storage technology used in buildings for the global warming solution," *Lecture Notes in Energy*, vol. 33, pp. 611-644, 2017. DOI: 10.1007/978-3-319-26950-4_31.

[45] J. Pereira da Cunha and P. Eames, "Thermal energy storage for low and medium temperature applications using phase change materials - A review," *Applied Energy*, vol. 177, pp. 227-238, Sep. 2016. DOI: 10.1016/j.apenergy.2016.05.097.

[46] K. Cellat, F. Tezcan, B. Beyhan, G. Kardaş, and H. Paksoy, "A comparative study on corrosion behavior of rebar in concrete with fatty acid additive as phase change material," *Constr Build Mater*, vol. 143, pp. 490-500, Jul. 2017. DOI: 10.1016/j.conbuildmat.2017.03.165.

[47] J. Giro-Paloma, C. Barreneche, M. Martínez, B. Šumiga, L. F. Cabeza, and A. I. Fernández, "Comparison of phase change slurries: Physicochemical and thermal properties," *Energy*, vol. 87, pp. 223-227, Jul. 2015. DOI: 10.1016/j.energy.2015.04.071.

[48] Y. E. Milián, A. Gutiérrez, M. Grageda, and S. Ushak, "A review on encapsulation techniques for inorganic phase change materials and the influence on their thermophysical properties," *Renewable and Sustainable Energy Reviews*, vol. 73, pp. 983-999, 2017. DOI: 10.1016/j.rser.2017.01.159.

[49] A. Bland, M. Khzouz, T. Statheros, and E. I. Gkanas, "PCMs for residential building applications: A short review focused on disadvantages and proposals for future development," *Buildings,* vol. 7, no. 3, 2017. DOI: 10.3390/buildings7030078.

[50] P. K. S. Rathore and S. K. Shukla, “An experimental evaluation of thermal behavior of the building envelope using macroencapsulated PCM for energy savings,” *Renew Energy*, vol. 149, pp. 1300-1313, Apr. 2020. DOI: 10.1016/j.renene.2019.10.130.

[51] P. K. S. Rathore and S. K. Shukla, “Potential of macroencapsulated pcm for thermal energy storage in buildings: A comprehensive review,” *Construction and Building Materials*, vol. 225, pp. 723-744, Nov. 2019. DOI: 10.1016/j.conbuildmat.2019.07.221.

[52] Z. Liu, Z. Yu, T. Yang, D. Qin, S. Li, G. Zhang,F Haghighat, and M. Joybari, “A review on macro-encapsulated phase change material for building envelope applications,” *Building and Enviroment*, vol. 144, pp. 281-294, Oct. 2018. DOI: 10.1016/j.buildenv.2018.08.030.

[53] M. Frigione, M. Lettieri, and A. Sarcinella, “Phase change materials for energy efficiency in buildings and their use in mortars,” *Materials*, Apr. 2019. DOI: 10.3390/ma12081260.

[54] W. Cheng, B. Xie, R. Zhang, Z. Xu, and Y. Xia, “Effect of thermal conductivities of shape stabilized PCM on under-floor heating system,” *Appl Energy*, vol. 144, pp. 10-18, Apr. 2015. DOI: 10.1016/j.apenergy.2015.01.055.

[55] A. Fallahi, G. Guldentops, M. Tao, S. Granados-Focil, and S. Van Dessel, “Review on solid-solid phase change materials for thermal energy storage: Molecular structure and thermal properties,” *Applied Thermal Engineering*, 2017. DOI: 10.1016/j.applthermaleng.2017.08.161.

[56] N. Beemkumar, D. Yuvarajan, M. Arulprakasajothi, S. Ganesan, K. Elangovan, and G. Senthilkumar, “Experimental investigation and numerical modeling of room temperature control in buildings by the implementation of phase change material in the roof,” *Journal of Solar Energy Engineering, Transactions of the ASME*, vol. 142, no. 1, Feb. 2020. DOI: 10.1115/1.4044564.

[57] B. P. Jelle and S. E. Kalnæs, “Phase Change Materials for Application in Energy-Efficient Buildings,” *Cost-Effective Energy Efficient Building Retrofitting*, Elsevier Inc., pp. 57–11, 2017. DOI: 10.1016/B978-0-08-101128-7.00003-4.

[58] L. Navarro, A. Sole, M. Marrtin, C. Barrenecha, L. Olivieri, J. Tenorio, and L. Cabeza, “Benchmarking of useful phase change materials for a building application,” *Energy Build*, vol. 182, pp. 45-50, Jan. 2019. DOI: 10.1016/j.enbuild.2018.10.005.

[59] A. Aranda-Usón, G. Ferreira, A. M. López-Sabirón, M. D. Mainar-Toledo, and I. Zabalza Bribián, “Phase change material applications in buildings: An environmental assessment for some Spanish climate severities,” *Science of the Total Environment*, vol. 444, pp. 16-25, Feb. 2013. DOI: 10.1016/j.scitotenv.2012.11.012.

[60] J. Yu, Q. Yang, H. Ye, J. Huang, Y. Liu, and J. Tao, "The optimum phase transition temperature for building roof with outer layer PCM in different climate regions of China," in *Energy Procedia*, pp. 3045-3051, 2019. DOI: 10.1016/j.egypro.2019.01.989.

[61] X. Jin, M. A. Medina, and X. Zhang, "Numerical analysis for the optimal location of a thin PCM layer in frame walls," *Appl Therm Eng*, vol. 103, pp. 1057-1063, Jun. 2016. DOI: 10.1016/j.applthermaleng.2016.04.056.

[62] A. Vukadinovic, J. Radosavljevic, and A. Dordevic, "Energy performance impact of using phase-change materials in thermal storage walls of detached residential buildings with a sunspace," *Solar Energy*, vol. 206, pp. 228-244, Aug. 2020. DOI: 10.1016/j.solener.2020.06.008.

[63] S. Lu, B. Xu, and X. Tang, "Experimental study on double pipe PCM floor heating system under different operation strategies," *Renew Energy*, vol. 145, pp. 1280-1291, Jan. 2020. DOI: 10.1016/j.renene.2019.06.086.

[64] T. Silva, R. Vicente, C. Amaral, and A. Figueiredo, "Thermal performance of a window shutter containing PCM: Numerical validation and experimental analysis," *Appl Energy*, vol. 179, pp. 64-84, Oct. 2016. DOI: 10.1016/j.apenergy.2016.06.126.

[65] V. V. Rao, R. Parameshwaran, and V. V. Ram, "PCM-mortar based construction materials for energy efficient buildings: A review on research trends," *Energy and Buildings*, vol. 158, pp. 95-122, Jan. 2018. DOI: 10.1016/j.enbuild.2017.09.098.

[66] H. Do Yun, K. L. Ahn, S. J. Jang, B. S. Khil, W. S. Park, and S. W. Kim, "Thermal and Mechanical Behaviors of Concrete with Incorporation of Strontium-Based Phase Change Material (PCM)," *Int J Concr Struct Mater*, vol. 13, no. 1, Dec. 2019. DOI: 10.1186/s40069-018-0326-8.

[67] L. F. Cabeza *et al.*, "Behaviour of a concrete wall containing micro-encapsulated PCM after a decade of its construction," *Solar Energy*, vol. 200, pp. 108-113, Apr. 2020. DOI: 10.1016/j.solener.2019.12.003.

[68] A. Adesina, "Use of phase change materials in concrete: current challenges," *Renewable Energy and Environmental Sustainability*, vol. 4, pp. 9, 2019. DOI: 10.1051/rees/2019006.

[69] A. Frazzica *et al.*, "Thermal performance of hybrid cement mortar-PCMs for warm climates application," *Solar Energy Materials and Solar Cells*, vol. 193, pp. 270-280, May 2019. DOI: 10.1016/j.solmat.2019.01.022.

[70] J. Hu and X. Yu, "Thermo and light-responsive building envelope: Energy analysis under different climate conditions," *Solar Energy*, vol. 193, pp. 866-877, Nov. 2019. DOI: 10.1016/j.solener.2019.10.021.

[71] M. Ahangari and M. Maerefat, “An innovative PCM system for thermal comfort improvement and energy demand reduction in building under different climate conditions,” *Sustain Cities Soc*, vol. 44, pp. 120-129, Jan. 2019. DOI: 10.1016/j.scs.2018.09.008.

[72] X. Kong, L. Wang, H. Li, G. Yuan, and C. Yao, “Experimental study on a novel hybrid system of active composite PCM wall and solar thermal system for clean heating supply in winter,” *Solar Energy*, vol. 195, pp. 259-270, Jan. 2020. DOI: 10.1016/j.solener.2019.11.081.

[73] W. Sun, R. Huang, Z. Ling, X. Fang, and Z. Zhang, “Numerical simulation on the thermal performance of a PCM-containing ventilation system with a continuous change in inlet air temperature,” *Renew Energy*, vol. 145, pp. 1608-1619, Jan. 2020. DOI: 10.1016/j.renene.2019.07.089.

[74] T. Barz, J. Emhofer, K. Marx, G. Zsembinszki, and L. F. Cabeza, “Phenomenological modelling of phase transitions with hysteresis in solid/liquid PCM,” *J Build Perform Simul*, vol. 12, no. 6, pp. 770–788, Nov. 2019. DOI: 10.1080/19401493.2019.1657953.

[75] M. T. Plytaria, E. Bellos, C. Tzivanidis, and K. A. Antonopoulos, “Numerical simulation of a solar cooling system with and without phase change materials in radiant walls of a building,” *Energy Convers Manag*, vol. 188, pp. 40-53, May 2019. DOI: 10.1016/j.enconman.2019.03.042.

[76] A. Dashtaki, A. Nadooshan, and A. Abedi, “Effect of type and location of a phase change material (PCM) layer in a building wall on energy consumption using numerical simulation,” *Int. J. Adv. Design Manuf. Technol.*, vol. 12, no. 4, pp. 33-46, 2019

[77] S. Nayak, N. M. A. Krishnan, and S. Das, “Microstructure-guided numerical simulation to evaluate the influence of phase change materials (PCMs) on the freeze-thaw response of concrete pavements,” *Constr Build Mater*, vol. 201, pp. 246-256, Mar. 2019. DOI: 10.1016/j.conbuildmat.2018.12.199.

[78] M. Kheradmand, R. Vicente, M. Azenha, and J. L. B. de Aguiar, “Influence of the incorporation of phase change materials on temperature development in mortar at early ages: Experiments and numerical simulation,” *Constr Build Mater*, vol. 225, pp. 1036-1051, Nov. 2019. DOI: 10.1016/j.conbuildmat.2019.08.028.

[79] Y. A. Cengel, “Heat transfer a practical approach, ” *New York: McGraw-Hill*, 2002.

[80] B. Zivkovic and I. Fujii, “An analysis of isothermal phase change of phase change material within rectangular and cylindrical containers,” *Solar Energy*, vol. 70, no. 1, pp. 51-61, 2001. DOI: 10.1016/S0038-092X(00)00112-2.

[81] “Chapter 23: Modeling Solidification and Melting.” [Online]. Available: https://ansyshelp.ansys.com/account/secured?returnurl=/Views/Secured/corp/v221/en/flu_ug/flu_ug_chp_melt_freeze.html (last accessed Jun. 2025).

[82] "Chapter 16: Solidification and Melting." [Online]. Available: https://ansyshelp.ansys.com/account/secured?returnurl=/Views/Secured/corp/v221/en/flu_th/flu_th_chp_melt_freeze.html (last accessed Jun. 2025).

[83] "Rubitherm GmbH." [Online]. Available: https://www.rubitherm.eu/en/pcm.html (last accessed Jun. 2025).

[84] N. S. Dhaidan and J. M. Khodadadi, "Melting and convection of phase change materials in different shape containers: A review," *Renewable and Sustainable Energy Reviews*, vol. 43, pp. 449-477, 2015. DOI: 10.1016/j.rser.2014.11.017.

[85] M. S. M. Al-Jethelah, S. H. Tasnim, S. Mahmud, and A. Dutta, "Melting of nano-phase change material inside a porous enclosure," *Int J Heat Mass Transf*, vol. 102, pp. 773–787, Nov. 2016. DOI: 10.1016/j.ijheatmasstransfer.2016.06.070.

[86] H. Ambarita, I. Abdullah, C. A. Siregar, R. E. T. Siregar, and A. D. Ronowikarto, "Experimental study on melting and solidification of phase change material thermal storage," in *IOP Conference Series: Materials Science and Engineering*, Institute of Physics Publishing, Mar. 2017. DOI: 10.1088/1757-899X/180/1/012030.

[87] Z. Li, C. Du, D. Ahmadi, R. Kalbasi, and S. Rostami, "Numerical modeling of a hybrid PCM-based wall for energy usage reduction in the warmest and coldest months," *J Therm Anal Calorim*, vol. 144, no. 5, pp. 1985–1998, Jun. 2021. DOI: 10.1007/s10973-020-09861-y.

[88] R. and A.-C. Engineers. American Society of Heating, "2009 Ashrae Handbook : fundamentals," *ASHRAE*, 2009.

[89] J. Holman, "Heat Transfer," *New York: McGraw-Hill*, 2009.

[90] "Free Open-Source Weather API | Open-Meteo.com." [Online]. Available: https://open-meteo.com/ (last accessed Jun. 2025).

[91] C. Gentilini, E. Franzoni, G. Graziani, and S. Bandini, "Mechanical properties of fired-clay brick masonry models in moist and dry conditions," *Key Engineering Materials*, vol. 624, pp. 307–312, 2014. DOI: 10.4028/www.scientific.net/KEM.624.307.

LIST OF PUBLICATIONS RELATED TO THE TOPIC OF THE RESEARCH FIELD

(1) A. Saliby and B. Kovács, "Minimization of annual energy consumption by incorporating phase change materials into building components: a comprehensive review," *Heat Transfer Research*, vol. 54, no. 13 pp. 65-91, 2023.

DOI: 10.1615/HeatTransRes.2023047570. **(Q_2, IF: 1.7)**

(2) A. Saliby and B. Kovács, "Melting process simulation of phase change material layer used in the building envelope," *Heat Transfer Research*, vol. 55, no. 4 pp. 15-26, 2024.

DOI: 10.1615/HeatTransRes.2023048367. **(Q_2, IF: 1.7)**

(3) A. Saliby and B. Kovács, "CFD modelling for phase change materials integrated to building envelope," *Pollack Periodica*, vol. 19, no. 1 pp. 67-72, 2024.

DOI: 10.1556/606.2023.00930. **(Q_3)**

(4) A. Saliby and B. Kovács, "Enhancing thermal performance of phase change materials in building envelopes," *Pollack Periodica*, vol. 20, no. 1 pp. 87-94, 2025.

DOI: 10.1556/606.2024.01153. **(Q_3)**

(5) A. Saliby and B. Kovács, "Optimizing PCM capsule shape for enhanced building envelope thermal management," *Heat Transfer Research*, vol. 56, no. 13 pp. 19-31, 2025.

DOI: 10.1615/HeatTransRes.2025056163. **(Q_2, IF: 1.7)**

(6) A. Saliby and B. Kovács, "Combining aesthetics and efficiency: PCM applications in Flemish bond walls," *Pollack Periodica,* 2025.

DOI: 10.1556/606.2025.01346. **(Q_3)**